

Measurement of NO_x and NO_y with a thermal dissociation cavity ring-down spectrometer (TD-CRDS): Instrument characterisation and first deployment.

5 Nils Friedrich¹, Ivan Tadic¹, Jan Schuladen¹, James Brooks², Eoghan Darbyshire², Frank Drewnick¹,
Horst Fischer¹, Jos Lelieveld¹, John N. Crowley¹

¹Atmospheric Chemistry Department, Max Planck Institute for Chemistry, Mainz, 55128, Germany

²Centre of Atmospheric Science, University of Manchester, Manchester, UK

Correspondence to: John N. Crowley (john.crowley@mpic.de)

Abstract. We present a newly constructed, two channel Thermal Dissociation Cavity Ring-Down Spectrometer (TD-CRDS)
10 for the **detection measurement** of NO_x (NO + NO₂), NO_y (NO_x + HNO₃ + RO₂NO₂ + N₂O₅ etc.), NO_z (NO_y - NO_x) and
particulate nitrate (pNit). NO_y-containing trace gases are detected as NO₂ by CRDS at 405 nm following sampling through
inlets at ambient temperature (NO_x), or at 850 °C (NO_y). In both cases, O₃ was added to the air sample directly upstream of
the cavities to convert NO (either ambient, or formed in the 850 °C oven) to NO₂. An activated carbon denuder was used to
remove gas-phase components of NO_y when sampling pNit. **Detection limits, defined as the 2σ precision for 1 minute**
15 **averaging, are 40 pptv for both NO_x and NO_y.** The total measurement uncertainties (at 50% RH) in the NO_x and NO_y channels
are 11% + 10 pptv and 16% + 14 pptv for NO_z, respectively. **Thermograms of various trace-gases of the NO_z family** confirm
stoichiometric conversion to NO₂ (and / or NO) at the oven temperature and rule out significant interferences from NH₃
detection (**< 2%**) or radical recombination reactions under ambient conditions. While fulfilling the requirement of high particle
transmission (**> 80% between 30 and 400 nm**) and essentially complete removal of reactive nitrogen under dry conditions (**>**
20 **99%**), the denuder suffered from NO_x breakthrough and memory effects (i.e. release of stored NO_y) under humid conditions,
which may potentially bias measurements of particle nitrate.
Summertime NO_x measurements obtained from a ship sailing through the Red Sea, Indian Ocean and Arabian Gulf (NO_x levels
from < 20 pptv to 25 ppbv) were in excellent agreement with those taken by a chemiluminescence detector of NO and NO₂. A
dataset obtained locally under vastly different conditions (urban location in winter) revealed large diel variations in the NO_z to
25 **NO_y ratio which could be attributed to the impact of local emissions by road-traffic.**

1 Introduction

1.1 Atmospheric NO_x and NO_y

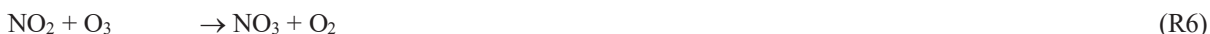
Total reactive nitrogen NO_y (= NO_x + NO_z) consists of nitrogen oxide NO, nitrogen dioxide NO₂ (NO + NO₂ = NO_x) and their reservoir species NO_z (NO₃ + 2N₂O₅ + HNO₃ + HONO + RONO₂ + RO₂NO₂ + XONO₂ + XNO₂ + pNit), where X is a halogen atom. HCN and NH₃ are generally not considered to be components of NO_y (Logan, 1983).

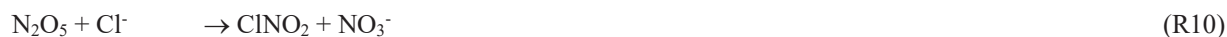
The formation of both peroxy nitrates (RO₂NO₂, PNs) and alkyl nitrates (RONO₂, ANs) requires the presence of organic peroxy radicals (RO₂), which are formed e.g. in the reaction of OH radicals with volatile organic compounds (VOCs) and oxygen (reaction R1). RO₂ radicals react subsequently with NO₂ or NO to form peroxy-nitrates (RO₂NO₂, PNs) or alkyl-nitrates (RONO₂, ANs, reactions R2 and R3). Reaction R3 competes with the formation of an alkoxy radical (RO) and the oxidation of NO to NO₂ (reaction R4), which consumes the dominant fraction of RO₂. The branching ratio between these two pathways depends on atmospheric conditions such as pressure and temperature and on the structure and length of the organic backbone (Lightfoot et al., 1992). HNO₃ is produced mainly via the reaction of NO₂ with OH (reaction R5).



The lifetimes of peroxy nitrates in the low troposphere are mainly governed by the temperature. PNs with an additional acyl group (PANs), such as peroxyacetyl nitrate (PAN), are generally more stable than PNs without an acyl group (e.g. pernitric acid HO₂NO₂), which are observed only in cold regions (Slusher et al., 2002). Thus, of the peroxy nitrates only PANs are considered able to act as transportable reservoirs for NO_x. At higher altitudes in the troposphere (above ca. 7 km) photolysis becomes the most important loss process for PAN, while the reaction with OH is negligible in the entire troposphere (Talukdar et al., 1995).

The absence of photolysis reactions and low levels of the OH radical at nighttime open alternative pathways to formation of NO_z species. NO₂ is oxidised by O₃ to produce the nitrate radical NO₃, which exists in thermal equilibrium with N₂O₅ (reactions R6 and R7). The reaction of NO₃ with hydrocarbons represents a nighttime source of alkyl nitrates (reaction R8), N₂O₅ can be hydrolysed on aqueous aerosol resulting in the formation of HNO₃ (reaction R9) and ClNO₂ (reaction R10) if particulate chloride is available (Finlayson-Pitts et al., 1989).





Nitric acid formation via the reaction of NO_2 and OH (reaction R5), followed by wet or dry deposition of HNO_3 , is considered to be the dominant daytime loss process for atmospheric NO_x (Roberts, 1990), though the reduction of NO_x may result in an increasingly important role for organic nitrates, e.g. in the USA (Present et al., 2020). As some organic nitrates are longer lived than HNO_3 , the atmospheric transport of NO_x to remote locations would lead to a more even distribution of NO_x , instead of hotspots in polluted regions close to emission sources. Atmospheric removal processes for ANs include oxidation by OH or O_3 (which may lead to a loss of the nitrate functionality), deposition to the earth's surface and photolysis. Additionally, partitioning into the aerosol phase is possible for large and multifunctional ANs (Perring et al., 2013). Alkyl-nitrates possessing no further functionality (e.g. double bonds or hydroxyl groups) can be unreactive and have long lifetimes (Talukdar et al., 1997). On the global average, RONO_2 has a lifetime of close to 3 hours (2.6 – 3 hours) with ~ 30% being lost by hydrolysis (Zare et al., 2018).

The formation of NO_z in the lower atmosphere reduces the NO_x lifetime and the partitioning of NO_y into NO_x and NO_z can provide information about the chemical history of an air-mass (Day et al., 2002; Wild et al., 2014). In regions impacted by biogenic emissions, the sources and sinks of ANs account for a large fraction of NO_x lost both during the day and night and thus control the lifetime of NO_x (Romer et al., 2016; Sobanski et al., 2017).

Laboratory experiments have shown that particulate nitrates (pNit) are formed at high yields in the atmospheric degradation of terpenoids in the presence of NO_x and play an important role in the formation and growth of secondary organic aerosol (SOA) (Ng et al., 2017; IUPAC, 2019). This has been confirmed in field studies, which provide evidence for the partitioning of organic nitrate to the aerosol phase both during day- and nighttime (Rollins et al., 2012; Fry et al., 2013; Palm et al., 2017) with formation of highly functionalised molecules and large contributions (up to 25%) of particulate organic nitrates to the total aerosol mass (Xu et al., 2015; Lee et al., 2016; Huang et al., 2019).

1.2 Detection of NO_x

Methods for the detection of NO and NO_2 include Chemiluminescence (CLD), Differential Optical Absorption Spectroscopy (DOAS), Laser Induced Fluorescence (LIF) and Cavity Ring-Down Spectroscopy (CRDS). A description and inter-comparison of these methods is given in Fuchs et al. (2010) and we restrict the following discussion to an outline of the basic principles. The CLD method detects NO by chemiluminescent emission in its reaction with O_3 ; detection of ambient NO_2 by CLD follows its catalytic or photolytic conversion to NO . The best CLD devices have detection limits for NO and NO_2 in single-digit pptv range (Beygi et al., 2011; Reed et al., 2016; Tadic et al., 2020). Detection of NO_2 via LIF involves photo-excitation in its visible absorption band at wavelengths > 400 nm and detection of fluorescent emission at wavelengths > 600 nm, with detection limits of the order of pptv achieved for an integration time of a few seconds (Day et al., 2002; Javed et al., 2019). The structured spectrum of NO_2 between ≈ 400 and 600 nm is used to detect light absorption by ambient NO_2 by DOAS, using either broadband light sources (long-path DOAS, over a few km pathlength) or natural sunlight (Platt et al., 1979; Leser et al., 2003; Pöhler et al., 2010; Merten et al., 2011).

The CRDS detection method for NO₂ also utilises its visible absorption spectrum, high sensitivity being achieved by achieving very long pathlengths for optical extinction in an optical resonator (see Sect. 2.1). Limits of detection for NO₂ with CRDS of < 20 pptv in 1 second integration time have been reported (Wild et al., 2014). NO can be detected as NO₂ following its oxidation by O₃ (R6) (Fuchs et al., 2009).

5 1.3 Detection of NO_y

The first NO_y measurements were based on the conversion of all reactive nitrogen trace gases (apart from NO) to NO on catalytic metal surfaces of gold at ~ 300-320 °C or of molybdenum oxide at ~ 350-400 °C (Fahey et al., 1985; Williams et al., 1998), with subsequent CLD detection of NO. Au converters were designed to exclude particulate nitrates, while MoO setups aimed at a response towards pNit (Williams et al., 1998). In recent years, the thermal decomposition of NO_z to NO₂ has been used to detect NO_z using inlets held at temperatures high enough (> 650-700 °C) to thermally dissociate the most strongly bound reactive nitrogen trace-gas, HNO₃, to NO₂ (Day et al., 2002; Rosen et al., 2004; Wooldridge et al., 2010; Perring et al., 2013; Wild et al., 2014) and/or using multiple inlets at intermediate temperatures (Paul et al., 2009; Paul and Osthoff, 2010; Sadanaga et al., 2016; Sobanski et al., 2016; Thieser et al., 2016). Subsequent to thermal decomposition, the NO₂ product can be detected using LIF (Day et al., 2002; Day et al., 2003; Rosen et al., 2004; Murphy et al., 2006; Wooldridge et al., 2010) or cavity enhanced absorption spectroscopy (Paul et al., 2009; Wild et al., 2014; Sadanaga et al., 2016; Sobanski et al., 2016; Thieser et al., 2016). These techniques are impacted to various degrees by secondary reactions at high temperatures including loss of NO₂ via recombination with α -carbonyl peroxy radicals or reaction with O-atoms (formed by the ~~pyrolysis~~ **thermolysis** of ambient O₃) and the generation of extra NO₂ from the oxidation of NO via reactions with peroxy radicals (Day et al., 2002; Sobanski et al., 2016; Thieser et al., 2016; Womack et al., 2017). Measures to reduce potential measurement artefacts and avoid excessive data correction include operation at low pressures (Day et al., 2002; Womack et al., 2017) and addition of surfaces to scavenge peroxy radicals (Sobanski et al., 2016). Nonetheless, data correction may still be necessary, which may involve laboratory characterisation and chemical simulation of the chemical reactions within the heated inlet (Sobanski et al., 2016; Thieser et al., 2016).

In this paper we present a two-channel TD-CRDS instrument for detection of NO_x, NO_y, NO_z and pNit which overcomes these limitations. **Compared to the setups described by Thieser et al. (2016) the following changes were implemented: (1) Addition of O₃ for NO_x detection; (2) higher oven temperature (to detect HNO₃) and location directly at the front of the inlet; and (3) use of a charcoal denuder for separate measurement of pNit and gas-phase NO_z. The addition of O₃ (after the TD-inlet) ensures that we detect NO as well as NO₂ and thus removes bias caused e.g. by the pyrolysis of O₃ and reactions of O(³P) which reduce NO₂ to NO.**

2 Experimental

Our TD-CRDS instrument consists of two identically constructed cavities to monitor NO₂ at 405 nm which are largely unchanged compared to those described by Thieser et al. (2016). In the present set-up, the two cavities are connected to three different inlets. One cavity monitors NO_x via an inlet at ambient temperature, the second samples air via either of two heated inlets (one equipped with a denuder, see below) and thereby monitors either NO_y or particle nitrate. A schematic diagram (not to scale) of the instrument is given in Fig. 1.

2.1 CRDS Operation principals

The optical resonator consists of two mirrors (1 m radius of curvature) with nominal 0.999965 reflectivity at 405 nm (Advanced Thin Films), which are mounted 70 cm apart. The cavity volumes are defined by Teflon (FEP) coated Duran glass tubes with an inner diameter of 10 mm.

Under normal operating conditions each cavity samples 3.0 L (STP) min⁻¹ (slm) of ambient air (where STP refers to 0°C and 1013 hPa). Additional purge flows (0.14 slm dry synthetic air) are introduced directly in front of each mirror to prevent surface degradation by atmospheric trace gases. The cavities are operated at pressures of 540 to 580 Torr (1 Torr = 1.333 hPa), resulting in residence time of ~1.2 s. 405 nm laser light (square-wave modulated at 1666 Hz and a 50% duty cycle) is provided by a laser diode (Laser Components), the emission of which is coupled into an optical fibre with a Y-piece for splitting into both cavities. Temperature and current control of the laser diode are achieved by a Thorlabs ITC 502 control unit. The laser emission spectrum is monitored continuously by coupling scattered light from one of the cavity mirrors into a 3648 pixel CCD-spectrograph (OMT, ~ 0.1 nm resolution).

The intensity of light exiting the cavity is measured with a photomultiplier (Hamamatsu Photonics), with ring-up and ring-down profiles recorded by a digital oscilloscope (PicoScope 3000). NO₂ mixing ratios are derived from the decay constant (k or k_0) describing the exponential decrease in light intensity after the laser has been switched off:

$$[\text{NO}_2] = \frac{l}{d} \cdot \frac{1}{\sigma c} (k - k_0), \quad (1)$$

where c is the speed of light, σ is the effective absorption cross-section of NO₂ over the emission spectrum of the laser (Vandaele et al., 2002) and k and k_0 are the decay constant with and without NO₂ present in the cavity, respectively. k_0 is thus defined by the mirror reflectivity and light scattering by the dry, synthetic air.

The ratio l/d accounts for the difference between the physical length of the cavity (l) and the effective optical path length (d) in which NO₂ is present, and for dilution effects. d is shorter than l due to the purge flows of zero air in front of the mirrors and a value of $l/d = 0.98 \pm 0.01$ was determined by adding a constant flow of NO₂ and varying the purge-gas flow rate (Schuster et al., 2009; Thieser et al., 2016). k_0 is typically determined every five minutes (for one minute) by overflowing the inlets with zero air from a commercial zero air generator (CAP 180, Fuhr GmbH) attached to a source of compressed ambient air. PTFE filters (47 mm diameter, 2 µm pore size) prevent aerosol particles entering the cavities. The filter's efficiency, tested with laboratory air containing 1.8×10^3 particles cm⁻³ and a CPC (TSI 3025 A), was > 98%.

Raw data sets (i.e. ring-down constants) undergo a few basic corrections before further analysis: 1) Interpolation of k_0 onto the k time-grid. The first three data points after switching from sampling to zeroing are discarded, to enable stabilisation of the zero signal. The remaining data points of each zero cycle are averaged. Finally, a linear interpolation between the averaged k_0 values is performed, allowing subtraction of k_0 for each individual data point. 2) Depending on conditions of flow, pressure and inlet set-up (see sections 2.2 and 2.3), changes in flow resistance between the zeroing and sampling periods result in slight changes in the cavity pressure. The resulting change in Rayleigh scattering of the 405 nm light owing to a pressure change of 6.5 Torr was found to be equivalent to a change of ca. 300 pptv in the NO₂ mixing ratio, which is in accordance with earlier experiments using previous versions of this instrumental setup (Thieser et al., 2016). We have also used an alternative setup, in which the inlet is overflowed with zero air added close to the tip of the inlet (downstream of the oven), which reduces the pressure difference, but has the disadvantage that hot air is blown out of the instrument when zeroing, which may interfere with co-located inlets. Addition of zero air upstream of the quartz inlets would remove this problem but increase the complexity of the inlet and potentially result in loss of sticky molecules such as HNO₃. 3) A further correction is associated with the difference in the Rayleigh scattering coefficient between dry air (during zeroing) and humid air (whilst taking ambient measurements). This effect was corrected using the H₂O scattering cross-sections reported by Thieser et al. (2016), leading e.g. to a correction of 116 pptv at 70% RH and 20 °C.

2.2 Detection of NO_x

In order to measure NO (which does not absorb at 405 nm), it is converted to NO₂ by reaction (R6) with an excess of ozone (O₃) which was generated by passing zero air over a Hg Pen-Ray lamp emitting at 185 nm, which was housed inside a glass vessel at ca. 980 torr pressure. The gas-stream containing O₃ is split up equally by critical orifices and directed into two identical reaction-volumes made of 88 cm long PFA tubing (1/2 inch outer diameter, residence time 1.05 s). The concentration of O₃ (monitored by a commercial monitor, Model 202, 2B Technologies) was optimised in laboratory experiments in which the efficiency of conversion of NO to NO₂ was varied by variation of the flow of air over the Pen-Ray lamp. The maximum concentration of NO₂ (corresponding to 96% of the NO in the gas bottle) was observed when the flow over the pen-ray lamp was between 60 and 80 cm³ (STP) min⁻¹ (hereafter sccm), which resulted in 19 ppmv O₃ in the reaction volumes. This result could be confirmed by numerical simulation (see Table S1) of the reactions involved in the formation and loss of NO₂ when NO reacts with O₃. According to the simulation, maximum conversion of NO to NO₂ during the 1.05 s residence time occurs between ca. 12 and 20 ppmv O₃. The conversion efficiency decreases at higher O₃ concentrations due to the formation of N₂O₅ and NO₃. The results from experiments to determine the optimum parameters for O₃ generation are summarised in Fig. S1. For NO₂, the performance of the instrument was first described by Thieser et al. (2016), who reports a measurement uncertainty of 6% + (20 pptv * RH/100) which is dominated by uncertainty in the effective cross section of NO₂ and the wavelength stability of the laser diode. The NO_x detection limit of 40 pptv (2σ, 1 minute average) for the present instrument (laboratory conditions) was derived from an Allan variance analysis and is worse than that reported by Thieser et al. (2016) (6 pptv at 40 s) due to degradation of the mirror reflectivity. Corrections applied to take into account humidity and pressure changes are discussed

in Sect. 2.1. The total uncertainty in NO_y will depend on the uncertainty in the conversion to NO_x of both gaseous and particulate nitrate and thus depends on the individual components of NO_y in the air sampled. For purely gaseous NO_y , the major problem is likely to be related to loss of sticky molecules at the inlet and we choose to quote a “worst case” uncertainty of 15%.

5 2.3 Thermal dissociation inlets: Detection of NO_y

The thermal dissociation inlets used to dissociate NO_y to NO_2 are quartz tubes housed in commercial furnaces (Carbolite, MTF 10/15/130). The oven temperature was regulated with a custom made electronic module, which enabled spatial separation between the heating elements and insulation and the control electronics. The distance between the heated section of the quartz tubes and the point at which air was taken into the inlet was kept short (ca. 30 cm) in order to minimise losses of trace gases with a high affinity for surfaces, especially HNO_3 (Neuman et al., 1999). Experiments characterising the thermal conversion of various trace gases to NO_2 are described in Sect. 3.1. An electronic, PTFE 3-way valve (Neptune Research, Inc., type 648T032, orifice diameter 4 mm) under software control switches between the two heated inlets, one of which is equipped with a denuder. Memory effects on the valves surfaces were not observed for NO_2 . Bypassing the valve under normal sampling conditions led to an 0.6 Torr pressure change. The sampling flow through both heated inlets is 3.0 slm. When sampling ambient air via the denuder we expect to remove all gas phase NO_y components and thus measure only particulate nitrate (pNit). Experiments to characterise the transmission of the denuder for particles and various trace gases are presented in Sect. 3.3.

2.4 Active carbon denuder

The active carbon denuder (DynamicAQS) has a honeycomb structure with 225 quadratic channels (1mm \times 1 mm) of length 10 cm in a cylindrical form (diameter 3 cm) which is housed inside an aluminium casing with $\frac{1}{2}$ inch connections (see Fig. 1). The geometric surface area of the denuder is $\sim 45 \text{ cm}^2$. Assuming a specific surface area for activated carbon of $1000 \text{ m}^2\text{g}^{-1}$ (Atsuko et al., 1996), we calculate a BET (Brunauer-Emmett-Teller, Brunauer et al. (1938) surface area in the order of 10^8 cm^2 .

2.5 Chemicals

A stock, liquid sample of PAN in n-tridecane (98+%, Alfa Aesar) was synthesized according to the procedures described by Gaffney et al. (1984) and Talukdar et al. (1995). Samples of lower concentration (as used in the experiments described below) were produced by diluting the original sample with additional n-tridecane. Acetone (> 99%), isopropyl nitrate (> 98.0%) and (R)-(+)-limonene (97%) were obtained from Sigma-Aldrich. An ammonia permeation source (324 ng/min) was supplied by VICI Metronics. Methanol (> 99.9%) was acquired from Merck, isoprene (98%, stabilised) from Acros Organics and ethanol from Martin und Werner Mundo oHG. Both nitric acid (65%) and β -pinene (pure) were obtained from Roth. N_2O_5 crystals were synthesized according to Davidson et al. (1978), by reacting NO (5%) with excess O_3 in a glass reactor. O_3 was produced via electrical discharge through O_2 using a commercial ozone generator (Ozomat Com, Anseros). The crystals were trapped and stored at $-78 \text{ }^\circ\text{C}$ in dry-ice and ethanol.

3 Results and discussion

3.1 Trace-gas thermograms

The fractional conversion of NO_z to NO_2 in the TD-inlets was investigated in a series of experiments in which constant flows of various NO_z trace-gases were passed through the heated-inlet (bypassing the denuder) while the temperature was varied and NO_2 was monitored. NO_x impurity levels were determined either via the simultaneous operation of the NO_x channel or via the NO_y channel mixing ratio at room temperature, before and after heating the inlet. By inserting a thermocouple into the middle part of the heated section under normal sampling conditions we were able to show that the temperature of the gas was $\approx 80^\circ\text{C}$ lower than that indicated by the oven's internal temperature sensor in the 200-300 $^\circ\text{C}$ temperature range and about 40 $^\circ\text{C}$ lower at a set temperature of 600 $^\circ\text{C}$ (see Fig. S3a)). We were unable to measure the temperatures of the gas stream at oven temperatures above about 600 $^\circ\text{C}$ and throughout the manuscript we refer only to the temperature indicated by the internal sensor of the oven.

We show below that the thermograms (plots of fractional dissociation of NO_z to NO_x versus temperature) which we measure with this instrument are broader and shifted in temperature compared to other examples found in the literature including those from this laboratory. As this instrument is built for measurement of NO_y and not intended for separate measurement of e.g. PNs, ANs and HNO_3 , overlap of the individual thermograms does not represent a problem.

3.1.1 PAN

A stream of 200 sccm synthetic air was used to elute a constant supply of gaseous PAN from its solution (held at a constant temperature of 0 $^\circ\text{C}$ in a glass vessel) into the CRDS inlet. The thermogram is presented in Fig. 2, the absolute NO_2 mixing ratios are depicted in Fig. S2a). In this experiment the maximum amount of NO_2 observed (at temperatures $> 400^\circ\text{C}$) was 2.2 ppbv. At temperatures $< 100^\circ\text{C}$, there was no measureable thermal decomposition of PAN to NO_2 . Increasing the temperature from 100 $^\circ\text{C}$ to 300 $^\circ\text{C}$ results in a sharp increase in NO_2 which flattens off at temperature $> 380^\circ\text{C}$. We conclude that PAN is stoichiometrically converted to NO_2 at temperatures above 400 $^\circ\text{C}$ in our oven. The steepest part of the isotherm at $\sim 200^\circ\text{C}$, i.e. 50% conversion of PAN to NO_2 , is therefore shifted by ca. 80 $^\circ\text{C}$ compared to those reported in the literature by Wild et al. (2014), Thieser et al. (2016) and Sobanski et al. (2016). This is a consistent feature of our TD-ovens and is related to the short time available for thermal decomposition (see below) and a significantly lower gas-temperature than indicated by the oven's internal temperature sensor.

3.1.2 Isopropyl nitrate

A 10 L stainless-steel canister containing 10.3 ppmv of isopropyl nitrate (iPN) at a pressure of 4 bar N_2 was prepared using a freshly vacuum-distilled liquid sample using standard manometric methods. NO_x impurities were ~ 4.7 ppbv, though we note that diluted iPN stored in stainless-steel canisters for periods of several weeks degrades to form NO_2 and HNO_3 .

The thermogram is displayed in Fig. 2, the absolute concentrations in Fig. S2b). Based on the mixing ratio of iPN in the canister and the dilution flows, 10.7 ppbv represents $(101 \pm 11)\%$ conversion. The shaded area around the expected iPN mixing ratio in Fig. S2b) signifies the uncertainty of this value, based on propagation of the errors during the manometric and dilution procedures (2% for flow rates, 5% for pressures measured with digital pressure gauges and 10% for the last dilution step using the analog pressure gauge of the canister).

Between 550 and 850 °C we observe a weak increase in NO₂ from 10.7 to 11.2 ppbv, which is likely due to small amounts of HNO₃ in the sample. For iPN, the temperature at 50% conversion is 50 °C higher than those reported by Thieser et al. (2016) and Sobanski et al. (2016). Wild et al. (2014) employed a gaseous mixture of different alkyl nitrates and also observed a broad thermogram, with an initial increase in NO₂ (up to 80% conversion) for temperatures < 300 °C, followed by a slower increase up to 800 °C. The alkyl nitrates thermogram of Wild et al. (2014) has been included into Fig. S2b) to illustrate this behaviour and to facilitate direct comparison.

3.1.3 HNO₃

A custom-made permeation source was used to provide a constant, known flow of HNO₃ (with ~ 8% NO_x impurity) to the TD-CRDS inlet. The permeation source consisted of a length (\approx 1m) of PFA tubing immersed in 66% HNO₃ solution held at 50 °C through which 100 sccm of dry, zero-air was passed. The concentration of HNO₃ and thus its permeation rate, $(1.62 \pm 0.2) \times 10^{-4}$ sccm, was derived by measuring the optical extinction of HNO₃ at 185 nm using the absorption cross section of Dulitz et al. (2018). The uncertainty is related to uncertainty in the absorption cross-section and the reproducibility of the output. The HNO₃ thermogram (Fig. 2 and Fig. S2c)) has a plateau at temperatures above \approx 800 °C. In the plateau region of Fig. 2, the HNO₃ mixing ratio measured is 13.0 ± 0.8 ppb, which (within combined uncertainties) is in agreement with the expected value (15.2 ± 1.98 ppbv) calculated from the permeation rate and uncertainty in the dilution factor. We cannot rule out some loss of HNO₃ in the tubing connecting the permeation source to the TD-CRDS, through previous studies have shown that irreversible losses are ~ of 5% or less under dry conditions (Neuman et al., 1999). We note that inlet loss of HNO₃ is minimized under ambient sampling conditions as only a short section (\sim 20 cm) quartz tubing at ambient temperature is upstream of the heated section in which HNO₃ is converted to NO₂. Our observations are thus in accord with previous studies that found complete conversion of HNO₃ to NO₂ in similar set-ups (Day et al., 2002; Di Carlo et al., 2013; Wild et al., 2014; Womack et al., 2017).

3.1.4 N₂O₅

A sample of N₂O₅ was prepared by flowing 80 sccm of synthetic air over N₂O₅ crystals, kept at -70 °C, with further dilution with 20 slm synthetic air. An 8.5 cm long Nylon tube was used to reduce HNO₃ impurity. Two distinct dissociation steps can be observed in Fig. 2, the first between 50 °C and 185 °C (in which NO₂ increases to 4.2 ppbv, see Fig. S2d)) is due to the dissociation of N₂O₅ to NO₂ + NO₃. In the second step, in which NO₃ is dissociated to NO_x between 450 °C and 800 °C, the NO₂ mixing ratio was 9.2 ppbv. As the amount of N₂O₅ derived from the first dissociation step was in accord with simultaneous

measurements of N_2O_5 using a further TD-CRDS set-up (Sobanski et al., 2016) we conclude that some HNO_3 was present in the sample, presumably the result of N_2O_5 hydrolysis. Our thermogram is similar to that reported by Womack et al. (2017) who also observed two steps, the first with a plateau at $T > 100$ °C and the second at $T > 650$ °C. The shift in temperature (100-150 °C) compared to our results is rationalised in Sect. 3.1.8.

5 3.1.5 HONO

Gaseous HONO was produced by flowing HCl in air (22 ppbv, relative humidity RH ca. 50 %), over a bed of continuously stirred sodium nitrate crystals (Wollenhaupt et al., 2000). In our setup, the thermal dissociation of HONO to NO starts at ~ 400 °C and reaches a plateau (6.2 ppbv) between ca. 800 °C and 850 °C (Fig. 2). We did not have access to independent instrumentation to characterise the concentrations of HONO and potential impurities generated using this method. Previous investigations report that HONO thermally dissociates between 450 and 650 °C (Perez et al., 2007), and between 200 and 700 °C (Wild et al., 2014). The reasons for such large divergence in the positions and widths of the thermograms may be partially related to the presence of impurities in the HONO samples used, though the details of the ovens used to thermally dissociated HONO also play an important role as described in see Sect. 3.1.8.

3.1.6 ClNO₂

15 ClNO₂ was generated by passing Cl₂ (33 ppbv in air) over sodium nitrate at room temperature. The thermogram, depicted in Fig. 2 has two steps, one with an apparent plateau at ~ 500 °C and a second at ~ 800 °C. The lower temperature plateau in which ClNO₂ dissociates to NO₂ corresponds to that reported previously (Thaler et al., 2011; Sobanski et al., 2016; Thieser et al., 2016). The observation of further NO₂ formation at higher temperature is consistent with the observations of Wild et al. (2014). We hypothesize, that the second dissociation step might be associated with the presence of ClNO which dissociates to NO
20 (and would therefore not have been detected by instruments that monitor NO₂ rather than NO_x). Even at temperatures > 850 °C, we still see an increase in NO₂ signal. However, as ClNO is not considered to be an important atmospheric trace gas, this has no repercussions for deployment of the instrument.

3.1.7 NH₄NO₃ and NaNO₃ particles

NH₄NO₃ and NaNO₃ particles were generated from an aqueous solution (ca. 1 g in 500 mL deionized water) using an atomizer
25 (TSI 3076). The particles were dried prior to size selection (DMA, TSI 3080), diluted in a total flow of 6 slm synthetic air which was split between a CPC and the heated TD-CRDS inlet (after further dilution). The relative thermogram for NH₄NO₃ is displayed in Fig. 2 and, similar to HNO₃, displays a plateau region at temperatures above 830 °C. The shift in the thermogram when comparing HNO₃ and NH₄NO₃ (which we expect to detect in a two-step process in which NH₄NO₃ first decomposes to HNO₃) may be related to the time required to fully thermally decompose particles (e.g. of 200 nm diameter) containing several
30 million molecules. Particle numbers (in cm⁻³) detected by the CPC were converted to molar-mixing ratios via the diameters and densities of the dry particles (1.72 g cm⁻³ for NH₄NO₃, and 2.26 g cm⁻³ for NaNO₃). The fraction of NH₄NO₃ detected as

NO_x following passage through the oven is illustrated in Fig. S5 which indicates values between $\approx 60\%$ and 120% depending on particle size. The total uncertainty in the concentration was estimated as 41% , which includes 10% uncertainty in the particle diameter (based on measured size distributions of Latex calibration particles), 20% uncertainty in the particle number (including the error in the multiple charge correction) and 10% uncertainty in the density, due to possible differences between
5 single crystal and bulk density. As the particle mass scales to the third-order with the particle diameter, the correction for double charged particles introduces a large uncertainty in the calculated mixing ratios, the effect being largest in the size range between 100 to 150 nm, which probably explains the lower NH₄NO₃ detection efficiencies in this range. We consider the data obtained at 200 nm to be the most reliable and conclude that, similar to other TD-instruments (Womack et al., 2017; Garner et al., 2020), ours also detects NH₄NO₃ particles as NO₂ with close to 100% efficiency. In contrast, our experiments using NaNO₃
10 resulted in much smaller NO_x concentrations despite identical experimental conditions in back-to-back experiments and resulted in detection efficiencies of close to 25% . While the inefficient detection of NaNO₃ is consistent with a previous reports suggesting that NaNO₃ would not be detected in TD-inlets (Womack et al., 2017) it contrasts strongly with the very recent result of Garner et al. (2020) who observe quantitative conversion of NaNO₃ to NO₂ at 600 °C. The difference may be related to residence times in the heated section of the inlet.

15 3.1.8 Summary of thermograms

The thermograms obtained by the present instrument deviate from others reported in the literature, the temperatures required for 50% dissociation being generally higher by e.g. 80 °C for PAN, 50 °C for iPN and 150 °C for HNO₃, respectively (Day et al., 2002; Wild et al., 2014; Sobanski et al., 2016; Thieser et al., 2016; Womack et al., 2017). This lack of agreement with
20 other setups is not unexpected as the degree of dissociation of a trace gas at any temperature depends not only on the temperature but also on the time over which the molecule is exposed to that temperature (Womack et al., 2017). To illustrate this, based on rate coefficients (related to bond-dissociation energies, BDE) for the thermal dissociation of PAN (Bridier et al., 1991), iPN (Barker et al., 1977), HNO₃ (Glänzer and Troe, 1974), N₂O₅ (IUPAC, 2019), ClNO₂ (Baulch et al., 1981), and HONO (Tsang and Herron, 1991), we calculated the theoretical 50% conversion temperature for each molecule as a function of residence time inside the oven (see Fig. S3b)). At short residence times the dependence on temperature is very steep
25 (especially for large BDEs) which partially explains the differences between our short heated section inlet and longer ones. However, in practise, we know neither the precise average temperature of the gas at the centre of the oven, nor can we characterise the axial and radial gradients in temperature in the quartz tubes so that calculations of fractional dissociation (or complete thermograms) based on bond-dissociation energies are at best only a rough guide. We note that use of different flows, oven diameters and operational pressures will strongly affect heat transfer from the oven walls to the gas, so that reporting the
30 temperature of the external oven-wall (as done here and in all reports in the literature) to some extent precludes comparison between different setups. The width of the thermograms (i.e. the temperature difference between e.g. 10% and 90% dissociation) will also depend on details of axial and radial temperature gradients in the tubing located within the oven and also in the downstream section of tubing, which represents a transition regime between oven and room temperature. The impact

of temperature gradients inside the quartz tube was explored by calculating the HNO₃ thermogram using an Arrhenius expression for its thermal dissociation and the gas residence time within the quartz tube. First we assumed that all HNO₃ molecules experience the same temperature and then compared this to the situation in which 20% of the HNO₃ molecules are 80 °C lower in, and 20% are 80 °C higher in temperatures. The resultant thermograms are displayed in Fig S3c) and indicate that the presence of temperature gradients results in an increase in the width of the thermogram from 250 °C to 350 °C. The thermograms we report here serve only to determine the temperature needed to ensure ~~complete~~ maximum conversion of each trace gas to NO₂. This is achieved in the present setup with a temperature of 850 °C. Where possible, we have verified that operation at the plateau of the thermogram resulted in quantitative conversion of the traces gases and particles studied, with one exception, NaNO₃ particles. We further note that, in an instrument designed only to measure NO_y, there is no need to ensure separation (in temperature) of the thermograms for different classes of molecules.

3.1.9 Detection of NH₃

As described previously (Wild et al., 2014; Womack et al., 2017) ammonia represents a potential interference in NO_y measurements. In order to quantify this interference, we measured NO₂ formation in air containing 131 ppbv NH₃ delivered by a calibrated permeation source (VICI METRONICS, permeation rate 324 ng min⁻¹ at 45 °C). The results are summarised in Fig. 2. In NH₃ – air mixtures, we observe a small NO₂ signal, increasing at first slowly and then (from ≈ 700 °C) rapidly with temperature; the amount of NO₂ observed at 850 °C corresponds to a fractional conversion of NH₃ to NO₂ of 0.006 ± 0.002. This result is in broad agreement with Wild et al. (2014), who found a conversion efficiency of < 0.01 at 700 °C. In experiments with NH₃ in zero-air with relative humidities of 17%, 31% and 53% we were unable to observe conversion of NH₃ to NO₂, again consistent with humidity related suppression of NO₂ formation observed by Wild et al. (2014). In additional experiments, we investigated the potential influence of ozone on the NH₃ to NO₂ conversion efficiency in zero-air containing O₃. The addition of O₃ results in a significant increase in NO₂ with a linear dependence on the O₃ mixing ratio (Fig. 3) with up to 11.4% conversion of NH₃ to NO₂ at 200 ppbv O₃. This was not reduced measurably by the addition of water vapour to the air / O₃ mixture. In further experiments we spiked air with the head-space of various organic liquids (acetone, methanol, ethanol, beta-pinene, limonene and isoprene). The gas-phase mixing ratios of the organic trace gases were unknown but in each case the formation of NO₂ was suppressed or completely stopped. A more quantitative investigation was carried out using a known concentration (1 ppmv gas bottle) of isoprene. We found that addition of 30 ppbv isoprene to zero-air (containing 330 ppbv O₃) did not significantly reduce the NH₃-to-NO₂ conversion efficiency under dry conditions, but reduced it by a factor of two when the RH was increased to 50%.

A tentative chemical mechanism, based partially on Womack et al. (2017) to explain the formation of NO₂ from NH₃ and O₃ at high temperatures and the processes that suppress it is given in reactions (R11 to R15). In this scheme, the oxidation of NH₃ is initiated and propagated by O(³P), formed from the thermal dissociation of O₃ (Peukert et al., 2013). This leads to formation of NO and HNO (R13a and R13b), both of which can be oxidised to NO₂ (R14 and R15). Forward and reverse rate coefficients for reaction (R11) indicate that O₃ is converted almost stoichiometrically to O(³P) in the ≈ 10 ms reaction time in the heated

inlet. The rate constants (at 1123 K) for the subsequent reactions involving O(³P) are: $k_{12} = 4.4 \times 10^{-13} \text{ cm}^3 \text{ molec}^{-1} \text{ s}^{-1}$ $k_{13a} = 8.3 \times 10^{-12} \text{ cm}^3 \text{ molec}^{-1} \text{ s}^{-1}$ and $k_{13b} = 7.5 \times 10^{-11} \text{ cm}^3 \text{ molec}^{-1} \text{ s}^{-1}$ (Cohen and Westberg, 1991). Reaction (R12) converts 0.3% of the initial NH₃ molecules to NH₂ within 10 ms (at 100 ppbv O₃ and 1123 K).



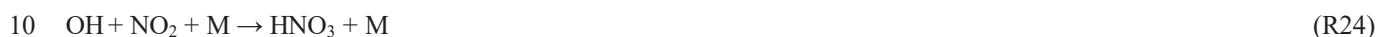
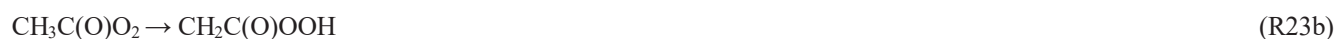
The experimental results obtained in zero-air indicate that reactions involving O(³P) from O₃ ~~pyrolysis~~ ~~thermolysis~~ can result in the conversion of NH₃ to NO and NO₂. These results could however not be reproduced when adding NH₃ to ambient air sampled from outside of the building. In this case, the addition of NH₃ (at 50-60 ppbv O₃) did not result in a measureable increase in NO₂, which was in accord with the observations of Womack et al. (2017). The scavenging of NH₂ radicals and O(³P) by both volatile organic compounds and H₂O provides a likely explanation for this. Womack et al. (2017) also found that addition of 100 ppbv CO can reduce the conversion of NH₃ to NO_x.

In summary, our experiments indicate that the conversion of NH₃ to NO₂ is suppressed in ambient air samples, or in synthetic air with added VOCs and water. The ambient air used in these experiments was from an urban and polluted environment (typical NO_x levels between 10 and 50 ppbv, see Sect. 4.2). As high levels of atmospheric NH₃ are associated with agricultural activity (Langford et al., 1992; Schlesinger and Hartley, 1992) and are often accompanied by high NO_x and VOC levels, the NH₃ interference under these conditions is most likely to be small compared to ambient NO_z levels. Long term measurements of NH₃ have additionally found a positive correlation between NH₃ concentrations and ambient temperature (Yamamoto et al., 1988; Wang et al., 2015; Yao and Zhang, 2016), the latter promoting the presence of high levels of biogenic VOCs, such as isoprene (Tingey et al., 1979), which would also help to minimize the NH₃-related interference.

25 3.2 Bias caused by secondary reactions in the TD-ovens

Thermal dissociation techniques coupled to CRD-systems for measurement of organic nitrates suffer bias to different degrees owing to reactions of organic peroxy radicals with NO and NO₂ (Sobanski et al., 2016; Thieser et al., 2016). According to previous studies (Day et al., 2002; Rosen et al., 2004; Thieser et al., 2016), in experiments using iPN at an oven temperature of 450 °C, an overestimation of ANs in the presence of NO is caused by reactions of the initially formed alkoxy radical, C₃H₇O, which results in the formation of both HO₂ and CH₃O₂ (R16-R21).





In order to investigate the potential bias in the measurement of ANs under the present experimental conditions, a set of experiments was conducted in which NO (up to 12 ppbv) was added to various amounts of iPN. The NO mixing ratio was determined by modulating the addition of O₃. The results (Fig. 4a)), show that NO₂ derived from the thermal decomposition of iPN increases with the amount of NO added and results in overestimation (factor of ~1.6) at 12 ppbv NO, which is consistent with the observations by Thieser et al. (2016). This disappears when 19 ppmv ozone is added in front of the cavity so that NO_x rather than NO₂ is measured (blue data points). This is readily explained by the compensation of the additional NO₂ formed via reactions of NO with RO₂ by an equal loss in NO, which is only detected when introducing O₃. This is illustrated graphically in Fig. S4.

20 We also explored the potential for bias caused by the recombination of CH₃C(O)O₂ and NO₂ ~~when measuring PAN~~ (reaction R22b), following the thermal decomposition of PAN (reaction R22a). Thieser et al. (2016) reported that PAN was underestimated by a factor 0.45 when adding 10 ppbv NO₂ to an air sample containing PAN at 200 °C. This behaviour was not apparent at 450 °C, which is related to the decomposition (reaction R23a) or isomerisation (reaction R23b) of CH₃C(O)O₂ at the higher temperature. The results of a similar experiment with our 850 °C inlet are presented in Fig. 4b). In this plot, the measured NO_z relative to the input PAN is plotted versus the mixing ratio of added NO₂. For PAN concentrations from 1.5-2.2 ppbv no effect was observed for NO₂ concentrations of up to 10 ppbv. This is consistent with the reaction scheme presented by Thieser et al. (2016) at 450 °C.

A potential source of bias when measuring HNO₃ includes its reformation via the reaction of OH and NO₂ (reaction R24). Compared to the RO and RO₂ radicals formed in the thermal dissociation of PNs and ANs, OH exhibits a higher affinity for surfaces and is likely to be efficiently removed at the oven wall. Day et al. (2002) estimated that wall losses are the dominant OH sink and that the resulting underestimation of HNO₃ would be < 2%, for NO_y levels < 5 ppbv. At our oven temperature, the diffusion coefficient for OH (D_{OH}) can be calculated according to Tang et al. (2014):

$$D_{\text{OH}}(1123 \text{ K}) = D_{\text{OH}}(296 \text{ K}) \cdot \frac{296^{-1.75}}{T} \quad (2)$$

Using an average of the literature values for D_{OH} at room temperature from Ivanov et al. (2007) (165 Torr $\text{cm}^2 \text{s}^{-1}$) and Bertram et al. (2001) (192 Torr $\text{cm}^2 \text{s}^{-1}$), a value of $D_{OH}(1123 \text{ K}) = 1841 \text{ Torr cm}^2 \text{s}^{-1}$ was derived. The maximum rate constant for OH wall loss (assuming laminar flow) can subsequently be approximated according to Zasytkin et al. (1997):

$$k_{\text{wall}} = \frac{D_{OH} \cdot 3.66}{r^2 \cdot p}, \quad (3)$$

5 With the radius of the oven quartz tube r (0.45 cm) and the pressure p (760 torr), the maximum value of k_{wall} is 44 s^{-1} . The first-order loss rate coefficient for reaction of OH with NO_2 is given by $k_{(\text{OH}+\text{NO}_2)}[\text{NO}_2]$, where $k_{(\text{OH}+\text{NO}_2)}$ is the rate coefficient for reaction between OH and NO_2 at 1123 K ($\sim 5 \times 10^{-14} \text{ cm}^3 \text{ molec}^{-1} \text{ s}^{-1}$ (IUPAC, 2019) and $[\text{NO}_2] = 6.5 \times 10^{10} \text{ molecule cm}^{-3}$ the concentration of 10 ppb NO_2 at the pressure and temperature of the oven. The first-order loss rate of OH via reaction with NO_2 is then $3 \times 10^{-3} \text{ s}^{-1}$. Clearly, the efficiency of uptake of OH to the wall would have to be very low in order to reduce the
 10 maximum value of 44 s^{-1} to values that are comparable to reaction with NO_2 , which is very unlikely. We conclude that reformation of HNO_3 via reaction (R24) will not bias measurements of HNO_3 with the present set-up.

3.3 Denuder characterisation

The efficiency of removal of NO_y trace gases and transmission of submicron particles was determined in a series of experiments, which are described below.

15 3.3.1 Transmission of ammonium nitrate particles (10 – 414 nm)

In order to characterise the transmission of the denuder for particles of different diameter a constant flow of particles was generated by passing 3.3 slm of nitrogen through an atomizer (TSI 3076) containing an aqueous solution of ammonium nitrate. The flow rate (3.3 slm) was matched to the typical sampling flow through the denuder. 0.28 slm of the flow was sampled into an SMPS/CPC system (TSI 3080 and TSI 3025A) to measure the number density and size distribution (10 – 414 nm) of the
 20 ammonium nitrate particles. The flow was delivered either directly to the SMPS/CPC via straight metal tubing (length 27 cm, inner diameter 0.9 cm), for which we assume 100% particle transmission, or via the denuder. The ratio of the particle numbers in each size bin thus represents the size-dependent denuder transmission. As shown in Fig. 5, the transmission of the denuder is $> 80\%$ for particles between 30 and 400 nm diameter. As expected, some diffusive loss is observed for particles $< 20 \text{ nm}$ diameter and loss due to impaction / settling is observed for particles $> 300 \text{ nm}$. The particle transmission T as a function of
 25 particle diameter d can be represented by the following empirical expression:

$$T(\%) = \frac{d(\text{nm}) - 5.79}{0.035 + 0.010 \cdot (d - 5.79) + 1.78 \cdot 10^{-6} \cdot (d - 5.79)^2} \quad (4)$$

The particle transmission through the denuder channels was also calculated using the *Particle Loss Calculator (PLC)* developed by von der Weiden et al. (2009). The results of this calculation are also plotted in Fig. 5. The observed loss of
 30 particles smaller than 40 nm are not replicated by the *PLC*, which was developed for cylindrical piping and not the square honeycomb shape of the denuder and also does not take into account losses due to impact at the finite surface area which the

gas/particle flow is exposed to at the entrance to the honeycomb. The PLC does a better job in predicting a reduction in transmission for the largest particles which we measured and indicates a transmission of 74% at 1 μm and 45% at 2 μm . In certain environments, nitrate associated with coarse mode particles thus represents a potential bias for TD-CRDS measurements of NO_y .

5 3.3.2 Efficiency of removal of NO_y trace gases.

The efficiency of removal of trace gases in the denuder under typical flow conditions (3.3 slm) was investigated for NO , NO_2 , PAN, iPN, HONO, N_2O_5 , ClNO_2 and HNO_3 as representative NO_y species. The efficiency of removal of each trace gas (generally present at 5-40 ppbv) was determined by measuring its relative concentration when flowing through the denuder (pNit-channel) and when bypassing the denuder (NO_y channel). The results (Fig. 6) indicate that, in dry air, all of these trace
10 gases were removed with an efficiency of close to 100%. However, when the main dilution flow was humidified significant, RH-dependent breakthrough of NO was observed, with only 60% stripped from the gas-phase at RH close to 100%. HONO was removed with 85% efficiency at an RH of 46%, and ClNO_2 with 75% efficiency at an RH of 60%. In contrast, humidification had only a marginal effect on the scrubbing efficiency for NO_2 , iPN and HNO_3 for which an efficiency of $\geq 95\%$ was observed. The precise values from which the removal efficiencies in Fig. 6 were determined are listed in Table S2.

15 In further experiments, we examined the potential for re-release of NO_y that had previously been stored in the activated carbon substrate of the denuder. In these experiments, in which either NO_x or NO_y was continuously monitored, the denuder was exposed to a flow of 9.5 ppm iPN in dry nitrogen for 90 minutes during which 2.30×10^{17} molecules of iPN were stripped from the gas phase and deposited onto the denuder. This exposure is equivalent to a month-long exposure to 20 ppb of iPN. The air passing through the denuder was subsequently humidified to RH = 65%. The results (Fig. 7a)) indicate a high initial
20 (11:40 – 11:50) rate of release of NO_x under humid conditions (resulting in a maximum mixing ratio of 2 ppbv at 11:45). At 11:50, humidification of the air was stopped and the rate of release of NO_x dropped gradually towards zero. During a second period, in which the air was again humidified (from 11:50 on), NO_x was released from the denuder, albeit at a lower rate than during the first humidification. From 12:25 onwards, the oven behind the denuder was heated to 850 $^\circ\text{C}$ so that NO_y was added. No significant increase in NO_2 was observed indicating that the trace-gas(es) species released from the denuder surface upon
25 humidification are predominantly NO_x . During this experiment, 2.55×10^{15} molecules of NO_x desorbed from the denuder, indicating that the major fraction of iPN molecules remained stored on the denuder surface upon humidification.

Similar denuder exposure experiments were performed with HNO_3 and NO_2 . For HNO_3 , no evidence for desorption of NO_x or NO_y during exposure to humidified air was observed, whereas NO_2 exhibited a similar behaviour to iPN (Fig. 7b)). After
30 loading the denuder with 5 sccm from a 0.831 ppm NO_2 gas bottle for 4.8 days (a total of 7.60×10^{17} molecules were deposited as derived from the flow rate, the exposure time and the gas bottle mixing ratio), the effect of passing humidified air through the denuder was to release NO_x , which was observed at concentrations up to ≈ 39 ppbv. While the relative humidity was kept constant at close to 100%, the NO_x released decreased over time so that after 30 minutes, 3.2 ppbv NO_x could still be detected. By switching the O_3 source off (at $\approx 10:45$) the NO_2 measured went to \approx zero indicating that predominantly NO was released

(and not NO₂). Integrating these results over time yielded a value of 1.63×10^{16} molecules desorbed NO from the denuder surface in humid air. **Qualitatively similar results, i.e. humidity induced formation and release of NO_x from the denuder, were observed when the denuder was exposed for periods of weeks to variable levels of NO_x (i.e. up to 20 ppbv) under dry conditions.**

5 Clearly, adsorption of water molecules onto the denuder surface can initiate / catalyse chemical transformation at the surface than convert stored NO_z into forms than can desorb and be detected as NO_x. To further our understanding of underlying processes that occur upon humidification, a series of experiments were conducted to examine the adsorption of water on the denuder. In these experiments the denuder was first dried by exposing it to dry air for several hours until the relative humidity of the air exiting the denuder was close to zero. Subsequently, humidified air was passed through the denuder and the RH of
10 air exiting it was continuously monitored. The results of an experiment in which the air was humidified to 68% are shown in Fig. 8a). After 77 minutes of exposure to this humidity, the RH of the air exiting the denuder acquired a maximum value of 64%. After switching back to dry synthetic air (at 09:37 UTC), ~60 minutes passed before the RH dropped to values close to zero. In this period, the RH did not decrease monotonically, the rate of change of relative humidity exiting the denuder revealing a number of discreet steps. Figure 8b) plots the derivatives (dRH/dt) of the drying phases of a series of experiments
15 in which the initial RH was varied between 47 and 75%. A similar pattern emerges for each experiment with the greatest desorption rates occurring at the beginning of the drying phase followed by a minimum in the desorption rate and a second maximum (at $\approx 15\%$ relative humidity). This behaviour is a clear indication that H₂O is bound to more than one chemically or physically distinct surface sites on the activated-activated carbon.

By measuring the change in RH of the air flowing into and out of the denuder we can derive an equilibrium adsorption isotherm
20 for H₂O at the active carbon surface. An example is given in Fig. 9 where it is also compared to a literature isotherm for adsorption of water vapour on activated carbon fibre (Kim et al., 2008). The data of Kim et al. (2008) have been scaled, by matching the number of adsorbed water molecules at 65.9% RH to our observed value at 67.2% RH. The exposure of carbonaceous surfaces to inert gases at high temperatures (2000 °C) reduces the capacity for water uptake, whereas functionalising the carbon surface with oxygen containing groups (e.g. from HNO₃) enhances the water adsorption capacity
25 (Dubinin et al., 1982; Barton and Koresh, 1983; Liu et al., 2017). In our experiments, the uptake of gas-phase NO_y is thus expected to generate oxygenated sites on our denuder surface, which in turn will influence water uptake and thus further trace-gas accommodation.

The chemistry leading to the formation of gas-phase NO_x from NO_y trace-gases adsorbed at the denuder surface under humid conditions cannot be elucidated in detail with our experimental setup. However, a strong humidity dependence in the
30 heterogeneous generation of HONO and NO from NO₂ adsorbed on soot particles has been reported (Kalberer et al., 1999; Kleffmann et al., 1999). Formation of HONO from NO_x has also been observed on wet aerosol and ground surfaces in field studies (Lammel and Perner, 1988; Notholt et al., 1992). Previous investigations report the adsorption of NO₂ on activated carbon at ambient or close to ambient temperatures (30-50 °C), followed by its reduction to NO, with the simultaneous oxidation of the carbon surface (Shirahama et al., 2002; Zhang et al., 2008; Gao et al., 2011). These results are consistent with

our observation of e.g. conversion of NO_2 to NO at the denuder surface under humid conditions. In our experiments, we observed that NO_2 was converted to NO (rather than HONO) at the denuder surface. It is possible that the initial step is formation of HONO (e.g. by the surface catalysed hydrolysis of NO_2 or iPN) which undergoes further reduction on the surface to NO . Release of HONO and NO has also been observed from soil, after the nitrification of $\text{NH}_3/\text{NH}_4^+$ or the reduction of NO_3^- (Su et al., 2011; Pilegaard, 2013; Meusel et al., 2018). Oswald et al. (2013) found comparable HONO and NO emission fluxes from non-acidic soils, providing another example of heterogeneous formation of HONO from other atmospheric nitrogen species, followed by the gas phase release of NO .

We conclude that the use of this denuder type (and assumption of complete removal of gaseous NO_y) may potentially result in a positive bias in measurements of particle nitrate owing to variable breakthrough and release of NO_x (dependent on the historical exposure of the denuder and relative humidity). Our findings may be applicable (at least in a qualitative sense) to similar denuders using activated carbon surfaces, and careful characterisation of the capacity to adsorb, breakthrough and release of NO_y components should be carried out prior to use in the field.

Reliable surface re-activation techniques for similar denuders would be useful to ensure continuous, efficient scrubbing of NO_y and NO_x and circumnavigate the potential overestimation of pNit . In this regard, attempts to “reactivate” the denuder by cleaning with distilled water, drying at 50°C and exposure to ca. 300 ppbv O_3 for one hour did not result in an improvement of the direct NO -breakthrough or in the background pNit signal upon humidification. Surface sensitive, spectroscopic investigation of the water-induced transformation of organic and inorganic NO_y to NO_x (and its subsequent release to the gas-phase) on denuder surfaces would be useful in resolving these issues.

3.4 Comparison of the TD-CRDS with existing methods for NO_x and NO_y and instruments

In this section, our instrument’s performance is compared to other methods for NO_x and NO_y detection. We consider only instruments which measure NO_x and / or NO_y and not those that measure individual trace-gases from each family.

NO_x has traditionally been measured by two-channel CLD instruments (one channel each for NO and NO_2) in which NO is detected by chemiluminescence from its reaction with O_3 and NO_2 is reduced converted to NO on a molybdenum converter or by photolysis at wavelengths close to 390 nm. Examples of this type of instrument and the reported LODs and overall uncertainties are listed in Table 2. In this Table we also list the LOD and uncertainty of a recently developed CRDS setup which is similar in principal of operation to the one described here (Fuchs et al., 2009).

NO_y has frequently been measured by CLD instruments with Au/MoO -coated thermal dissociation inlets that reduce NO_2 to NO which is detected as described above for CLD- NO_x instrument. Although such instruments have very low detection limits, they have been shown to be vulnerable to degradation of the NO_y conversion efficiency and suffer from interferences by HCN , CH_3CN and NH_3 (Kliner et al., 1997), as well as loss of NO_y in the inlet (Zenker et al., 1998; Parrish et al., 2004). Table 2 summarises the LODs and uncertainties reported by other NO_y instruments.

Table 2 indicates that the total uncertainty of the present instrument is comparable to those reported for both NO_x and NO_y . Our present detection limit for both NO_x and NO_y is however worse than that reported (for NO_2) for the same instrument in 2016 (Thieser et al., 2016), which is a result of mirror degradation since that study.

4 Application of the instrument in field experiments

5 4.1 NO_x intercomparison and pNit measurements during the AQABA campaign

The first deployment of the instrument was during the AQABA (*Air Quality and climate change in the Arabian Basin*) ship campaign in summer 2017. From the 31st of July to the 2nd of September, the ship “*Kommander Iona*” followed a route from southern France via the Mediterranean Sea, the Suez Channel, the Red Sea, the Arabian Sea and the Arabian Gulf to Kuwait and back. The instrument was located in a container in front of the ship, with the inlet ovens located in an aluminium box on the roof of the container. The (unheated) tips of quartz inlet tubes protruded about 15 cm from the side of the aluminium box. Here we compare the NO_x and pNit measurements with other measurements of these parameters made during the campaign.

During AQABA, NO_x levels ranged from a few pptv (maritime background) up to several tens of ppbv in heavily polluted air masses in shipping lanes or in harbours. In Fig. 10a) we compare NO_x measured with the TD-CRDS with the results of a chemiluminescence detector (CLD 790 SR, ECO Physics, Tadic et al. (2020)), which measured NO and NO_2 . The data points represent 1 minute averages for the entire campaign, excluding air-masses which were contaminated by the ships exhaust. Additionally, periods with very high NO_x variability were not included, a data point being discarded whenever the differences in mean values exceeded 2 ppbv for consecutive data points.

A bivariate fit to the datasets (York, 1966), which incorporates total uncertainties for both instruments (CLD: 8.6%; TD-CRDS: 11% + 20 pptv*RH/100) resulted in a slope of 0.996 ± 0.003 and an intercept of -1.3 pptv. The very good agreement, serves to underline the general applicability of the TD-CRDS in NO_x measurements even under difficult conditions (e.g. a non-static platform). In this context we note that the deployment on a ship resulted in a degradation in performance (LOD was ≈ 100 pptv) owing to the ship’s motions, especially in heavy seas, which resulted in drifts in the instrument zero.

Figure 10b) shows a ca. 10 hours time frame with pNit measurements from the denuder channel of the TD-CRDS. Unfortunately, the TD-oven of the denuder channel broke down very early in the campaign and was not operational afterwards. The data from the pNit channel are presented together with the NO_x and NO_y measurements along with particulate nitrate mass concentrations measured by an aerosol mass spectrometer (Aerodyne HR-ToF-AMS; DeCarlo et al. (2006), Brooks et al. (2020)). The night-to-day transition is indicated via NO_2 photolysis rates J_{NO_2} derived from a spectral radiometer (Metcon GmbH), the relative humidity was $> 80\%$ throughout the period shown. During the two periods when, apart from some short spikes, NO_x was very low (21:10-23:45 UTC and 02:20-03:40 UTC), TD-CRDS data indicate the presence of 300-400 pptv of pNit, which would then constitute $\sim 80\%$ of NO_y . Such mixing ratios of particulate nitrate are not commensurate with those measured by the AMS, which, on average, are a factor 6-8 lower. As the AMS does not detect particles larger than ~ 600 nm with high efficiency (Drewnick et al., 2005), the difference could potentially indicate that a significant fraction of the

particulate nitrate is associated with coarse mode aerosol. In the lower panel of Fig. 10b) we plot coarse mode aerosol mass concentration determined from measurements of an optical particle counter (OPC) that measures particles between 0.2 and 20 μm . In the two low NO_x periods outlined above, the OPC-derived aerosol mass concentrations were between 3 and 5 $\mu\text{g m}^{-3}$. If 10 % of this coarse mode aerosol mass concentration were nitrate, which is a typical value in the Mediterranean (Koulouri et al., 2008; Calzolari et al., 2015; Malaguti et al., 2015), this would account for 100-200 pptv of the pNit observed by the TD-CRDS and not by the AMS. However, the time profile of pNit measured by the TD-CRDS is not consistent with those of either the OPC or the AMS, but rather resembles the NO_x mixing ratios. This strongly suggests that the large difference between pNit reported by the TD-CRDS and the AMS does not result from the non/detection of supermicron particulate nitrate by the AMS, but result from the denuder artefacts described in Sect. 3.3.2. This short case-study serves to highlight the potential positive bias in denuder based, TD-CRDS measurements of pNit under humid field conditions.

4.2 Ambient NO_x and NO_y measurements in an urban environment (Mainz, Germany)

NO_x and NO_y mixing ratios were obtained in air sampled outside the Max-Planck-Institute for Chemistry (MPIC). The MPIC (49°59'27.5"N 8°13'44.4"E) is located on the outskirts of Mainz but within 200 m of two busy 2- and 4-lane roads and within 500 m of additional university buildings as well as commercial and residential areas. The city of Mainz (217k inhabitants) is located in the densely populated *Rhine-Main-Area* together with the cities of Frankfurt (753k) and Wiesbaden (278k) and the air is strongly influenced by local pollution. The sampling location was on the top floor of a three story building (ca. 12 m above ground level). Air was sub-sampled to the inlets of the instrument from a ~1 m long 0.5 inch outer diameter PFA tube which was connected to a membrane pump / flow controller to generate a 20 slm bypass flow. **Aerosol transmission was probably < 100% in these measurements.**

Figure 11a) summarises the 8-days of measurement (data coverage 82%) as a time series for NO_x , NO_y , NO_z , (10 min averages) wind speed (1 hour averages) and the NO_z/NO_y ratio. The NO_x and NO_y mixing ratios were highly variable throughout this period, with NO_x mixing ratios between 0.7 and 148.3 ppbv (mean and median values of 22.1 and 6.9 ppbv, respectively). Traffic-related morning rush-hour peaks in NO_x were observed on all weekdays (14th, 16th, 17th and 20th) between 5:00 and 10:00 UTC. The morning NO_x peak is reduced or absent on the weekends (18th and 19th). NO_x levels stayed above 50 ppbv for nearly a full day from 18:00 UTC on the 16th of January until 18:00 UTC on the 17th of January, which coincides with constantly low wind speeds and sampling of air masses that were predominantly local, and thus highly polluted. NO_z mixing ratios were usually between 0.5 and 2.5 ppbv (minimum < LOD, maximum 3.1 ppbv, mean 1.0 ppbv and median 0.9 ppbv), with NO_z/NO_y ratios below 0.5. These values indicate that the air masses have been impacted by recent (local) NO_x emissions. The NO_z/NO_y ratio can be used as indicator for the degree of chemical processing of an air mass. In Fig. 11b) a median diel profile (including all measurement days) for the NO_z/NO_y ratio from the ambient measurement is shown. The diel profile displays two distinct minima in NO_z/NO_y during the morning and evening rush hour, where NO_z only makes up 5-10% of the total NO_y . This fraction increases up to 15% during midday and up to 25% during nighttime during which emissions of NO_x are reduced. **The diel profiles of NO_z/NO_y are strongly influenced by fresh emissions of NO_x . As the measurement location is**

strongly influenced by traffic, there is a decrease in NO_x (and increase in NO_z/NO_y) at nighttime. Nighttime increases in NO_z (13th-14th, 15th-16th, 18th-19th and 19th-20th of January 2020) may also be partially caused by formation of N_2O_5 as previously observed (Schuster et al., 2009) and which would have been favoured by the low nighttime temperatures ($< 10\text{ }^\circ\text{C}$) in winter. These measurements serve to illustrate the applicability of our TD-CRDS over a wide range of NO_x and NO_y concentrations under realistic field conditions and in the investigation of processes that transform NO_x into its gas- and particle-phase reservoirs.

5 Conclusions

We report on the development, characterisation and first deployment of a TD-CRDS instrument for the measurement of NO_x , NO_y , NO_z and pNit. Our laboratory experiments suggest that the different gas-phase NO_z species investigated (PAN, iPN, N_2O_5 , HONO, ClNO_2 , HNO_3) are converted with near stoichiometric efficiency to NO_x at an oven temperature of $850\text{ }^\circ\text{C}$. NH_4NO_3 particles of diameter 200 nm are also detected quantitatively as NO_x , whereas the efficiency of detection of NaNO_3 particles of similar diameter was closer to 25%. The efficiency of detection of coarse mode particles will be further reduced by their lower transmission through the denuder.

The potential for NH_3 to bias NO_y measurements was assessed and found to be insignificant in ambient air or synthetic air containing VOCs and water. The conversion to NO_2 (by reaction with O_3) of atmospheric NO , and also NO formed in the heated inlet circumvents bias resulting from O_3 ~~pyrolysis~~ thermolysis (leading to an NO_2 overestimation) and secondary processes, initiated by the thermal dissociation of organic nitrates.

For our activated carbon denuder, we observed $> 90\%$ transmission for ammonium nitrate particles with diameters between 40 and 400 nm. Under humid conditions the denuder suffered from direct breakthrough of NO and the re-release of previously stored iPN and NO_2 in the form of NO , indicating a potential bias of pNit measurements using this technique and potentially limiting its deployment to low- NO_x and low- NO_z environments. When using comparable denuders, we recommend regular checks with humidified zero air to characterize potential breakthrough. Our experiments demonstrated that the release of NO_x from the denuder exposed humid zero-air for several hours can decrease to values below 1 ppbv, which, in a first approximation could be treated as an offset. Cycling between multiple denuders would help in reducing the size of any bias.

The performance of the instrument under field conditions was demonstrated by measurements in Mainz, Germany and during the AQABA ship campaign. NO_x measurements with the new instrument were in good agreement with those from an established, independent CLD-based instrument.

Author contributions

NF developed the TD-CRDS, performed all laboratory and campaign measurements, evaluated the data sets and wrote the manuscript. IT and HF provided the AQABA CLD NO_x measurements. JS designed the heated inlet system and performed

actinic flux measurements on AQABA. JB, ED and FD provided AMS and OPC measurements from AQABA. JL and JNC designed and supervised the study and the campaigns. JNC, JL and FD contributed to the manuscript.

Competing Interests

The authors declare that they have no conflict of interest.

5 Acknowledgements

We thank Ezra Wood for providing us with the activated-carbon denuder and Chemours for the provision of the FEP sample (FEPD 121) used to coat the cavity walls. This work was supported by the Max Planck Graduate Center with the Johannes Gutenberg-Universität Mainz (MPGC).

References

- 10 Atsuko, N., Kazuya, S., Toshiaki, E., Kei-ichi, K., Morinobu, E., and Norifumi, S.: Electronic and Magnetic Properties of Activated Carbon Fibers, *Bull. Chem. Soc. Jpn.*, 69, 333-339, 10.1246/bcsj.69.333, 1996.
- Barker, J. R., Benson, S. W., Mendenhall, G. D., and Goldern, D. M.: Measurements of rate constants of importance in smog, Rep. PB-274530, Natl. Tech. Inf. Serv., Springfield, Va., 1977.
- 15 Barton, S. S., and Koresh, J. E.: Adsorption Interaction of Water with Microporous Adsorbents .1. Water-Vapor Adsorption on Activated Carbon Cloth, *J. Chem. Soc. Faraday Trans. I*, 79, 1147-1155, DOI 10.1039/f19837901147, 1983.
- Baulch, D. L., Duxbury, J., Grant, S. J., and Montague, D. C.: Evaluated kinetic data for high temperature reactions. Volume 4 Homogeneous gas phase reactions of halogen- and cyanide- containing species, *J. Phys. Chem. Ref. Data*, 10, 1981.
- 20 Bertram, A. K., Ivanov, A. V., Hunter, M., Molina, L. T., and Molina, M. J.: The reaction probability of OH on organic surfaces of tropospheric interest, *Journal of Physical Chemistry a*, 105, 9415-9421, 2001.
- 25 Beygi, Z. H., Fischer, H., Harder, H. D., Martinez, M., Sander, R., Williams, J., Brookes, D. M., Monks, P. S., and Lelieveld, J.: Oxidation photochemistry in the Southern Atlantic boundary layer: unexpected deviations of photochemical steady state, *Atmos. Chem. Phys.*, 11, 8497-8513, 10.5194/acp-11-8497-2011, 2011.
- 30 Bridier, I., Caralp, F., Loirat, H., Lesclaux, R., Veyret, B., Becker, K. H., Reimer, A., and Zabel, F.: Kinetic and Theoretical-studies of the Reactions $\text{CH}_3\text{C}(\text{O})\text{O}_2 + \text{NO}_2 + \text{M} \leftrightarrow \text{CH}_3\text{C}(\text{O})\text{NO}_2 + \text{M}$ between 248 K and 393 K and Between 30-torr and 760-torr, *Journal of Physical Chemistry*, 95, 3594-3600, 1991.
- 35 Brooks, J., Darbyshire, E., Drewnick, F., Alfara, R., Struckmeier, C., Fachinger, F., Borrmann, S., Allen, G., and Coe, H.: Characterisation of accumulation mode aerosol across the Middle East and Mediterranean during a ship campaign in the summer of 2017, in preperation, 2020.
- Brunauer, S., Emmett, P. H., and Teller, E.: Adsorption of gases in multimolecular layers, *J. Amer. Chem. Soc.*, 60, 309-319, 1938.
- 40 Calzolari, G., Nava, S., Lucarelli, F., Chiari, M., Giannoni, M., Becagli, S., Traversi, R., Marconi, M., Frosini, D., Severi, M., Udisti, R., di Sarra, A., Pace, G., Meloni, D., Bommarito, C., Monteleone, F., Anello, F., and Sferlazzo, D. M.: Characterization of PM10 sources in the central Mediterranean, *Atmos Chem Phys*, 15, 13939-13955, 10.5194/acp-15-13939-2015, 2015.

- Cohen, N., and Westberg, K. R.: Chemical Kinetic Data Sheets for High-Temperature Reactions .2., *J. Phys. Chem. Ref. Data*, 20, 1211-1311, Doi 10.1063/1.555901, 1991.
- Davidson, J. A., Viggiano, A. A., Howard, C. J., Dotan, I., Fehsenfeld, F. C., Albritton, D. L., and Ferguson, E. E.: Rate Constants for Reactions of O₂⁺, NO₂⁺, NO⁺, H₃O⁺, Co₃⁻, NO₂⁻, and Halide Ions with N₂O₅ at 300 K, *Journal of Chemical Physics*, 68, 2085-2087, 1978.
- Day, D. A., Wooldridge, P. J., Dillon, M. B., Thornton, J. A., and Cohen, R. C.: A thermal dissociation laser-induced fluorescence instrument for in situ detection of NO₂, peroxy nitrates, alkyl nitrates, and HNO₃, *J. Geophys. Res. -Atmos.*, 107, doi:10.1029/2001jd000779, 2002.
- Day, D. A., Dillon, M. B., Wooldridge, P. J., Thornton, J. A., Rosen, R. S., Wood, E. C., and Cohen, R. C.: On alkyl nitrates, O₃, and the "missing NO_y", *Journal of Geophysical Research-Atmospheres*, 108, 4501, doi:10.1029/2003jd003685, 2003.
- DeCarlo, P. F., Kimmel, J. R., Trimborn, A., Northway, M. J., Jayne, J. T., Aiken, A. C., Gonin, M., Fuhrer, K., Horvath, T., Docherty, K. S., Worsnop, D. R., and Jimenez, J. L.: Field-deployable, high-resolution, time-of-flight aerosol mass spectrometer, *Anal. Chem.*, 78, 8281-8289, 10.1021/ac061249n, 2006.
- Di Carlo, P., Aruffo, E., Busilacchio, M., Giammaria, F., Dari-Salisburgo, C., Biancofiore, F., Visconti, G., Lee, J., Moller, S., Reeves, C. E., Bauguitte, S., Forster, G., Jones, R. L., and Ouyang, B.: Aircraft based four-channel thermal dissociation laser induced fluorescence instrument for simultaneous measurements of NO₂, total peroxy nitrate, total alkyl nitrate, and HNO₃, *Atmospheric Measurement Techniques*, 6, 971-980, 10.5194/amt-6-971-2013, 2013.
- Drewnick, F., Hings, S. S., DeCarlo, P., Jayne, J. T., Gonin, M., Fuhrer, K., Weimer, S., Jimenez, J. L., Demerjian, K. L., Borrmann, S., and Worsnop, D. R.: A new time-of-flight aerosol mass spectrometer (TOF-AMS) - Instrument description and first field deployment, *Aerosol Science and Technology*, 39, 637-658, 10.1080/02786820500182040, 2005.
- Dubinin, M. M., Andreeva, G. A., Vartapetyan, R. S., Vnukov, S. P., Nikolaev, K. M., Polyakov, N. S., Seregina, N. I., and Fedoseev, D. V.: Adsorption of Water and the Micropore Structures of Carbon Adsorbents .5. Pore Structure Parameters of Thermally Treated Carbon Adsorbents and the Adsorption of Water-Vapor on These Materials, *B Acad Sci Ussr Ch+*, 31, 2133-2137, Doi 10.1007/Bf00958379, 1982.
- Dulitz, K., Amedro, D., Dillon, T. J., Pozzer, A., and Crowley, J. N.: Temperature-(208-318 K) and pressure-(18-696 Torr) dependent rate coefficients for the reaction between OH and HNO₃, *Atmos. Chem. Phys.*, 18, 2381-2394, 2018.
- Fahey, D. W., Eubank, C. S., Hubler, G., and Fehsenfeld, F. C.: Evaluation of a Catalytic Reduction Technique for the Measurement of Total Reactive Odd-Nitrogen Noy in the Atmosphere, *J Atmos Chem*, 3, 435-468, Doi 10.1007/Bf00053871, 1985.
- Finlayson-Pitts, B. J., Ezell, M. J., and Pitts, J. N. J.: Formation of chemically active chlorine compounds by reactions of atmospheric NaCl particles with gaseous N₂O₅ and ClONO₂, *Nature*, 337, 241-244, 1989.
- Fischer, H., Waibel, A. E., Welling, M., Wienhold, F. G., Zenker, T., Crutzen, P. J., Arnold, F., Burger, V., Schneider, J., Bregman, A., Lelieveld, J., and Siegmund, P. C.: Observations of high concentrations of total reactive nitrogen (NO_y) and nitric acid (HNO₃) in the lower Arctic stratosphere during the stratosphere-troposphere experiment by aircraft measurements (STREAM) II campaign in February 1995, *J. Geophys. Res. -Atmos.*, 102, 23559-23571, 10.1029/97jd02012, 1997.
- Fry, J. L., Draper, D. C., Zarzana, K. J., Campuzano-Jost, P., Day, D. A., Jimenez, J. L., Brown, S. S., Cohen, R. C., Kaser, L., Hansel, A., Cappellin, L., Karl, T., Roux, A. H., Turnipseed, A., Cantrell, C., Lefer, B. L., and Grossberg, N.: Observations of gas- and aerosol-phase organic nitrates at BEACHON-RoMBAS 2011, *Atmospheric Chemistry and Physics*, 13, 8585-8605, doi:10.5194/acp-13-8585-2013, 2013.
- Fuchs, H., Dube, W. P., Lerner, B. M., Wagner, N. L., Williams, E. J., and Brown, S. S.: A Sensitive and Versatile Detector for Atmospheric NO₂ and NO_x Based on Blue Diode Laser Cavity Ring-Down Spectroscopy, *Environmental Science & Technology*, 43, 7831-7836, doi:10.1021/es902067h, 2009.
- Fuchs, H., Ball, S. M., Bohn, B., Brauers, T., Cohen, R. C., Dorn, H. P., Dube, W. P., Fry, J. L., Haseler, R., Heitmann, U., Jones, R. L., Kleffmann, J., Mentel, T. F., Musgen, P., Rohrer, F., Rollins, A. W., Ruth, A. A., Kiendler-Scharr, A., Schlosser, E., Shillings, A. J. L., Tillmann, R., Varma, R. M., Venables, D. S., Tapia, G. V., Wahner, A., Wegener, R., Wooldridge, P. J., and Brown, S. S.: Intercomparison of measurements of NO₂ concentrations in the atmosphere simulation chamber SAPHIR during the NO₃-Comp campaign, *Atmos. Meas. Tech.*, 3, 21-37, 2010.

- Gaffney, J. S., Fajer, R., and Senum, G. I.: An Improved Procedure for High-Purity Gaseous Peroxyacyl Nitrate Production - Use of Heavy Lipid Solvents, *Atmos Environ*, 18, 215-218, Doi 10.1016/0004-6981(84)90245-2, 1984.
- 5 Gao, X. A., Liu, S. J., Zhang, Y., Luo, Z. Y., Ni, M. J., and Cen, K. F.: Adsorption and reduction of NO₂ over activated carbon at low temperature, *Fuel Process Technol*, 92, 139-146, 10.1016/j.fuproc.2010.09.017, 2011.
- Garner, N. M., Matchett, L. C., and Osthoff, H. D.: Quantification of Non-refractory Aerosol Nitrate in Ambient Air by Thermal Dissociation Cavity Ring-Down Spectroscopy, *Environmental Science & Technology*, 10.1021/acs.est.0c01156, 2020.
- 10 Glänzer, K., and Troe, J.: Thermal Decomposition of Nitrocompounds in Shock Waves. IV: Decomposition of Nitric Acid, *Berichte der Bunsengesellschaft für physikalische Chemie*, 78, 71-76, 10.1002/bbpc.19740780112, 1974.
- Huang, W., Saathoff, H., Shen, X. L., Ramisetty, R., Leisner, T., and Mohr, C.: Chemical Characterization of Highly Functionalized Organonitrates Contributing to Night-Time Organic Aerosol Mass Loadings and Particle Growth, *Environmental Science & Technology*, 15 53, 1165-1174, 10.1021/acs.est.8b05826, 2019.
- IUPAC: Task Group on Atmospheric Chemical Kinetic Data Evaluation, (Ammann, M., Cox, R.A., Crowley, J.N., Herrmann, H., Jenkin, M.E., McNeill, V.F., Mellouki, A., Rossi, M. J., Troe, J. and Wallington, T. J.) <http://iupac.pole-ether.fr/index.html>, 2019.
- 20 Ivanov, A. V., Trakhtenberg, S., Bertram, A. K., Gershenson, Y. M., and Molina, M. J.: OH, HO₂, and ozone gaseous diffusion coefficients, *Journal of Physical Chemistry A*, 111, 1632-1637, 2007.
- Javed, U., Kubistin, D., Martinez, M., Pollmann, J., Rudolf, M., Parchatka, U., Reiffs, A., Thieser, J., Schuster, G., Horbanski, M., Pöhler, D., Crowley, J. N., Fischer, H., Lelieveld, J., and Harder, H.: Laser-induced fluorescence-based detection of atmospheric nitrogen dioxide and comparison of different techniques during the PARADE 2011 field campaign, *Atmos. Meas. Tech.*, 12, 1461-1481, 10.5194/amt-12-1461-2019, 2019.
- 25 Kalberer, M., Ammann, M., Arens, F., Gaggeler, H. W., and Baltensperger, U.: Heterogeneous formation of nitrous acid (HONO) on soot aerosol particles, *Journal of Geophysical Research-Atmospheres*, 104, 13825-13832, 1999.
- Kim, P., Zheng, Y. J., and Agnihotri, S.: Adsorption equilibrium and kinetics of water vapor in carbon nanotubes and its comparison with activated carbon, *Ind Eng Chem Res*, 47, 3170-3178, 10.1021/ie0713240, 2008.
- 35 Kleffmann, J., Becker, K. H., Lackhoff, M., and Wiesen, P.: Heterogeneous conversion of NO₂ on carbonaceous surfaces, *Phys. Chem. Chem. Phys.*, 1, 5443-5450, DOI 10.1039/a905545b, 1999.
- Kliner, D. A. V., Daube, B. C., Burley, J. D., and Wofsy, S. C.: Laboratory investigation of the catalytic reduction technique for measurement of atmospheric NO_y, *Journal of Geophysical Research-Atmospheres*, 102, 10759-10776, Doi 10.1029/96jd03816, 1997.
- 40 Koulouri, E., Saarikoski, S., Theodosi, C., Markaki, Z., Gerasopoulos, E., Kouvarakis, G., Makela, T., Hillamo, R., and Mihalopoulos, N.: Chemical composition and sources of fine and coarse aerosol particles in the Eastern Mediterranean, *Atmos Environ*, 42, 6542-6550, 10.1016/j.atmosenv.2008.04.010, 2008.
- 45 Lammel, G., and Perner, D.: The Atmospheric Aerosol as a Source of Nitrous-Acid in the Polluted Atmosphere, *J. Aerosol Sci.*, 19, 1199-1202, Doi 10.1016/0021-8502(88)90135-8, 1988.
- Langford, A. O., Fehsenfeld, F. C., Zachariassen, J., and Schimel, D. S.: Gaseous Ammonia Fluxes and Background Concentrations in Terrestrial Ecosystems of the United States, *Glob. Biogeochem. Cycles*, 6, 459-483, 10.1029/92gb02123, 1992.
- 50 Lee, B. H., Mohr, C., Lopez-Hilfiker, F. D., Lutz, A., Hallquist, M., Lee, L., Romer, P., Cohen, R. C., Iyer, S., Kurten, T., Hu, W. W., Day, D. A., Campuzano-Jost, P., Jimenez, J. L., Xu, L., Ng, N. L., Guo, H. Y., Weber, R. J., Wild, R. J., Brown, S. S., Koss, A., de Gouw, J., Olson, K., Goldstein, A. H., Seco, R., Kim, S., McAvey, K., Shepson, P. B., Starn, T., Baumann, K., Edgerton, E. S., Liu, J. M., Shilling, J. E., Miller, D. O., Brune, W., Schobesberger, S., D'Ambro, E. L., and Thornton, J. A.: Highly functionalized organic nitrates in the southeast United States: Contribution to secondary organic aerosol and reactive nitrogen budgets, *Proc. Natl. Acad. Sci. U. S. A.*, 113, 1516-1521, 10.1073/pnas.1508108113, 2016.
- 55

- Leser, H., Honninger, G., and Platt, U.: MAX-DOAS measurements of BrO and NO₂ in the marine boundary layer, *Geophysical Research Letters*, 30, 2003.
- 5 Lightfoot, P. D., Cox, R. A., Crowley, J. N., Destriau, M., Hayman, G. D., Jenkin, M. E., Moortgat, G. K., and Zabel, F.: Organic peroxy radicals - kinetics, spectroscopy and tropospheric chemistry, *Atmospheric Environment, Part A: General Topics*, 26, 1805-1961, 1992.
- Liu, L. M., Tan, S. L., Horikawa, T., Do, D. D., Nicholson, D., and Liu, J. J.: Water adsorption on carbon - A review, *Adv. Colloid Interface Sci.*, 250, 64-78, 10.1016/j.cis.2017.10.002, 2017.
- 10 Logan, J. A.: Nitrogen-Oxides in the Troposphere - Global and Regional Budgets, *J Geophys Res-Oceans*, 88, 785-807, DOI 10.1029/JC088iC15p10785, 1983.
- 15 Malaguti, A., Mircea, M., La Torretta, T. M. G., Telloli, C., Petralia, E., Stracquandano, M., and Berico, M.: Chemical Composition of Fine and Coarse Aerosol Particles in the Central Mediterranean Area during Dust and Non-Dust Conditions, *Aerosol Air Qual Res*, 15, 410-425, 10.4209/aaqr.2014.08.0172, 2015.
- Merten, A., Tschritter, J., and Platt, U.: Design of differential optical absorption spectroscopy long-path telescopes based on fiber optics, *Applied Optics*, 50, 738-754, 2011.
- 20 Meusel, H., Tamm, A., Kuhn, U., Wu, D. M., Leifke, A. L., Fiedler, S., Ruckteschler, N., Yordanova, P., Lang-Yona, N., Pohlker, M., Lelieveld, J., Hoffmann, T., Poschl, U., Su, H., Weber, B., and Cheng, Y. F.: Emission of nitrous acid from soil and biological soil crusts represents an important source of HONO in the remote atmosphere in Cyprus, *Atmos. Chem. Phys.*, 18, 799-813, 10.5194/acp-18-799-2018, 2018.
- 25 Murphy, J. G., Day, A., Cleary, P. A., Wooldridge, P. J., and Cohen, R. C.: Observations of the diurnal and seasonal trends in nitrogen oxides in the western Sierra Nevada, *Atmospheric Chemistry and Physics*, 6, 5321-5338, 2006.
- 30 Neuman, J. A., Huey, L. G., Ryerson, T. B., and Fahey, D. W.: Study of inlet materials for sampling atmospheric nitric acid, *Env. Sci. Tech.*, 33, 1133-1136, 1999.
- Ng, N. L., Brown, S. S., Archibald, A. T., Atlas, E., Cohen, R. C., Crowley, J. N., Day, D. A., Donahue, N. M., Fry, J. L., Fuchs, H., Griffin, R. J., Guzman, M. I., Herrmann, H., Hodzic, A., Iinuma, Y., Jimenez, J. L., Kiendler-Scharr, A., Lee, B. H., Luecken, D. J., Mao, J., McLaren, R., Mutzel, A., Osthoff, H. D., Ouyang, B., Picquet-Varrault, B., Platt, U., Pye, H. O. T., Rudich, Y., Schwantes, R. H., Shiraiwa, M., Stutz, J., Thornton, J. A., Tilgner, A., Williams, B. J., and Zaveri, R. A.: Nitrate radicals and biogenic volatile organic compounds: oxidation, mechanisms, and organic aerosol, *Atmos. Chem. Phys.*, 17, 2103-2162, 10.5194/acp-17-2103-2017, 2017.
- 35 Notholt, J., Hjorth, J., and Raes, F.: Formation of HNO₂ on Aerosol Surfaces During Foggy Periods in the Presence of NO and NO₂, *Atmospheric Environment Part a-General Topics*, 26, 211-217, 1992.
- 40 Oswald, R., Behrendt, T., Ermel, M., Wu, D., Su, H., Cheng, Y., Breuninger, C., Moravek, A., Mougou, E., Delon, C., Loubet, B., Pommerening-Roser, A., Sorgel, M., Poschl, U., Hoffmann, T., Andreae, M. O., Meixner, F. X., and Trebs, I.: HONO Emissions from Soil Bacteria as a Major Source of Atmospheric Reactive Nitrogen, *Science*, 341, 1233-1235, 10.1126/science.1242266, 2013.
- 45 Palm, B. B., Campuzano-Jost, P., Day, D. A., Ortega, A. M., Fry, J. L., Brown, S. S., Zarzana, K. J., Dube, W., Wagner, N. L., Draper, D. C., Kaser, L., Jud, W., Karl, T., Hansel, A., Gutierrez-Montes, C., and Jimenez, J. L.: Secondary organic aerosol formation from in situ OH, O₃, and NO₃ oxidation of ambient forest air in an oxidation flow reactor, *Atmos. Chem. Phys.*, 17, 5331-5354, 10.5194/acp-17-5331-2017, 2017.
- 50 Parrish, D. D., Ryerson, T. B., Holloway, J. S., Neuman, J. A., Roberts, J. M., Williams, J., Stroud, C. A., Frost, G. J., Trainer, M., Hubler, G., Fehsenfeld, F. C., Flocke, F., and Weinheimer, A. J.: Fraction and composition of NO_y transported in air masses lofted from the North American continental boundary layer, *Journal of Geophysical Research-Atmospheres*, 109, Artn D09302 10.1029/2003jd004226, 2004.
- 55 Pätz, H. W., Volz-Thomas, A., Hegglin, M. I., Brunner, D., Fischer, H., and Schmidt, U.: In-situ comparison of the NO_y instruments flown in MOZAIC and SPURT, *Atmos. Chem. Phys.*, 6, 2401-2410, 10.5194/acp-6-2401-2006, 2006.

- Paul, D., Furgeson, A., and Osthoff, H. D.: Measurements of total peroxy and alkyl nitrate abundances in laboratory-generated gas samples by thermal dissociation cavity ring-down spectroscopy, *Rev. Sci. Instrum.*, 80, Art. 114101, 10.1063/1.3258204 2009.
- 5 Paul, D., and Osthoff, H. D.: Absolute Measurements of Total Peroxy Nitrate Mixing Ratios by Thermal Dissociation Blue Diode Laser Cavity Ring-Down Spectroscopy, *Analytical Chemistry*, 82, 6695-6703, doi:10.1021/ac101441z, 2010.
- Perez, I. M., Wooldridge, P. J., and Cohen, R. C.: Laboratory evaluation of a novel thermal dissociation chemiluminescence method for in situ detection of nitrous acid, *Atmospheric Environment*, 41, 3993-4001, 10.1016/j.atmosenv.2007.01.060, 2007.
- 10 Perring, A. E., Pusede, S. E., and Cohen, R. C.: An observational perspective on the atmospheric impacts of alkyl and multifunctional nitrates on ozone and secondary organic aerosol, *Chemical Reviews*, 113, 5848-5870, doi:10.1021/cr300520x, 2013.
- 15 Peukert, S. L., Sivaramakrishnan, R., and Michael, J. V.: High temperature shock tube studies on the thermal decomposition of O₃ and the reaction of dimethyl carbonate with O-Atoms, *Journal of Physical Chemistry A*, 117, 3729-3738, doi:10.1021/jp400613p, 2013.
- Pilegaard, K.: Processes regulating nitric oxide emissions from soils, *Philos T R Soc B*, 368, ARTN 20130126 10.1098/rstb.2013.0126, 2013.
- 20 Platt, U., Perner, D., and Patz, H. W.: Simultaneous Measurement of Atmospheric CH₂O, O₃, and NO₂ by Differential Optical-Absorption, *Journal of Geophysical Research-Oceans and Atmospheres*, 84, 6329-6335, DOI 10.1029/JC084iC10p06329, 1979.
- Pohler, D., Vogel, L., Friess, U., and Platt, U.: Observation of halogen species in the Amundsen Gulf, Arctic, by active long-path differential optical absorption spectroscopy, *P Natl Acad Sci USA*, 107, 6582-6587, 10.1073/pnas.0912231107, 2010.
- 25 Present, P. S. R., Zare, A., and Cohen, R. C.: The changing role of organic nitrates in the removal and transport of NO_x, *Atmospheric Chemistry and Physics*, 20, 267-279, 10.5194/acp-20-267-2020, 2020.
- 30 Reed, C., Evans, M. J., Di Carlo, P., Lee, J. D., and Carpenter, L. J.: Interferences in photolytic NO₂ measurements: explanation for an apparent missing oxidant?, *Atmospheric Chemistry and Physics*, 16, 4707-4724, 10.5194/acp-16-4707-2016, 2016.
- Roberts, J. M.: The atmospheric chemistry of organic nitrates, *Atmospheric Environment, Part A: General Topics*, 24, 243-287, doi:10.1016/0960-1686(90)90108-y, 1990.
- 35 Rollins, A. W., Browne, E. C., Min, K.-E., Pusede, S. E., Wooldridge, P. J., Gentner, D. R., Goldstein, A. H., Liu, S., Day, D. A., Russell, L. M., and Cohen, R. C.: Evidence for NO_x Control over Nighttime SOA Formation, *Science*, 337, 1210-1212, 2012.
- Romer, P. S., Duffey, K. C., Wooldridge, P. J., Allen, H. M., Ayres, B. R., Brown, S. S., Brune, W. H., Crouse, J. D., de Gouw, J., Draper, D. C., Feiner, P. A., Fry, J. L., Goldstein, A. H., Koss, A., Misztal, P. K., Nguyen, T. B., Olson, K., Teng, A. P., Wennberg, P. O., Wild, R. J., Zhang, L., and Cohen, R. C.: The lifetime of nitrogen oxides in an isoprene-dominated forest, *Atmospheric Chemistry and Physics*, 16, 7623-7637, 10.5194/acp-16-7623-2016, 2016.
- 40 Rosen, R. S., Wood, E. C., Wooldridge, P. J., Thornton, J. A., Day, D. A., Kuster, W., Williams, E. J., Jobson, B. T., and Cohen, R. C.: Observations of total alkyl nitrates during Texas Air Quality Study 2000: Implications for O₃ and alkyl nitrate photochemistry, *Journal of Geophysical Research-Atmospheres*, 109, Art. Nr D07303, doi:10.1029/2003jd004227, 2004.
- 45 Sadanaga, Y., Takagi, R., Ishiyama, A., Nakajima, K., Matsuki, A., and Bandow, H.: Thermal dissociation cavity attenuated phase shift spectroscopy for continuous measurement of total peroxy and organic nitrates in the clean atmosphere, *Rev Sci Instrum*, 87, Artn 074102 10.1063/1.4958167, 2016.
- 50 Schlesinger, W. H., and Hartley, A. E.: A Global Budget for Atmospheric NH₃, *Biogeochemistry*, 15, 191-211, 1992.
- Schuster, G., Labazan, I., and Crowley, J. N.: A cavity ring down / cavity enhanced absorption device for measurement of ambient NO₃ and N₂O₅, *Atmospheric measurement techniques*, 2, 1-13, 2009.
- 55

- Shirahama, N., Moon, S. H., Choi, K. H., Enjoji, T., Kawano, S., Korai, Y., Tanoura, M., and Mochida, I.: Mechanistic study on adsorption and reduction of NO₂ over activated carbon fibers, *Carbon*, 40, 2605-2611, Pii S0008-6223(02)00190-2
Doi 10.1016/S0008-6223(02)00190-2, 2002.
- 5 Slusher, D. L., Huey, L. G., Tanner, D. J., Chen, G., Davis, D. D., Buhr, M., Nowak, J. B., Eisele, F. L., Kosciuch, E., Mauldin, R. L., Lefer, B. L., Shetter, R. E., and Dibb, J. E.: Measurements of pernitric acid at the South Pole during ISCAT 2000, *Geophysical Research Letters*, 29, Art. 2011, doi:10.1029/2002gl015703, 2002.
- 10 Sobanski, N., Schuladen, J., Schuster, G., Lelieveld, J., and Crowley, J. N.: A five-channel cavity ring-down spectrometer for the detection of NO₂, NO₃, N₂O₅, total peroxy nitrates and total alkyl nitrates, *Atmos. Meas. Tech.*, 9, 5103-5118, 10.5194/amt-9-5103-2016, 2016.
- Sobanski, N., Thieser, J., Schuladen, J., Sauvage, C., Song, W., Williams, J., Lelieveld, J., and Crowley, J. N.: Day- and Night-time Formation of Organic Nitrates at a Forested Mountain-site in South West Germany, *Atmos. Chem. Phys.*, 17, 4115-4130, 2017.
- 15 Su, H., Cheng, Y. F., Oswald, R., Behrendt, T., Trebs, I., Meixner, F. X., Andreae, M. O., Cheng, P., Zhang, Y., and Poschl, U.: Soil Nitrite as a Source of Atmospheric HONO and OH Radicals, *Science*, 333, 1616-1618, 10.1126/science.1207687, 2011.
- 20 Tadic, I., Crowley, J. N., Dienhart, D., Eger, P., Harder, H., Hottmann, B., Martinez, M., Parchatka, U., Paris, J. D., Pozzer, A., Rohloff, R., Schuladen, J., Shenolikar, J., Tauer, S., Lelieveld, J., and Fischer, H.: Net ozone production and its relationship to nitrogen oxides and volatile organic compounds in the marine boundary layer around the Arabian Peninsula, *Atmospheric Chemistry and Physics*, 20, 6769-6787, 10.5194/acp-20-6769-2020, 2020.
- 25 Talukdar, R. K., Burkholder, J. B., Schmoltner, A. M., Roberts, J. M., Wilson, R. R., and Ravishankara, A. R.: Investigation of the loss processes for peroxyacetyl nitrate in the atmosphere: UV photolysis and reaction with OH, *J. Geophys. Res. -Atmos.*, 100, 14163-14173, doi:10.1029/95jd00545, 1995.
- Talukdar, R. K., Herndon, S. C., Burkholder, J. B., Roberts, J. M., and Ravishankara, A. R.: Atmospheric fate of several alkyl nitrates .1. Rate coefficients of the reactions alkyl nitrates with isotopically labelled hydroxyl radicals, *Journal of the Chemical Society-Faraday Transactions*, 93, 2787-2796, 1997.
- 30 Tang, M. J., Cox, R. A., and Kalberer, M.: Compilation and evaluation of gas phase diffusion coefficients of reactive trace gases in the atmosphere: volume 1. Inorganic compounds, *Atmos. Chem. Phys.*, 14, 9233-9247, 10.5194/acp-14-9233-2014, 2014.
- 35 Thaler, R. D., Mielke, L. H., and Osthoff, H. D.: Quantification of nitril chloride at part per trillion mixing ratios by thermal dissociation cavity ring-down spectroscopy, *Analytical Chemistry*, 83, 2761-2766, doi:10.1021/ac200055z, 2011.
- 40 Thieser, J., Schuster, G., Phillips, G. J., Reiffs, A., Parchatka, U., Pöhler, D., Lelieveld, J., and Crowley, J. N.: A two-channel, thermal dissociation cavity-ringdown spectrometer for the detection of ambient NO₂, RO₂NO₂ and RONO₂, *Atmos. Meas. Tech.*, 9, 553-576, 10.5194/amt-9-553-2016, 2016.
- Tingey, D. T., Manning, M., Grothaus, L. C., and Burns, W. F.: Influence of Light and Temperature on Isoprene Emission Rates from Live Oak, *Physiol. Plant.*, 47, 112-118, DOI 10.1111/j.1399-3054.1979.tb03200.x, 1979.
- 45 Tsang, W., and Herron, J. T.: Chemical kinetic data base for propellant combustion. I. Reactions involving NO, NO₂, HNO, HNO₂, HCN and N₂O, *JPCRD*, 20, 609-663, 1991.
- Vandaele, A. C., Hermans, C., Fally, S., Carleer, M., Colin, R., Merienne, M. F., Jenouvrier, A., and Coquart, B.: High-resolution Fourier transform measurement of the NO₂ visible and near-infrared absorption cross sections: Temperature and pressure effects, *J. Geophys. Res. -Atmos.*, 107, Art. 4348, 10.1029/2001JD000971, 2002.
- 50 von der Weiden, S. L., Drewnick, F., and Borrmann, S.: Particle Loss Calculator - a new software tool for the assessment of the performance of aerosol inlet systems, *Atmos. Meas. Tech.*, 2, 479-494, DOI 10.5194/amt-2-479-2009, 2009.
- 55 Wang, S. S., Nan, J. L., Shi, C. Z., Fu, Q. Y., Gao, S., Wang, D. F., Cui, H. X., Saiz-Lopez, A., and Zhou, B.: Atmospheric ammonia and its impacts on regional air quality over the megacity of Shanghai, China, *Sci Rep-Uk*, 5, ARTN 15842
10.1038/srep15842, 2015.

- 5 Wild, R. J., Edwards, P. M., Dube, W. P., Baumann, K., Edgerton, E. S., Quinn, P. K., Roberts, J. M., Rollins, A. W., Veres, P. R., Warneke, C., Williams, E. J., Yuan, B., and Brown, S. S.: A measurement of total reactive nitrogen, NO_y, together with NO₂, NO, and O₃ via cavity ring-down spectroscopy, *Environmental Science & Technology*, 48, 9609-9615, doi:10.1021/es501896w, 2014.
- Williams, E. J., Baumann, K., Roberts, J. M., Bertman, S. B., Norton, R. B., Fehsenfeld, F. C., Springston, S. R., Nunnermacker, L. J., Newman, L., Olszyna, K., Meagher, J., Hartsell, B., Edgerton, E., Pearson, J. R., and Rodgers, M. O.: Intercomparison of ground-based NO_y measurement techniques, *J Geophys Res-Atmos*, 103, 22261-22280, Doi 10.1029/98jd00074, 1998.
- 10 Wollenhaupt, M., Carl, S. A., Horowitz, A., and Crowley, J. N.: Rate coefficients for reaction of OH with acetone between 202 and 395 K, *Journal of Physical Chemistry* 104, 2695-2705, 2000.
- Womack, C. C., Neuman, J. A., Veres, P. R., Eilerman, S. J., Brock, C. A., Decker, Z. C. J., Zarzana, K. J., Dube, W. P., Wild, R. J., Wooldridge, P. J., Cohen, R. C., and Brown, S. S.: Evaluation of the accuracy of thermal dissociation CRDS and LIF techniques for atmospheric measurement of reactive nitrogen species, *Atmospheric Measurement Techniques*, 10, 1911-1926, 10.5194/amt-10-1911-2017, 2017.
- 15 Wooldridge, P. J., Perring, A. E., Bertram, T. H., Flocke, F. M., Roberts, J. M., Singh, H. B., Huey, L. G., Thornton, J. A., Wolfe, G. M., Murphy, J. G., Fry, J. L., Rollins, A. W., LaFranchi, B. W., and Cohen, R. C.: Total Peroxy Nitrates (ΣPNs) in the atmosphere: the Thermal Dissociation-Laser Induced Fluorescence (TD-LIF) technique and comparisons to speciated PAN measurements, *Atmospheric measurement techniques*, 3, 593-607, doi:10.5194/amt-3-593-2010, 2010.
- 20 Xu, L., Suresh, S., Guo, H., Weber, R. J., and Ng, N. L.: Aerosol characterization over the southeastern United States using high-resolution aerosol mass spectrometry: spatial and seasonal variation of aerosol composition and sources with a focus on organic nitrates, *Atmospheric Chemistry and Physics*, 15, 7307-7336, 10.5194/acp-15-7307-2015, 2015.
- Yamamoto, N., Kabeya, N., Onodera, M., Takahashi, S., Komori, Y., Nakazuka, E., and Shirai, T.: Seasonal-Variation of Atmospheric Ammonia and Particulate Ammonium Concentrations in the Urban Atmosphere of Yokohama over a 5-Year Period, *Atmos Environ*, 22, 2621-2623, Doi 10.1016/0004-6981(88)90498-2, 1988.
- 30 Yao, X. H., and Zhang, L. M.: Trends in atmospheric ammonia at urban, rural, and remote sites across North America, *Atmos Chem Phys*, 16, 11465-11475, 10.5194/acp-16-11465-2016, 2016.
- York, D.: Least-Squares Fitting of a Straight Line, *Can. J. Phys.*, 44, 1079-+, DOI 10.1139/p66-090, 1966.
- 35 Zare, A., Romer, P. S., Nguyen, T., Keutsch, F. N., Skog, K., and Cohen, R. C.: A comprehensive organic nitrate chemistry: insights into the lifetime of atmospheric organic nitrates, *Atmos. Chem. Phys.*, 18, 15419-15436, 10.5194/acp-18-15419-2018, 2018.
- Zasypkin, A. Y., Grigoreva, V. M., Korchak, V. N., and Gershenson, Y. M.: A formula for summing of kinetic resistances for mobile and stationary media: 1. Cylindrical reactor, *Kinetics and Catalysis*, 38, 772-781, 1997.
- 40 Zenker, T., Fischer, H., Nikitas, C., Parchatka, U., Harris, G. W., Mihelcic, D., Müsgen, P., Pätz, H. W., Schultz, M., Volz-Thomas, A., Schmitt, R., Behmann, T., Weißenmayer, M., and Burrows, J. P.: Intercomparison of NO, NO₂, NO_y, O₃, and RO_x measurements during the Oxidizing Capacity of the Tropospheric Atmosphere (OCTA) campaign 1993 at Izaña, *Journal of Geophysical Research: Atmospheres*, 103, 13615-13634, 10.1029/97jd03739, 1998.
- 45 Zhang, W. J., Bagreev, A., and Rasouli, F.: Reaction of NO₂ with activated carbon at ambient temperature, *Ind Eng Chem Res*, 47, 4358-4362, 10.1021/ie800249s, 2008.

50

Table 1: Comparison of NO_x and/or NO_y measurements.

Species	Reference	Method	2 σ Level of detection (integration time)	Uncertainty (%)
NO _x	Parrish et al. (2004)	CLD	20 pptv (1 s)	10
	Fuchs et al. (2009)	CRDS	22 pptv (1 s)	5
	Wild et al. (2014)	CRDS	< 30 pptv (1 s)	5
	Reed et al. (2016)	CLD Lab	2.5 pptv (60 s)	5
		CLD Aircraft	~ 1.0 pptv (60 s)	5
	This Study	CRDS	40 pptv (60 s)	6
NO _y	Fischer et al. (1997)	CLD	200 pptv (6 s)	25
	Williams et al. (1998)	CLD “BNL”	~ 50 pptv (1 s)	10
		CLD “NOAA”	20 pptv (1 s)	18
	Day et al. (2002)	LIF	~ 10 pptv (10 s)	< 5
	Parrish et al. (2004)	CLD	36 pptv (1 s)	10
	Wild et al. (2014)	CRDS	< 30 pptv (1 s)	12
	Pätz et al. (2006)	CLD	51 pptv (1 s)	13
		CLD	100 pptv (1s)	9
	This Study	CRDS	40 pptv (60 s)	15 ^a

Notes: ^aRefers to gas-phase NO_y only.

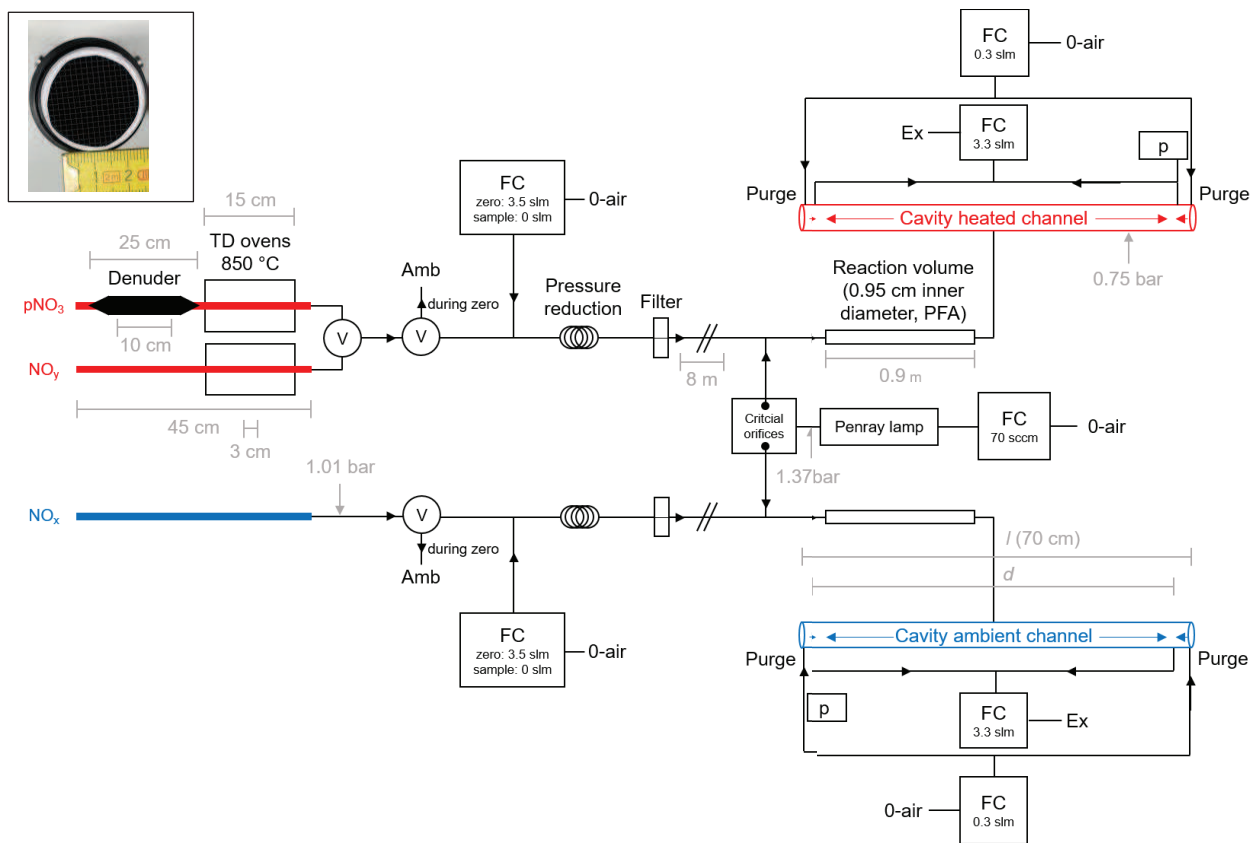


Figure 1: Schematic diagram of the TD-CRDS instrument (not to scale). NO_y and $p\text{NO}_3$ are detected via the heated channel, NO_x via the ambient channel. Ozone is generated via a Pen-Ray lamp (185 nm) and serves to convert NO to NO_2 . TD = Thermal Dissociation, FC = flow controller. The flows listed are those used under normal operating conditions, p = pressure sensor, Ex = membrane pump and exhaust, Amb = ambient air outside of the chamber, V = electronically switchable PTFE valve. Filter = PTFE filter, 2 μm pore size). The inset (photo) shows the honeycomb structure of the activated carbon denuder. The critical orifices have diameters of ≈ 0.05 mm.

5

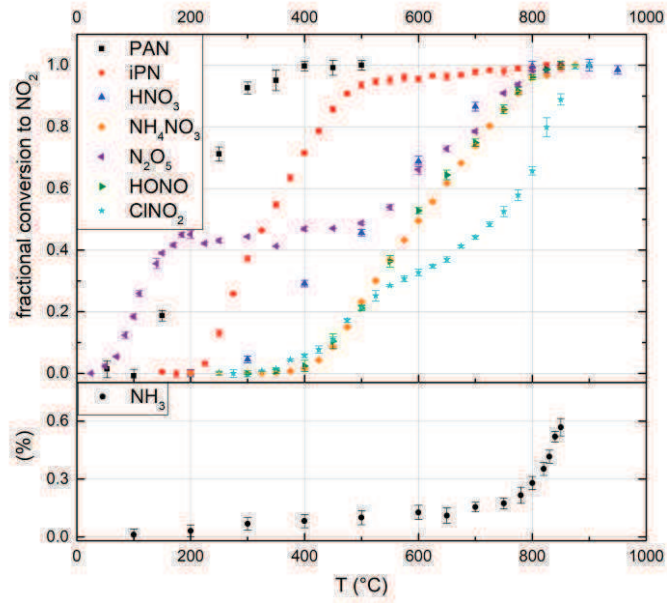


Figure 2: Thermograms of the NO_2 species PAN, iPN, HNO_3 , NH_4NO_3 , N_2O_5 , HONO, ClNO_2 and the potential interference NH_3 (without added O_3). The NH_3 fractional conversion is calculated relative to the calibrated output of the employed permeation source, all others relative to the observed mixing ratio at maximum conversion. Error bars are derived from the normed standard deviations during the averaging intervals. At the set temperature of 850 °C PAN, iPN, NH_4NO_3 , N_2O_5 (x2), HONO and HNO_3 are converted quantitatively to NO_2 , while the NH_3 interference is negligible under common ambient conditions.

5

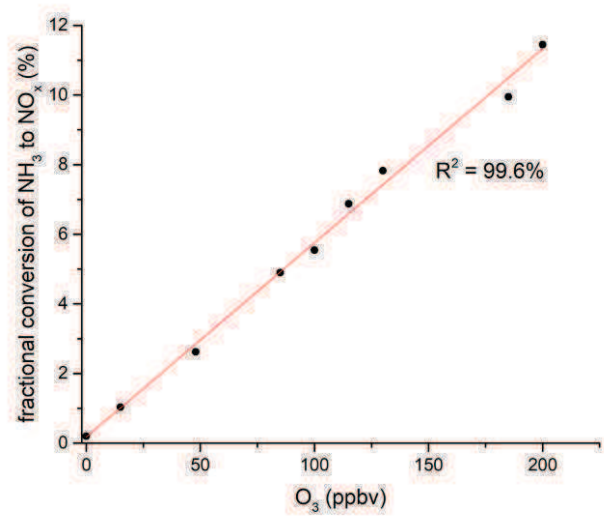
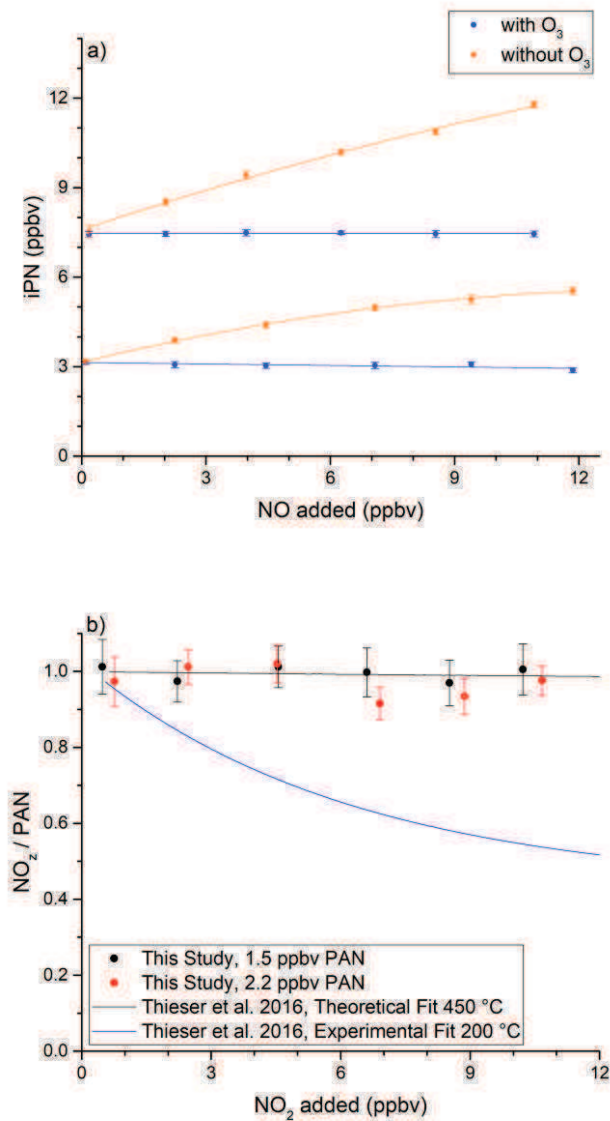


Figure 3: NH₃ to NO_x conversion in the heated inlet channel of the instrument in the presence of O₃. The fractional conversion of NH₃ to NO_x is calculated from the 13.1 ppmv of NH₃ from the permeation source.

5

10



5 **Figure 4:** Investigation of bias caused by reactions of NO with HO₂ and RO₂ when measuring iPN. *a)* NO varied for two initial iPN mixing ratios in the presence (blue data points) and absence (orange data points) of added O₃. The NO_x background signal from the iPN cylinder was subtracted from the iPN mixing ratios. *b)* Investigation of bias caused by the recombination of RO₂ and NO₂ during the thermal decomposition of PAN. In both experiments the oven temperature was 850 °C. In both plots, the error bars indicate standard deviation over the averaging interval.

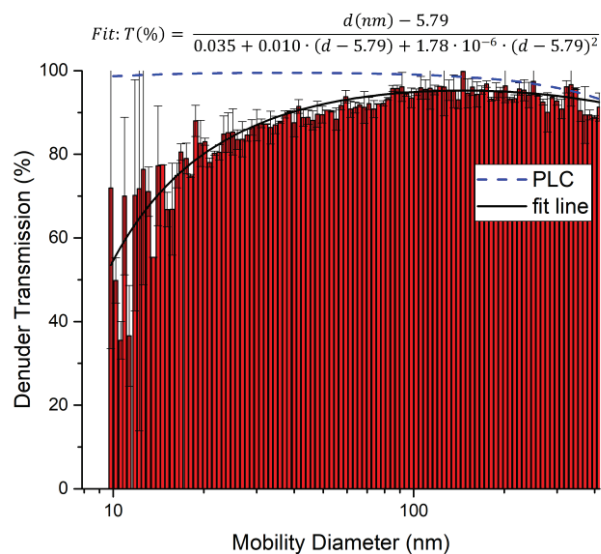


Figure 5: Transmission of ammonium nitrate particles through the denuder inlet. Relative transmissions are derived by dividing the number size distribution when sampling through the denuder by a size distribution obtained without the denuder. Error bars are based on the standard deviation of three consecutive measurements with and without the denuder. An aerosol flow of 3.3 slm was directed through the denuder (diameter 3 cm, see Sect. 2.4) and subsequently a DMA sampled 0.3 slm from the stream exiting the denuder. The plot also includes a fit of the experimental (solid, black line) data and a theoretical transmission distribution computed with the *Particle Loss Calculator (PLC)*.

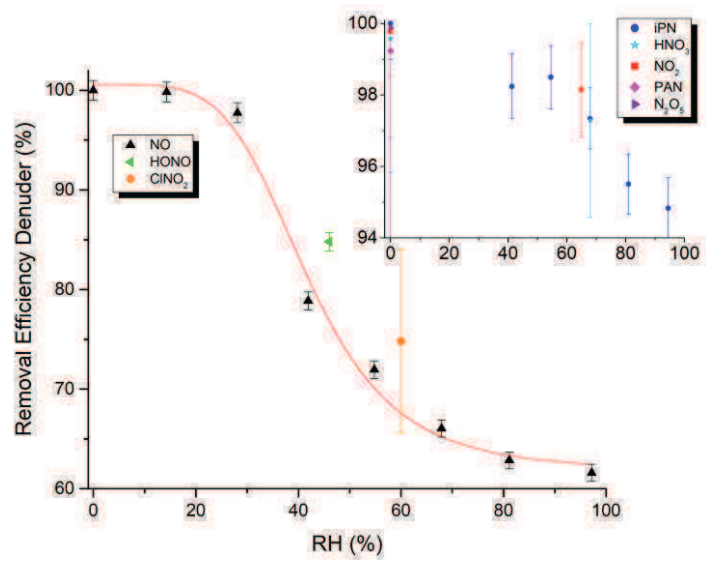


Figure 6: Removal efficiency of the denuder for various NO_y trace-gases as a function of RH. Units of the inset are identical to the main graph. See Table S2 for the exact values and information on the error determination.

5

10

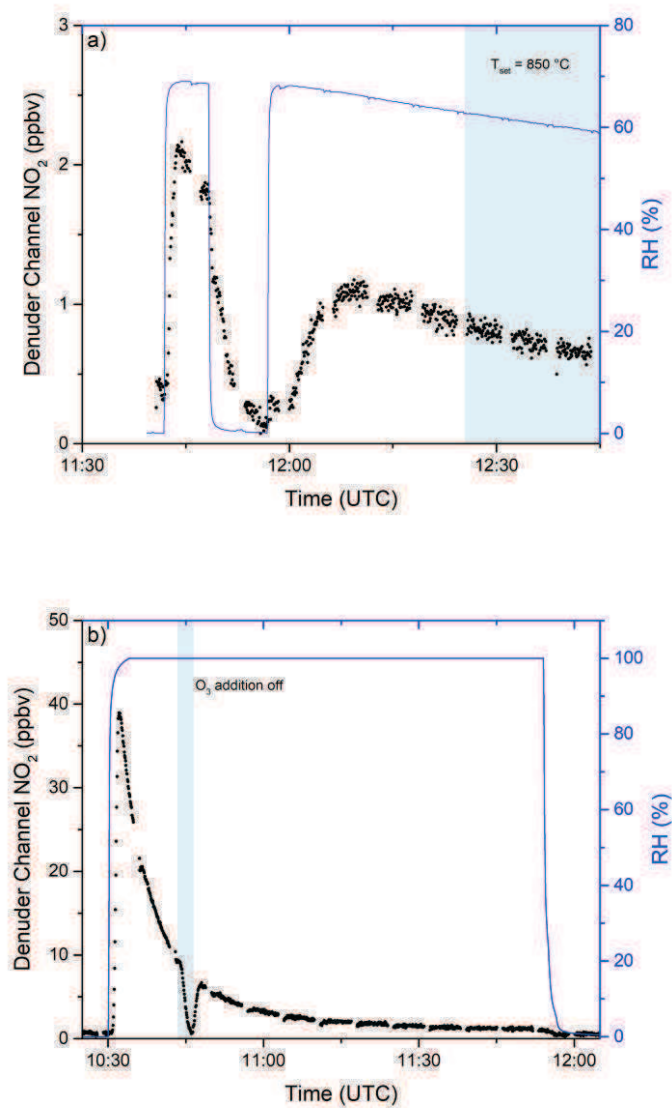


Figure 7: a) Release of NO_x from the denuder in humid air after exposure to 9.5 ppmv iPN for 1.5 hours. Relative humidity was measured before passing through the denuder. The blue shaded area signifies the period in which the inlet oven was heated to 850 °C. Changes in RH are achieved by flowing parts of the zero air stream through deionized water. b) Release of NO_x from the denuder in humid air after exposure to 0.83 ppmv NO₂ for 4.8 days. O₃ addition was switched off during the blue shaded period.

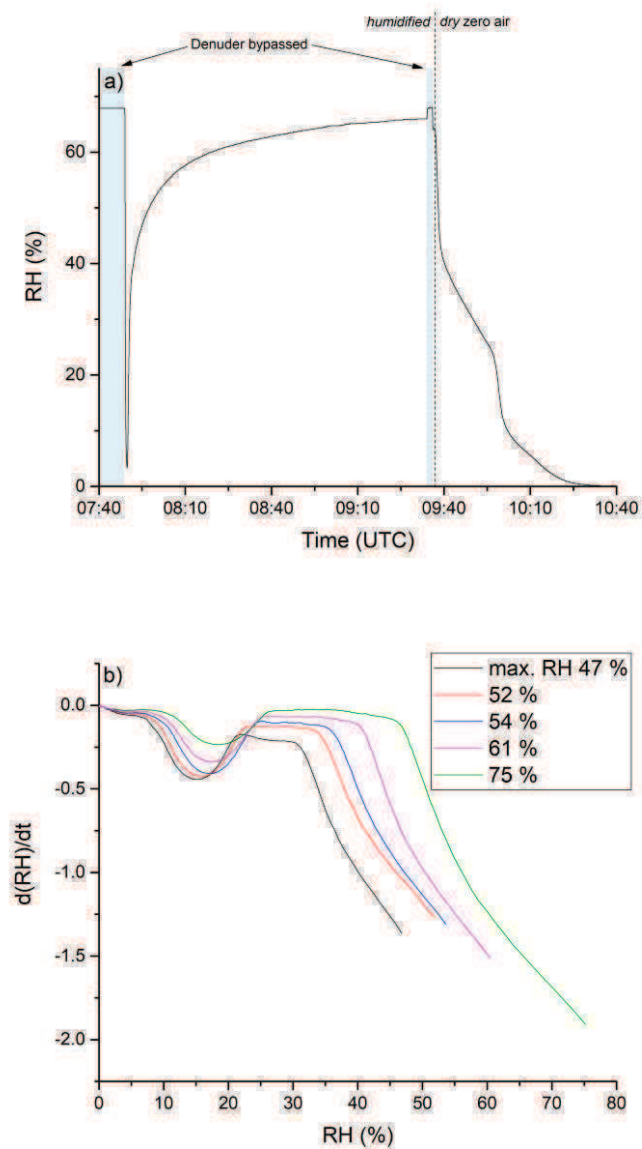


Figure 8: a) RH of humidified synthetic zero air after passing through the denuder. The initial RH was determined by bypassing the denuder before and after the experiment. Zero air was humidified by flowing a fraction of the stream through deionized water stored in a glass vessel. The time at which the experiment was conducted is given on the x-axis. Until ca. 09:35 UTC, zero-air with constant humidity (RH ca. 68%) was sent through the denuder. Afterwards the denuder was exposed to dry zero air. b) Derivative of the measured RH during the drying period. The step during the drying phase occurs in a higher RH area when starting the drying from a larger RH value.

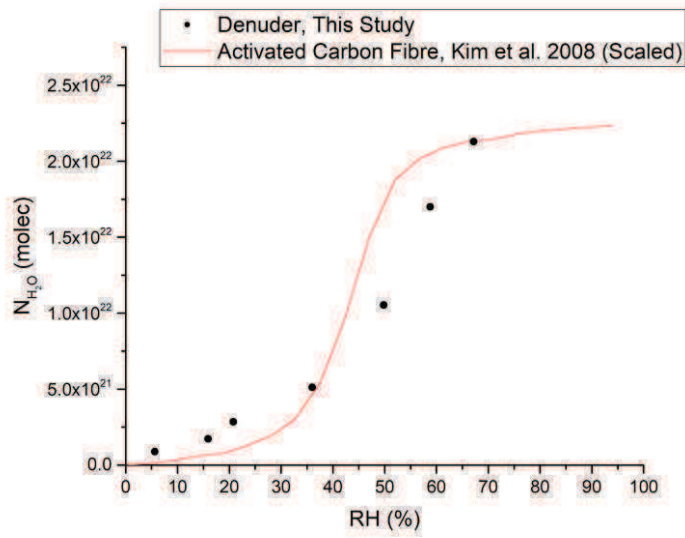
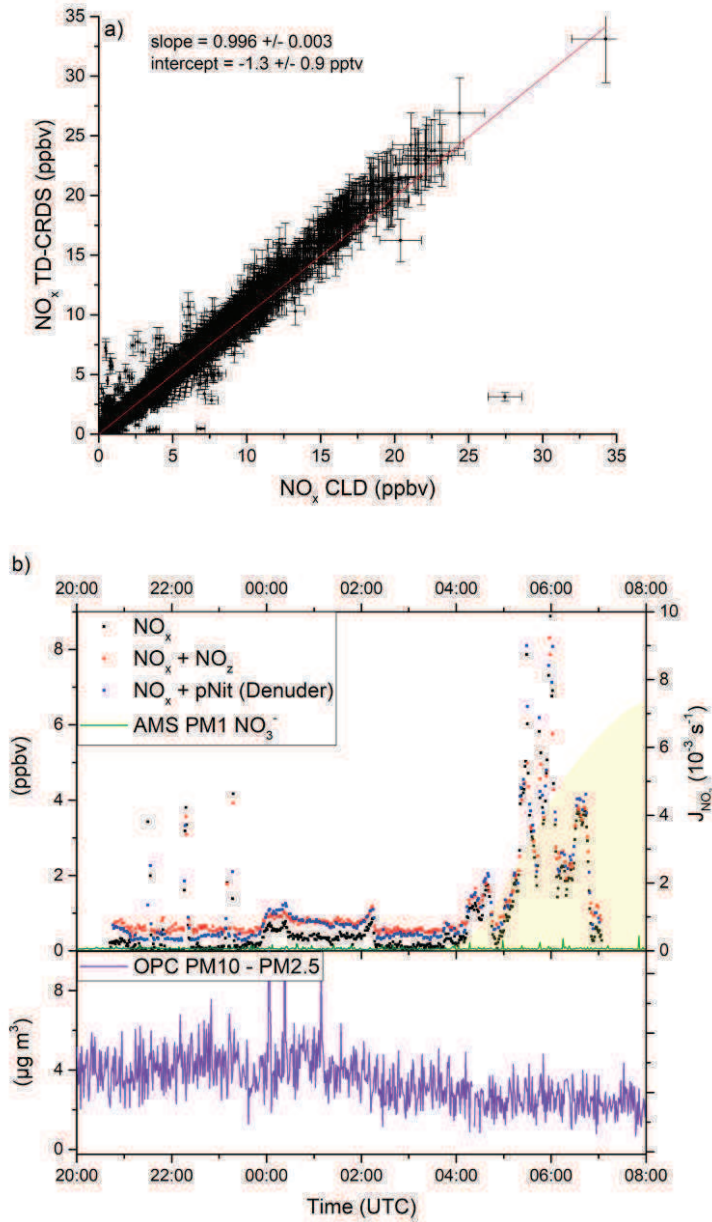


Figure 9: Number of adsorbed water molecules onto the denuder surface at equilibrium versus RH. The red line represents (scaled) results from a study on activated carbon fibre (Kim et al., 2008).

5

10

15



5 **Figure 10:** a) Correlation between the TD-CRDS NO_x measurements (1 min averages) and an independent CLD NO_x instrument from the AQABA. Data obtained during phases of very high NO_x variability have been excluded (see Sect. 4.1). See Fig. S6 for a histogram of the NO_x data points. b) pNit measurements using the denuder channel (blue data points) during AQABA and comparison with particulate NO_3^- from an AMS. The discrepancy towards the AMS and the correlation with the NO_x mixing ratios indicate a positive bias in the pNit measurements, caused by humidity effects on the denuder surface. OPC measurements are added in the lower panel to assess the potential influence of coarse mode aerosol nitrates.

10

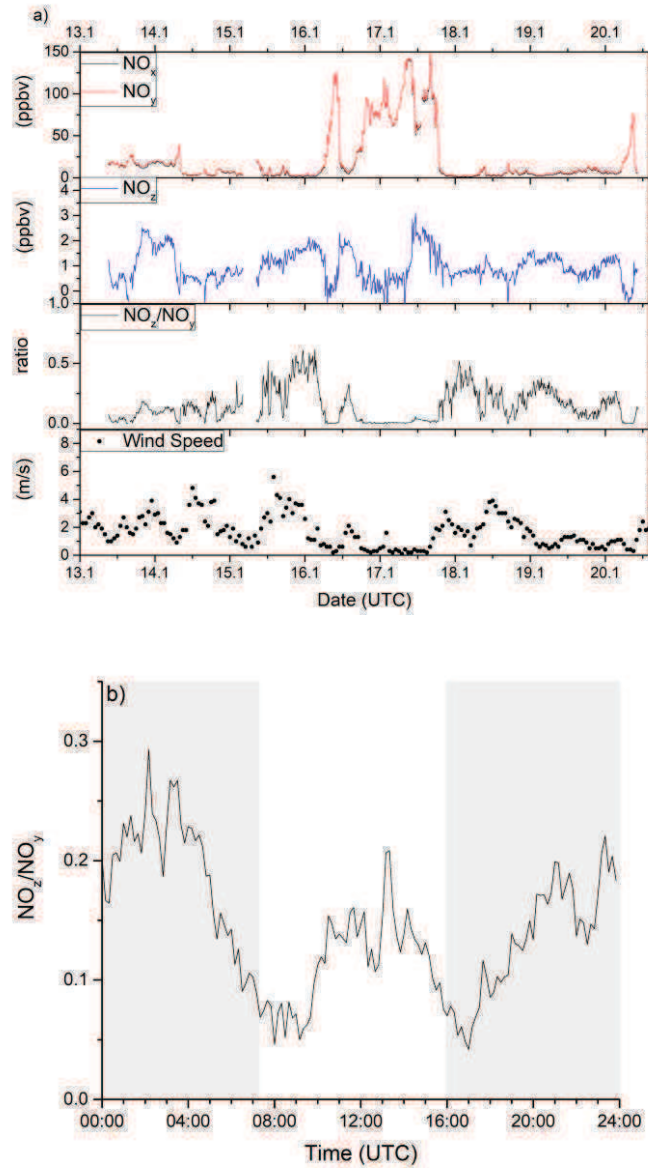


Figure 11: a) Time series of NO_x , NO_y , NO_z , NO_z/NO_y and wind speed from ambient measurements in Mainz, Germany in January 2020. Highly variable NO_x (between 0 and 150 ppbv) and moderate NO_z (between 0 and 3 ppbv) mixing ratios were observed, identifying the sampled air masses as dominated by anthropogenic emissions. Wind speed data was obtained from *Agrarmeteorologie Rheinland-Pfalz* (wetter.rlp.de) b) Diel profile of the NO_z/NO_y ratio including all measurement days, showing distinct minima during the morning and evening rush hours. Shaded areas signify the time between sunset and sunrise.

5

Measurement of NO_x and NO_y with a thermal dissociation cavity ring-down spectrometer (TD-CRDS): Instrument characterisation and first deployment.

5 Nils Friedrich¹, Ivan Tadic¹, Jan Schuladen¹, James Brooks², Eoghan Darbyshire², Frank Drewnick¹,
Horst Fischer¹, Jos Lelieveld¹, John N. Crowley¹

¹Atmospheric Chemistry Department, Max Planck Institute for Chemistry, Mainz, 55128, Germany

²Centre of Atmospheric Science, University of Manchester, Manchester, UK

Correspondence to: John N. Crowley (john.crowley@mpic.de)

10

Supplement

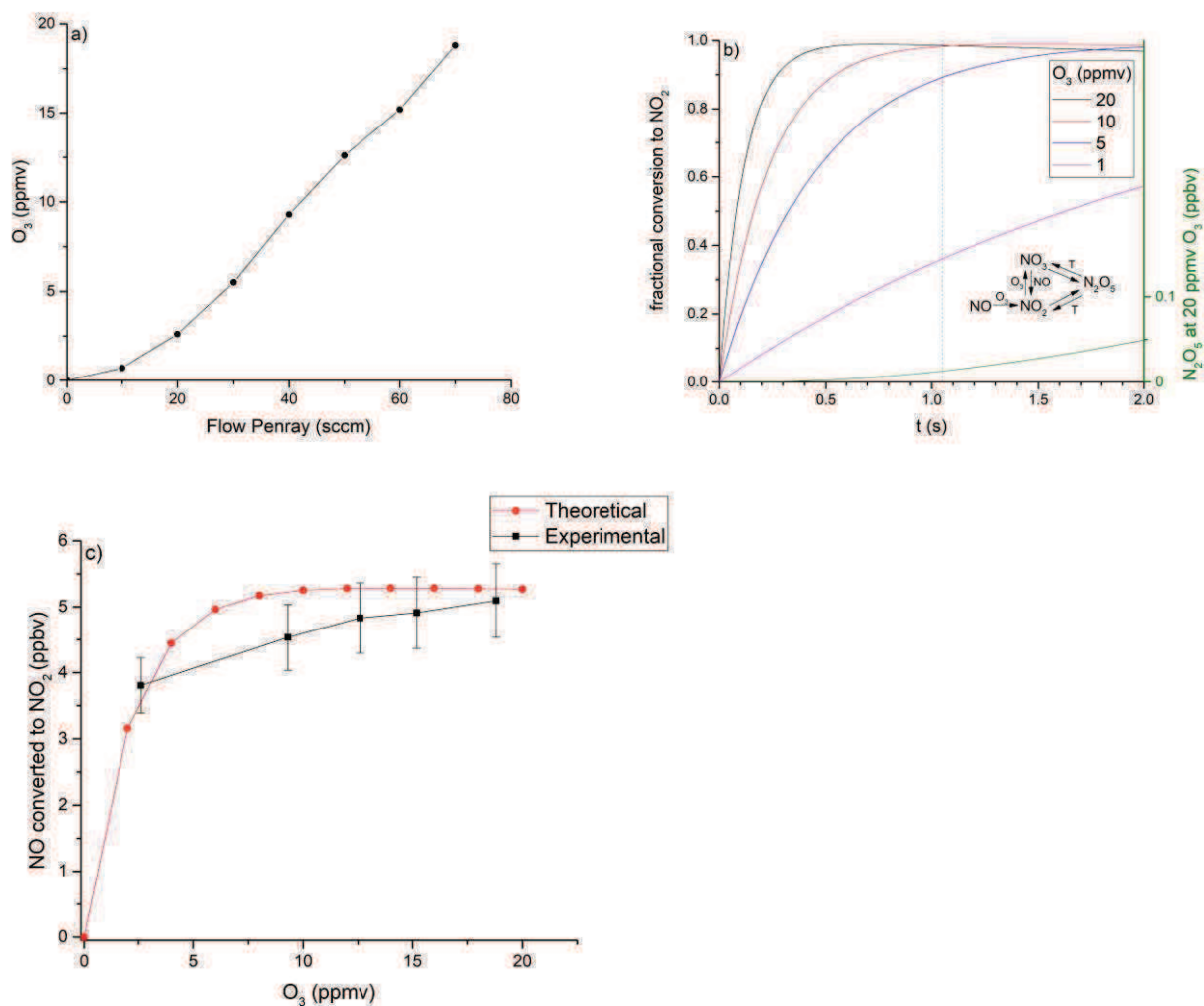


Figure S1: Optimisation of NO to NO₂ conversion via the addition of O₃. *a)* Ozone generated by passing synthetic air over the Pen-Ray lamp as a function of the flow rate. *b)* Numerical simulation of the fractional NO conversion as a function of reaction time and a chemical scheme showing reactions included in the model. High concentrations of O₃ can lead to the formation of significant amounts of N₂O₅ (50 pptv at 20 ppmv O₃ and 2 s reaction time). *c)* Conversion of 5.3 ppbv NO to NO₂ as a function of O₃ in 1.05 s reaction time. Both laboratory results and predictions of a numerical simulation are shown. Quantitative conversion is achieved for O₃ concentrations above 15 ppmv. The error bars indicate total overall uncertainty.

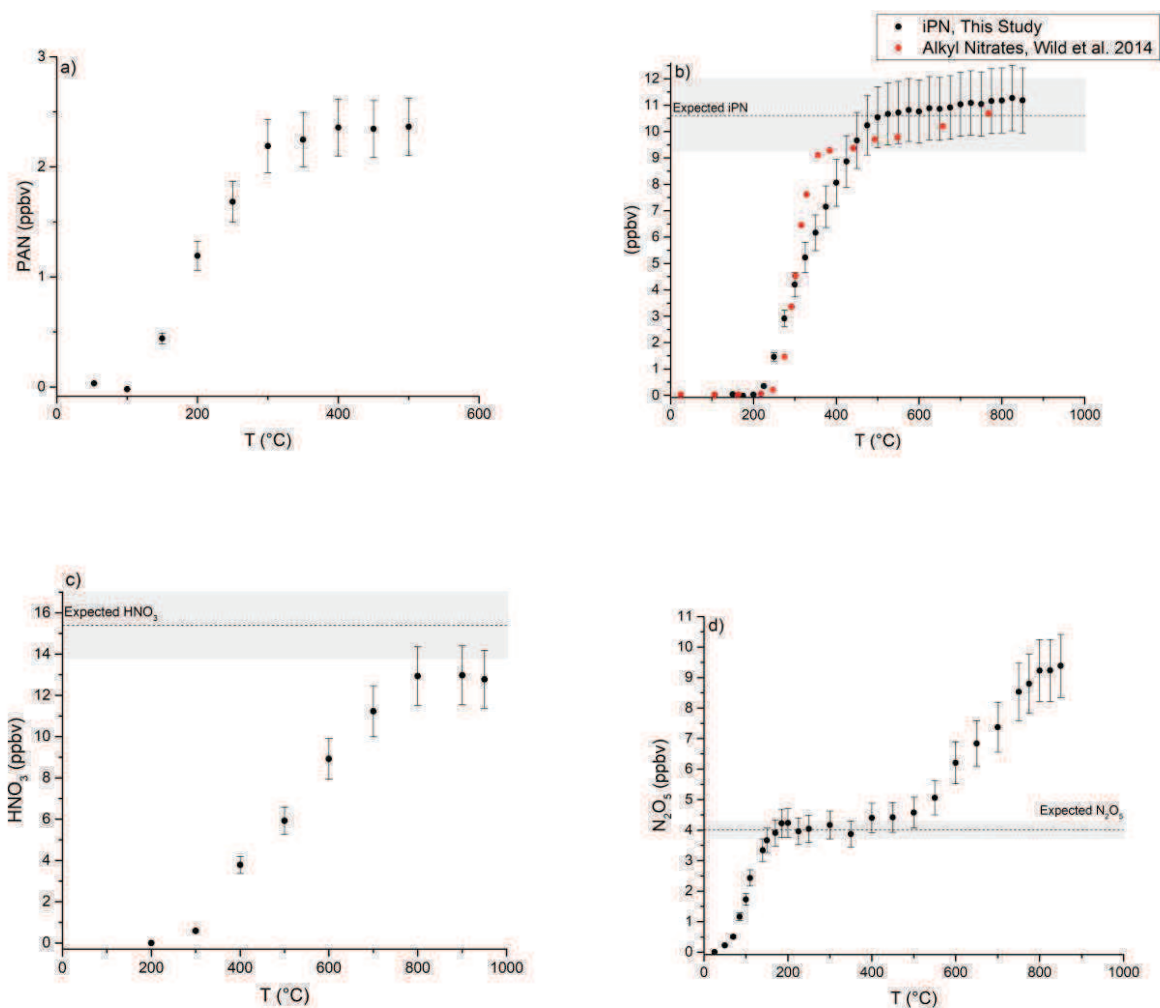
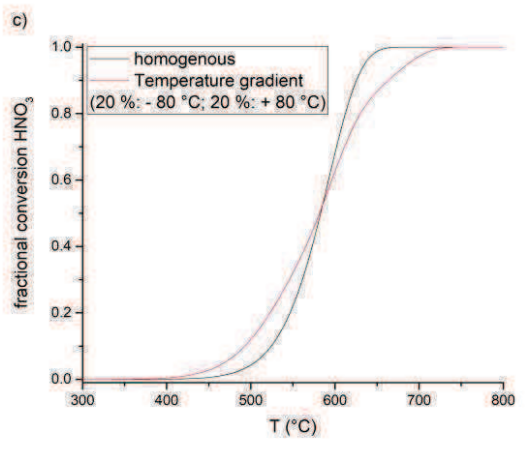
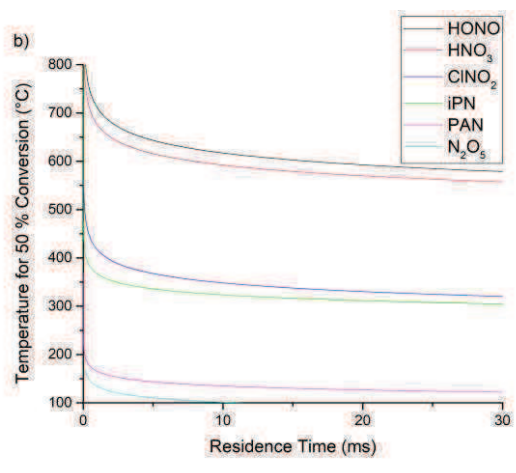
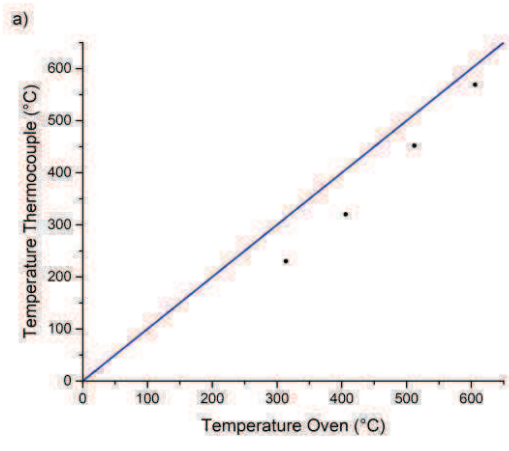


Figure S2: Absolute thermograms of PAN (a), iPN (b) and HNO₃ (c) and N₂O₅ (d). Error bars represent the total measurement uncertainty measurements (see Sect. 2.2). Shaded areas show the estimated uncertainty ranges for the expected iPN and HNO₃ concentrations, based on errors during sample preparation and gas stream dilution. Within combined uncertainties we observe quantitative conversion of PAN, iPN, 2x N₂O₅ and HNO₃ to NO₂ at the TD-CRDS set temperature of 850 °C. (b) also includes data points for an alkyl nitrates mixtures from Wild et al. (2014), to illustrate broader dissociation steps the continuous increases in signal above 400 °C.

- 10 Wild, R. J., Edwards, P. M., Dube, W. P., Baumann, K., Edgerton, E. S., Quinn, P. K., Roberts, J. M., Rollins, A. W., Veres, P. R., Warneke, C., Williams, E. J., Yuan, B., and Brown, S. S.: A measurement of total reactive nitrogen, NO_y, together with NO₂, NO, and O₃ via cavity ring-down spectroscopy, *Env. Sci. Tech.*, 48, 9609-9615, doi:doi:10.1021/es501896w, 2014



5 **Figure S3:** a) Plot of temperature from the internal reading of the TD-oven and a thermocouple located in the gas stream. The blue line shows a 1:1 correlation. b) Calculated threshold temperature for 50% conversion of N_2O_5 , PAN, iPN, $ClNO_2$, HNO_3 and HONO to NO_x relative to the residence time in the heated inlet and based on kinetic parameters of their thermal dissociation (see Sect. 3.1.8). For HNO_3 , the threshold temperature increases by 40 °C when the residence time decreases from 30 to 10 ms. c) Impact of temperature gradients inside the TD-inlet on the shape of the calculated HNO_3 thermogram. The width of the thermogram increases by ca. 100 °C.

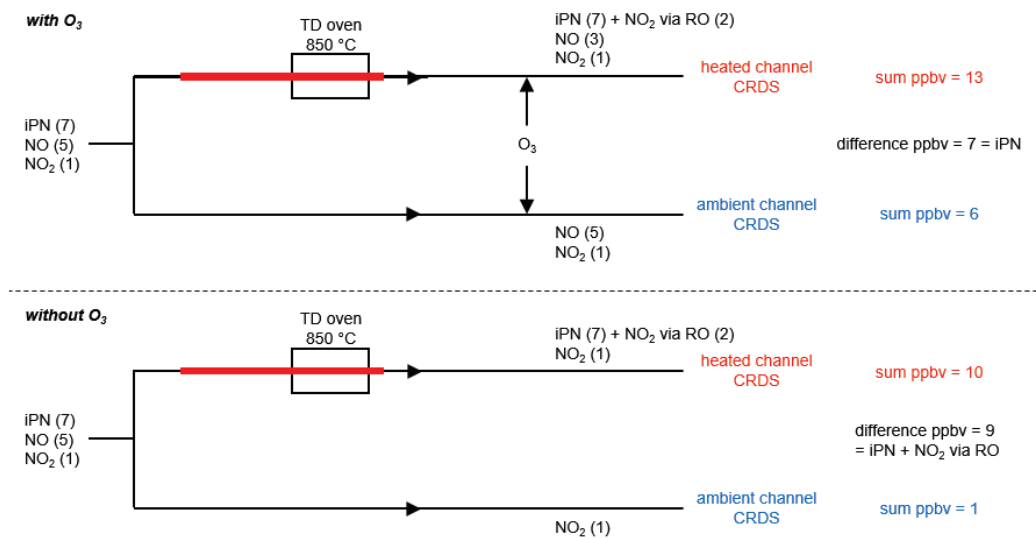


Figure S4: Graphical representation of the bias caused by $RO_2 + NO$ reactions in detecting iPN. In both cases an initial mixing ratio of 7 ppbv iPN is present, along with 5 ppbv NO and 1 ppbv NO_2 . When passed through the oven the iPN is converted to 7 ppbv NO_2 and (in this scenario) 2 ppbv of NO are converted to NO_2 via reaction with HO_2 . In total 13 ppbv of NO_2 are detected in the cavity sampling via the oven. In the cavity at ambient temperature 6 ppbv of NO_2 are detected so that a (correct) iPN mixing ratio of 7 ppbv is derived. In the lower part of the figure, the same initial conditions apply, but O_3 is not added. The conversion of 2 ppbv NO to NO_2 occurs as above, so that 10 ppbv NO_2 are detected when sampling from the oven. The NO_2 mixing ratio in the cavity sampling at ambient is 1 ppbv, resulting in a derived (incorrect) NO_2 iPN mixing ratio of 9 ppbv.

15

20

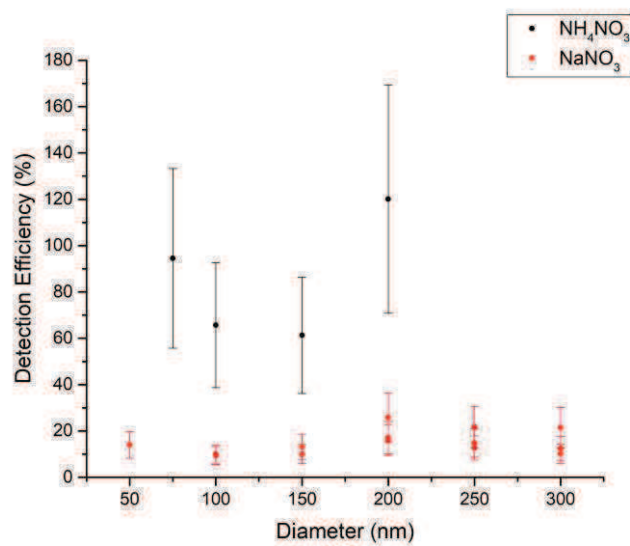


Figure S5: Detection efficiencies of NH₄NO₃ and NaNO₃ in the TD-CRDS, as a function of particle diameter. The CPC measured particle numbers were converted to mixing ratios and compared to the TD-CRDS. Errors inherent for this method are explained in Sect. 3.1.7. The particle conversion to NO₂ is clearly more efficient for NH₄NO₃, in direct comparison to NaNO₃.

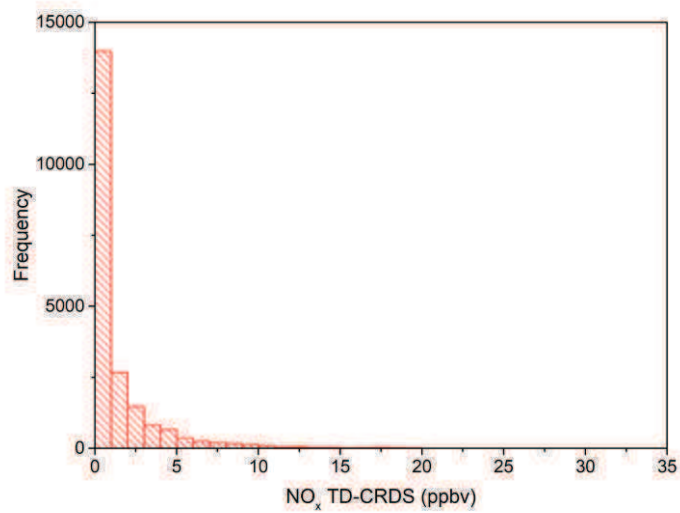


Figure S6: Histogram of the AQABA TD-CRDS NO_x mixing ratios shown in Fig. 10a). 92 % of the NO_x data points were at mixing ratios below 5 ppbv.

Table S1: Reactions included in the numerical simulations used to generate Fig. S1.

Reaction	Rate coefficients (Burkholder et al. (2015))
$\text{NO}_2 + \text{O}_3 \rightarrow \text{NO}_3 + \text{O}_2$	$1.2\text{E-}13 \cdot \exp(-2450/T)$
$\text{NO} + \text{NO}_3 \rightarrow \text{NO}_2 + \text{NO}_2$	$1.5\text{E-}11 \cdot \exp(170/T)$
$\text{NO} + \text{O}_3 \rightarrow \text{NO}_2 + \text{O}_2$	$3.0\text{E-}12 \cdot \exp(-1500/T)$
$\text{N}_2\text{O}_5 \rightarrow \text{NO}_3 + \text{NO}_2$	$\frac{((2.0\text{E-}30 \cdot (T/300)^{-4.4}) \cdot M / (1 + ((2.0\text{E-}30 \cdot (T/300)^{-4.4}) \cdot M / (1.4\text{E-}12 \cdot (T/300)^{-0.7})))) \cdot 0.6^{(1 + (\text{LOG}_{10}((2.0\text{E-}30 \cdot (T/300)^{-4.4}) \cdot M / (1.4\text{E-}12 \cdot (T/300)^{-0.7})))^2)^{-1}}}{(3.0\text{E-}27 \cdot \exp(10990/T))}$
$\text{NO}_2 + \text{NO}_3 \rightarrow \text{N}_2\text{O}_5$	$\frac{((2.0\text{E-}30 \cdot (T/300)^{-4.4}) \cdot M / (1 + ((2.0\text{E-}30 \cdot (T/300)^{-4.4}) \cdot M / (1.4\text{E-}12 \cdot (T/300)^{-0.7})))) \cdot 0.6^{(1 + (\text{LOG}_{10}((2.0\text{E-}30 \cdot (T/300)^{-4.4}) \cdot M / (1.4\text{E-}12 \cdot (T/300)^{-0.7})))^2)^{-1}}}{(3.0\text{E-}27 \cdot \exp(10990/T))}$

M = molecular density in molecule cm^{-3} , T = temperature in K.

- 5 *Burkholder, J. B., Sander, S. P., Abbatt, J., Barker, J. R., Huie, R. E., Kolb, C. E., Kurylo, M. J., Orkin, V. L., Wilmouth, D. M., and Wine, P. H.: Chemical Kinetics and Photochemical Data for Use in Atmospheric Studies, Evaluation No. 18, "JPL Publication 15-10, Jet Propulsion Laboratory, Pasadena, <http://jpldataeval.jpl.nasa.gov>., 2015.*

Table S2: Denuder characterisation

NO _y species	RH (%)	Reference mixing ratio (pptv) = I ₀ ± ΔI ₀	Mixing ratio with denuder (pptv) = I ± ΔI	Removal efficiency (%) = (R ± ΔR) x 100
NO	0	37036 ± 261	0 ± 43	100.0 ± 1.0
	14		62 ± 46	99.8 ± 1.0
	28		832 ± 94	97.8 ± 1.0
	42		7832 ± 60	78.9 ± 0.9
	55		10391 ± 65	71.9 ± 0.9
	68		12575 ± 45	66.0 ± 0.9
	81		13758 ± 51	62.9 ± 0.8
	97		14220 ± 74	61.6 ± 0.9
iPN	0	20181 ± 247	0 ± 22	100.0 ± 1.0
	14		-98 ± 91	100.5 ± 1.0
	27		-65 ± 58	100.3 ± 1.0
	41		355 ± 49	98.2 ± 0.9
	55		303 ± 41	98.5 ± 0.9
	68		537 ± 47	97.3 ± 0.9
	81		907 ± 46	95.5 ± 0.8
	95		1043 ± 33	94.8 ± 0.9
HNO ₃	0	8224 ± 214	35 ± 58	99.6 ± 2.7
	68	9104 ± 173	247 ± 50	97.3 ± 3.7
NO ₂	0	24259 ± 211	54 ± 45	99.8 ± 1.3
	65	24164 ± 225	448 ± 40	98.1 ± 1.2
PAN	0	7575 ± 93	58 ± 130	99.2 ± 2.4
N ₂ O ₅	0	4179 ± 230	5 ± 48	99.9 ± 7.8
HONO	46	10000 ± 61	1521 ± 47	84.8 ± 0.9
ClNO ₂	60	2068 ± 103	521 ± 141	74.8 ± 9.2

Mixing ratios (reference determined in heated inlet with bypassed denuder), standard deviations (1σ) during the averaging intervals and derived denuder removal efficiencies of various NO_y species, as a function of RH and as presented graphically in Fig. 6. R = (I₀ - I) / I₀. ΔR was determined by error propagation.

5

Author's Response to Referee #1

In this response, the referee comments (in black) are listed together with our replies (in blue) and the changes to the original manuscript (in red).

This paper reports the development of an instrument to measure NO₂, total NO_y and total particulate nitrate based on Cavity Ring-Down spectroscopy for measuring NO₂ and thermal dissociation for NO_y. The accurate measurement of NO_x down to low (ppt) levels is crucial for understanding the chemistry of remote atmosphere and combining such an instrument with thermal dissociation to measure total reactive nitrogen compounds and particulate nitrate further adds to the potential uses of such an instrument. Whilst a few examples of this type of approach exist in the literature, CRDS is a relatively new method and so work like this is important.

In general the paper details a comprehensive laboratory study of the instrument, including the thermal decomposition of different NO_y species and the performance of the denuder for the particulate measurements. It is well written, easy to follow and within scope of the journal. I recommend publication subject to the following, largely minor amendments and additions.

We thank the referee for the positive review of our paper and the constructive comments, which we address in the following responses.

A detailed description of the CRDS NO₂ / NO_x instrument is given in a previous paper (Thieser et al 2016), however I feel this new paper would benefit from some more details on the performance of the instrument to NO₂ and NO. There is no mention of how these species are calibrated, or what the precision / accuracy are. Whilst this data may be able to be found elsewhere, I believe the authors should include it here as well. It would greatly assist readers wishing to get a full understanding of the performance of the instrument. I would suggest at least adding what calibration gases were used for NO and NO₂, what is the accuracy and precision of these measurements at various time resolutions and what is the magnitude of any interferences.

We added the following paragraph to Sect. 2.2 as a short overview of the instrument's performance in detecting NO₂ and NO.

For NO₂, the performance of the instrument was first described by Thieser et al. (2016), who reports a measurement uncertainty of 6 % + (20 pptv * RH / 100) which is dominated by uncertainty in the effective cross section of NO₂ and the wavelength stability of the laser diode. The NO_x detection limit of 40 pptv (2σ, 1 minute average) for the present instrument (laboratory conditions) was derived from an Allan variance analysis and is worse than that reported by Thieser et al. (2016) (6 pptv at 40 s) due to degradation of the mirror reflectivity. Corrections applied to take into account humidity and pressure changes are discussed in Sect. 2.1. The total uncertainty in NO_y will depend on the uncertainty in the conversion to NO_x of both gaseous and particulate nitrate and thus depends on the individual components of NO_y in the air sampled. For purely gaseous NO_y, the major problem is likely to be related to loss of sticky molecules at the inlet and we choose to quote a "worst case" uncertainty of 15%.

We have amended the LOD we quote to that obtained on a stationary platform (the one mentioned in the last version was derived from the AQABA dataset obtained on a ship):

In this context we note that the deployment on a ship resulted in a degradation in performance (LOD was ≈ 100 pptv) owing to the ship's motions, especially in heavy seas, which resulted in drifts in the instrument zero.

On page 8 lines 17-20 it is stated that complete conversion of HNO₃ to NO₂ occurs at temperatures above 800°C, but then that the amount of NO₂ detected of 13 ppb is 85% of that expected based on the permeation and dilution flows. These two things do not seem to be consistent with each other – could the authors please clarify? Also, no mention is made of any potential losses of HNO₃ to the surface of the instrument or the inlet, something that is often a problem with this type of instrument?

The uncertainties of the measurements have to be taken into account. We have modified our text and now write:

A custom-made permeation source was used to provide a constant, known flow of HNO₃ (with $\sim 8\%$ NO_x impurity) to the TD-CRDS inlet. The permeation source consisted of a length (≈ 1 m) of PFA tubing immersed in 66% HNO₃ solution held at 50 °C through which 100 sccm of dry, zero-air was passed. The concentration of HNO₃ and thus its permeation rate, $(1.62 \pm 0.2) \times 10^{-4}$ sccm, was derived by measuring the optical extinction of HNO₃ at 185 nm using the absorption cross section of Dulitz et al. (2018). The uncertainty is related to uncertainty in the absorption cross-section and the reproducibility of the output. The HNO₃ thermogram (Fig. 2 and Fig. S2c) has a plateau at temperatures above ≈ 800 °C. In the plateau region of Fig. 2, the HNO₃ mixing ratio measured is 13.0 ± 0.8 ppb, which (within combined uncertainties) is in agreement with the expected value (15.2 ± 1.98 ppb) calculated from the permeation rate and uncertainty in the dilution factor. We cannot rule out some loss of HNO₃ in the tubing connecting the permeation source to the TD-CRD, through previous studies have shown that irreversible losses are \sim of 5% or less under dry conditions (Neuman et al., 1999). We note that inlet loss of HNO₃ is minimized under ambient sampling conditions as only a short section (~ 20 cm) quartz tubing at ambient temperature is upstream of the heated section in which HNO₃ is converted to NO₂. Our observations are thus in accord with previous studies that found complete conversion of HNO₃ to NO₂ in similar set-ups (Day et al., 2002; Di Carlo et al., 2013; Wild et al., 2014; Womack et al., 2017).

Could the authors comment on if there would be an effect of HONO on the NO_y channel?

We have performed additional experiments with other trace gases, including HONO. Our results indicate efficient conversion of HONO to NO_x in our heated inlet and are described in a new section 3.1.5.

In section 3.3.1 could the authors make some comment as to how much particles greater than 414 nm in diameter are transmitted? I would have thought that, especially in remote marine environments, particulate nitrate have a significant fraction on larger particles and thus provide an interference to the instrument.

We have addressed this comment by adding text in Sect. 3.3.1:

The PLC does a better job in predicting a reduction in transmission for the largest particles which we measured and indicates a transmission of 74% at 1 μ m and 45 % at 2 μ m. In certain environments, nitrate associated with coarse mode particles thus represents a potential bias for TD-CRDS measurements of NO_y.

In section 3.3.2 could the authors comment on how the efficiency of the denuder changes with age and how often it may need to be regenerate or replaced.

This will depend on the conditions of its deployment (e.g. highly polluted or remote) and we cannot suggest a regeneration schedule. Also, the behavior of our denuder is not necessarily identical to that of other designs.

In section 4.1 the authors state that they do not present an analysis of the NO_z data as it will be presented in a future publication. I think they should at least comment on the NO_z data observed. This paper is about the development of an instrument to measure NO_z and to not comment on the measurements made even a little seems very strange.

Unlike NO_x, there were no measurements during AQABA with which to directly compare our NO_z data set. The separate publication will be non-technical and will deal with the atmospheric chemistry of NO_z which is not in the scope of AMT. We see little value in reproducing information from the planned publication here. We now write:

Here we compare the NO_x and pNit measurements with other measurements of these parameters made during the campaign.

Likewise section 4.2 would also benefit from an expanded discussion of the NO_z data. For instance why is the diurnal cycle observed as it is, especially the nighttime peak values.

We expanded the discussion and now write:

The diel profiles of NO_z/NO_y are strongly influenced by fresh emissions of NO_x. As the measurement location is strongly influenced by traffic, there is a decrease in NO_x (and increase in NO_z/NO_y) at nighttime. Nighttime increases in NO_z (13th-14th, 15th-16th, 18th-19th and 19th-20th of January 2020) may also be partially caused by formation of N₂O₅ as previously observed (Schuster et al, 2009) and which would have been favoured by the low nighttime temperatures (< 10 °C) in winter.

Finally I wonder if the authors could comment on now the particulate nitrate measurement could be improved. There are some suggestions given in section 3 but I think there should be something in the conclusions about this. Currently I read the paper like there was not much hope that the technique could be used for accurate particulate nitrate measurements but I am sure this is not the case, thus the authors should say so.

The following text has been added to the conclusions:

Under humid conditions the denuder suffered from direct breakthrough of NO and the re-release of previously stored iPN and NO₂ in the form of NO, indicating a potential bias of pNit measurements using this technique and potentially limiting its deployment to low-NO_x and low-NO_z environments. When using comparable denuders, we recommend regular checks with humidified zero air to characterize potential breakthrough. Our experiments demonstrated that the release of NO_x from the denuder exposed humid zero-air for several hours can decrease to values below 1 ppbv, which, in a first approximation could be treated as an offset. Cycling between multiple denuders would help in reducing the size of any bias.

Page 13 line 6: 'humidified significant' does not make sense.

Typo has been removed

humidified significant

References

Day, D. A., Wooldridge, P. J., Dillon, M. B., Thornton, J. A., and Cohen, R. C.: A thermal dissociation laser-induced fluorescence instrument for in situ detection of NO₂, peroxy nitrates, alkyl nitrates, and HNO₃, *J. Geophys. Res. -Atmos.*, 107, doi:10.1029/2001jd000779, 2002.

Di Carlo, P., Aruffo, E., Busilacchio, M., Giammaria, F., Dari-Salisburgo, C., Biancofiore, F., Visconti, G., Lee, J., Moller, S., Reeves, C. E., Bauguitte, S., Forster, G., Jones, R. L., and Ouyang, B.: Aircraft based four-channel thermal dissociation laser induced fluorescence instrument for simultaneous measurements of NO₂, total peroxy nitrate, total alkyl nitrate, and HNO₃, *Atmospheric Measurement Techniques*, 6, 971-980, 10.5194/amt-6-971-2013, 2013.

Dulitz, K., Amedro, D., Dillon, T. J., Pozzer, A., and Crowley, J. N.: Temperature-(208-318 K) and pressure-(18-696 Torr) dependent rate coefficients for the reaction between OH and HNO₃, *Atmos. Chem. Phys.*, 18, 2381-2394, 2018.

Neuman, J. A., Huey, L. G., Ryerson, T. B., and Fahey, D. W.: Study of inlet materials for sampling atmospheric nitric acid, *Env. Sci. Tech.*, 33, 1133-1136, 1999.

Wild, R. J., Edwards, P. M., Dube, W. P., Baumann, K., Edgerton, E. S., Quinn, P. K., Roberts, J. M., Rollins, A. W., Veres, P. R., Warneke, C., Williams, E. J., Yuan, B., and Brown, S. S.: A measurement of total reactive nitrogen, NO_y, together with NO₂, NO, and O₃ via cavity ring-down spectroscopy, *Environmental Science & Technology*, 48, 9609-9615, doi:10.1021/es501896w, 2014.

Womack, C. C., Neuman, J. A., Veres, P. R., Eilerman, S. J., Brock, C. A., Decker, Z. C. J., Zarzana, K. J., Dube, W. P., Wild, R. J., Wooldridge, P. J., Cohen, R. C., and Brown, S. S.: Evaluation of the accuracy of thermal dissociation CRDS and LIF techniques for atmospheric measurement of reactive nitrogen species, *Atmospheric Measurement Techniques*, 10, 1911-1926, 10.5194/amt-10-1911-2017, 2017.

Author's Response to Referee #2

In this response, the referee comments (in black) are listed together with our replies (in blue) and the changes to the original manuscript (in red).

Friedrich et al. describe a 2-channel thermal dissociation cavity ring-down spectrometer (TD-CRDS) for quantification of NO_x, NO_y, and particulate nitrate (pNit). Thermograms of peroxyacyl nitrate (PAN), isopropyl nitrate and nitric acid are presented. The potential interference from NH₃ and secondary radical chemistry is evaluated. The use of an activated carbon denuder to suppress gas-phase components of NO_y and transmit pNit is described. Several experiments are presented to characterize the performance of this denuder: the transmission of ammonium nitrate particles in the 10 nm - 414 nm size range and the partial removal of several trace gases (NO, NO₂, PAN, iPN, and HNO₃) as a function of relative humidity (RH) which revealed inlet memory effects. Sample ambient air measurements from the 2017 AQABA campaign and ambient air measurements in Mainz, Germany are presented.

This research group has described similar instruments previously (Sobanski et al., 2016; Thieser et al., 2016) and in this paper extends the earlier measurement capabilities to now quantify NO_x, NO_y, and aerosol nitrate. The measurement of NO_x and NO_y (including NH₄NO₃) has previously been demonstrated by Fuchs et al. (2009) and Wild et al. (2014), so that the main novelty of this work is the use of the denuder to selectively quantify ammonium nitrate. A denuder was previously used by the Cohen group (Rollins et al., 2010) to quantify organic nitrates which dissociate at a lower inlet temperature than NH₄NO₃.

The measurement of NO_x by CRDS through the addition of O₃ is convincing. However, the paper will require considerable revision before it can be considered for acceptance. I have summarized my major concerns below. Most importantly, I am not convinced that the instrument presented here yields accurate NO_y and particulate nitrate data.

We thank the referee for the comprehensive and constructive comments on our paper, which we address in the following responses. We have performed additional laboratory experiments, as suggested.

Major comments

(1) Thermograms and temperature dependence of thermal dissociation:

(a) The thermograms presented in this paper are inconsistent with literature, but no convincing rationale is provided as to why that would be. (Day et al., 2002; Wild et al., 2014) have shown that thermograms of iPN and HNO₃ are considerably offset from each other, which is what one would expect from their Arrhenius parameters (and is shown in the SI of this paper as Figure S2D). The "rather short" heated section of the inlet likely broadens the thermograms which is undesirable but should not have resulted in their complete overlap.

We re-measured the iPN thermogram using a thoroughly cleaned canister and with a different liquid sample. The newly measured thermogram is much closer to that expected from our own previous measurements and we conclude that the previous sample was contaminated (presumably with HNO₃ as the referee suggested). Note that while this result is reassuring, it changes none of the conclusions drawn in the manuscript as the instrument is not designed to measure PNs, ANs, HNO₃ etc separately, but to provide a measurement of NO_y. We now write:

A 10 L stainless-steel canister containing 10.3 ppmv of isopropyl nitrate (iPN) at a pressure of 4 bar N₂ was prepared using a freshly vacuum-distilled liquid sample using standard manometric methods. NO_x impurities were ~ 4.7 ppbv, though we note that diluted iPN stored in stainless-steel canisters for periods of several weeks degrades to form NO₂ and HNO₃.

The thermogram is displayed in Fig. 2, the absolute concentrations in Fig. S2b). Based on the mixing ratio of iPN in the canister and the dilution flows, 10.7 ppbv represents (101 ± 11)% conversion. The shaded area around the expected iPN mixing ratio in Fig. S2b) signifies the uncertainty of this value, based on propagation of the errors during the manometric and dilution procedures (2% for flow rates, 5% for pressures measured with digital pressure gauges and 10% for the last dilution step using the analog pressure gauge of the canister).

Between 550 and 850 °C we observe a weak increase in NO₂ from 10.7 to 11.2 ppbv, which is likely due to small amounts of HNO₃ in the sample. For iPN, the temperature at 50% conversion is 50 °C higher than those reported by Thieser et al. (2016) and Sobanski et al. (2016). Wild et al. (2014) employed a gaseous mixture of different alkyl nitrates and also observed a broad thermogram, with an initial increase in NO₂ (up to 80% conversion) for temperatures < 300 °C, followed by a slower increase up to 800 °C. The alkyl nitrates thermogram of Wild et al. (2014) has been included into Fig. S2b) to illustrate this behaviour and to facilitate direct comparison.

(b) The thermogram for PAN is inconsistent with a large body of literature including work by the Mainz group (Phillips et al., 2013) which showed full dissociation of PAN at an inlet temperature of ~150 °C (not at ~400 °C). If the higher dissociation temperatures are a consequence of the short heater residence time, then this would be design flaw as the higher temperatures enable unwanted side reactions, increase thermal gradients, and reduce selectivity.

This instrument is not designed to be selective and separately measure PAN and ANs. It is designed to measure NO_y and the positions of the individual thermograms are not of central importance as long as the plateau region is reached. The Phillips 2013 instrument used a PFA tube wrapped with heating wire rather than a quartz tube inserted into a commercial oven and was operated at a lower flow rate. There is no reason to expect that thermograms obtained at different flows with different tube materials and diameters (and thus temperature gradients) should be similar. In order to more fully understand the source of the differences which the referee has highlighted, we have measured the gas temperature by inserting a thermocouple into the oven region. We found, for example that with the oven temperature set at 310 °C, the thermocouple reading was just 230 °C, which helps explain the shift to higher temperatures when using the present set-up. We have also assessed the impact of

thermal gradients on the thermograms in another supplementary figure (see Fig. S3c). The following text has been added:

By inserting a thermocouple into the middle part of the heated section under normal sampling conditions we were able to show that the temperature of the gas was ≈ 80 °C lower than that indicated by the oven's internal temperature sensor in the 200-300 °C temperature range and about 40 °C lower at a set temperature of 600 °C (see Fig. S3a). We were unable to measure the temperatures of the gas stream at oven temperatures above about 600 °C and throughout the manuscript we refer only to the temperature indicated by the internal sensor of the oven.

We have added a new general section explaining why thermograms measured in different setups may differ.

3.1.8 Summary of thermograms

The thermograms obtained by the present instrument deviate from others reported in the literature, the temperatures required for 50% dissociation being generally higher by e.g. 80 °C for PAN, 50 °C for iPN and 150 °C for HNO₃, respectively (Day et al., 2002; Wild et al., 2014; Sobanski et al., 2016; Thieser et al., 2016; Womack et al., 2017). This lack of agreement with other setups is not unexpected as the degree of dissociation of a trace gas at any temperature depends not only on the temperature but also on the time over which the molecule is exposed to that temperature (Womack et al., 2017). To illustrate this, based on rate coefficients (related to bond-dissociation energies, BDE) for the thermal dissociation of PAN (Bridier et al., 1991), iPN (Barker et al., 1977), HNO₃ (Glänzer and Troe, 1974), N₂O₅ (IUPAC, 2019), ClNO₂ (Baulch et al., 1981), and HONO (Tsang and Herron, 1991), we calculated the theoretical 50% conversion temperature for each molecule as a function of residence time inside the oven (see Fig. S3b)). At short residence times the dependence on temperature is very steep (especially for large BDEs) which partially explains the differences between our short heated section inlet and longer ones. However, in practise, we know neither the precise average temperature of the gas at the centre of the oven, nor can we characterise the axial and radial gradients in temperature in the quartz tubes so that calculations of fractional dissociation (or complete thermograms) based on bond-dissociation energies are at best only a rough guide. We note that use of different flows, oven diameters and operational pressures will strongly affect heat transfer from the oven walls to the gas, so that reporting the temperature of the external oven-wall (as done here and in all reports in the literature) to some extent precludes comparison between different setups. The width of the thermograms (i.e. the temperature difference between e.g. 10% and 90% dissociation) will also depend on details of axial and radial temperature gradients in the tubing located within the oven and also in the downstream section of tubing, which represents a transition regime between oven and room temperature. The impact of temperature gradients inside the quartz tube was explored by calculating the HNO₃ thermogram using an Arrhenius expression for its thermal dissociation and the gas residence time within the quartz tube. First we assumed that all HNO₃ molecules experience the same temperature and then compared this to the situation in which 20% of the HNO₃ molecules are 80 °C lower in, and 20% are 80 °C higher in temperatures. The resultant thermograms are displayed in Fig S3c) and indicate that the presence of temperature gradients results in an increase in the width of the thermogram from 250 °C to 350 °C.

The thermograms we report here serve only to determine the temperature needed to ensure ~~complete~~ maximum conversion of each trace gas to NO₂. This is achieved in the present setup with a temperature of 850 °C. Where possible, we have verified that operation at the plateau of the thermogram resulted in quantitative conversion of the traces gases and particles studied, with one exception, NaNO₃ particles. We further note that, in an instrument designed only to measure NO_y, there is no need to ensure separation (in temperature) of the thermograms for different classes of molecules.

(c) Have the authors independently confirmed the identity, purity and concentrations of the gases they sampled by CIMS (PAN, HNO₃) or GC (iPN)? For PAN, Figure S2a shows a step after ~300 °C which may be due to the presence of an alkyl nitrate. For iPN and HNO₃ Figure S2 shows "expected values" based on permeation and dilution flows, though I consider these methods reliable standards.

As the referee mentions, flows of HNO₃ and iPN were obtained from either permeation standards or canisters with known mixing ratios. Experiments on N₂O₅, carried out following a suggestion of this referee (see comment below), were conducted with parallel sampling by a further TD-CRD operated in this laboratory. Experiments on PAN, ClNO₂ and HONO were conducted without parallel measurements by other instruments. Note that TD methods have been used in the past to calibrate e.g. PAN and ClNO₂ signals for a CIMS, so reversing the logic and using a CIMS to calibrate the TD instrument in this work makes little sense.

We would like to re-emphasise that our instrument is not set-up to measure different members of the NO_z family but to measure NO_y. An impurity e.g. of HNO₃ in the iPN sample (see above) will surely change the shape of the thermogram, but will not prevent conversion of all NO_z to NO₂ and NO at the operational temperature of 850 °C. Text (section 3.1.8) has been added to emphasise this:

The thermograms we report here serve only to determine the temperature needed to ensure ~~complete~~ maximum conversion of each trace gas to NO₂. This is achieved in the present setup with a temperature of 850 °C. Where possible, we have verified that operation at the plateau of the thermogram resulted in quantitative conversion of the traces gases and particles studied, with one exception, NaNO₃ particles. We further note that, in an instrument designed only to measure NO_y, there is no need to ensure separation (in temperature) of the thermograms for different classes of molecules.

(d) The thermogram of NH₄NO₃ should be shown.

(e) N₂O₅, ClNO₂, and HONO are important NO_y components; their thermal dissociation should have been evaluated since the claim is made that the inlet's behaviour is different from that of Wild et al. (2014).

We have performed additional laboratory experiments, and now include thermograms for NH₄NO₃, N₂O₅, ClNO₂ and HONO.

See new Sections 3.1.4 to 3.1.7.

(2) Denuder performance:

(a) The denuder partially transmits gases but at a rate that appears to be dependent on environmental factors such as RH (Figure 6) and possible also ambient air temperature (not examined). The transmission of many potentially important components of NO_z (e.g., N₂O₅, ClNO₂, HONO) was not evaluated but should have been.

We have performed additional laboratory experiments with the denuder, and now include N_2O_5 , ClNO_2 and HONO in Fig. 6. The removal efficiency of N_2O_5 was only determined in dry air, to prevent the formation of HNO_3 . ClNO_2 and HONO were only tested under humid conditions, as humidity was required for their initial generation. The text has been modified:

The efficiency of removal of trace gases in the denuder under typical flow conditions (3.3 slm) was investigated for NO, NO_2 , PAN, iPN, HONO, N_2O_5 , ClNO_2 and HNO_3 as representative NO_y species. The efficiency of removal of each trace gas (generally present at 5–40 ppbv) was determined by measuring its relative concentration when flowing through the denuder (pNit-channel) and when bypassing the denuder (NO_y channel). The results (Fig. 6) indicate that, in dry air, all of these trace gases were removed with an efficiency of close to 100%. However, when the main dilution flow was humidified significant, RH-dependent breakthrough of NO was observed, with only 60% stripped from the gas-phase at RH close to 100%. HONO was removed with 85% efficiency at an RH of 46%, and ClNO_2 with 75% efficiency at an RH of 60%. In contrast, humidification had only a marginal effect on the scrubbing efficiency for NO_2 , iPN and HNO_3 for which an efficiency of $\geq 95\%$ was observed. The precise values from which the removal efficiencies in Fig. 6 were determined are listed in Table S2.

(b) Memory effects. The high-concentration experiments described on pg 13 are a poor way of assessing memory effects because there could be a limited number of surface sites that are overloaded when sampling a high concentration. A more realistic experiment would be to sample a low concentration of NO_x for a longer time period, and then examine what comes off the denuder while sampling zero air.

We do not aim to provide a quantitative analysis of memory effects but to indicate that such effects can be important for this denuder type. We also have data in which the denuder was exposed to “typical” concentrations of NO_x for long periods but under less controlled (i.e. more variable conditions). The qualitative result, a release of NO_x when exposed to humidity, is the same. We now write:

Qualitatively similar results, i.e. humidity induced formation and release of NO_x from the denuder, were observed when the denuder was exposed for periods of weeks to variable levels of NO_x (i.e. up to 20 ppbv) under dry conditions.

(c) NO_x and the aforementioned components of NO_z usually dominate NO_y , such that any transmission of these species constitutes a sizeable measurement error for pNit. This should have been taken into account in an explicit error analysis as part of the pNit data reduction.

After identifying the humidity issues of the denuder and in the absence of effective regeneration techniques, we refrained from detailed analysis (including assessment of errors) in our pNit measurements. Our findings, that the denuder suffers from humidity related breakthrough and release of reactive nitrogen indicates that measurements of pNit using similar denuders to remove gaseous NO_y may suffer from bias under some conditions. We are unable to quantify this. In the ambient measurements from Mainz we measured only total NO_y and did not attempt to separate between gas and particulate phase NO_y . The pNit measurements from AQABA serve to demonstrate the presence of humidity issues under campaign conditions and were not included as part of an analysis of gas-particle nitrogen partitioning. We write:

This strongly suggests that the large difference between pNit reported by the TD-CRDS and the AMS does not result from the inability of the AMS to detect supermicron particulate nitrate, but from denuder artefacts similar to those seen in the laboratory experiments described in Sect. 3.3.2. This short case-study serves to highlight the

potential positive bias in denuder based, TD-CRDS measurements of pNit under humid field conditions.

(3) Aerosol nitrate can be present on mineral dust as organic nitrates or on sea salt aerosol. Do other nitrate salts convert to NO₂ in this inlet?

We have performed extra experiments on NaNO₃ and compared the detection efficiency of NaNO₃ with that of NH₄NO₃ as a function of particle diameter.

The results are presented and discussed in the new section 3.1.7

(4) How does the instrument perform above the 1-micron size range? The latter dominates aerosol mass in many regions.

As we did not carry out experiments with super-micron particles, we can only assess this using the predicted transmission of the denuder according to the PLC. The following paragraph has been added in Sect. 3.3.1:

The PLC does a better job in predicting a reduction in transmission for the largest particles which we measured and indicates a transmission of 74% at 1 μm and 45% at 2 μm. In certain environments, nitrate associated with coarse mode particles represents a potential (negative) bias to TD-CRDS measurements of NO_y.

(5) Ambient air measurements of pNit:

(a) How was the error due to break-through of NO_x considered?

(b) How were denuder memory effects taken into account in the reduction of the field data?

(c) The RH dependence of denuder performance is a considerable issue considering the inlet is periodically flooded with dry zero air and then re-exposed to humid ambient air. How does this back-and-forth affect the field data?

See response to major comment (2) (c). We do not show pNit data sets that were corrected for the break-through and that can be considered as accurate pNit measurements. The denuder is never back-flooded with (hot) zero air, as this would melt the PFA fittings between denuder and quartz tube.

(d) How long was the inlet for the NO_y channel? Was conductive tubing used (or were aerosol lost on the inlet)?

During AQABA, sampling was directly through the denuder in the pNit channel and through the heated quartz inlet in the NO_y channel, so that aerosol losses to non-conductive tubing or bent inlet lines was avoided. In the Mainz ambient measurements, the pNit channel was not operated and the NO_x and NO_y channels sampled from a common overflow in a straight ca. 1 m long ½ inch PFA tube. Aerosol loss in the NO_y channel might be possible under this setup. We added in Sect. 4.2:

Aerosol transmission was probably < 100% in these measurements.

(e) Since the TD-CRDS data were not compared with an independent measurement of NO_y (Mo converter CL) or of total aerosol nitrate (High-volume impactors, PILS, MARGA or similar), the claim that this instrument accurately quantifies NO_y and particulate nitrate in ambient air is not substantiated and the conclusions need to be weakened accordingly.

In the conclusions we now write:

Our laboratory experiments suggest that the different gas-phase NO_z species investigated (PAN, iPN, N₂O₅, HONO, ClNO₂, HNO₃) are converted with near stoichiometric efficiency to NO_x at an oven temperature of 850 °C. NH₄NO₃ particles of diameter 200 nm are also detected quantitatively as NO_x, whereas the efficiency of

detection of NaNO_3 particles of similar diameter was closer to 25%. The efficiency of detection of coarse mode particles will be further reduced by their lower transmission through the denuder.

(6) The authors show several pages on the interference due to gas-phase NH_3 only to conclude it to be insignificant. However, much more NH_3 is typically present in the form of aerosol ammonium, which would evaporate in the NO_y inlet. The authors should also consider and examine conversion of $(\text{NH}_4)_2\text{SO}_4$ especially in the presence of O_3 . The concentration of NH_3 which we used (131 ppb) corresponds to an aerosol ammonium loading of about $100 \text{ microg m}^{-3}$, which is more than found in most environments. As there is no obvious reason why NH_3 from $(\text{NH}_4)_2\text{SO}_4$ should behave differently to gas phase NH_3 . We do not see any value in performing experiments on $(\text{NH}_4)_2\text{SO}_4$.

(7) General organization:

(a) The introduction with its lengthy discussion of nitrogen oxide chemistry misses the mark (see detailed comment below).

We would argue that some description of NO_y chemistry is essential to put this work in context and describe our motivation for the development of the instrument. Too much is probably better than too little and the well informed reader has the choice of simply skipping this section. See specific comment below for changes made.

(b) A critical comparison of the performance of this new instrument to existing methods (in terms of detection limits, selectivity, instrument including heater designs, etc.) is lacking and should be provided.

We have added an additional section (3.4) in which we compare the instrument to others. Note that we restrict this discussion to instruments that measure NO_x and NO_y and not single components thereof.

Specific comments

pg 1 line 10 "detection" replace with quantification
"detection" has been replaced with "measurement"

pg 1 line 14 "detection limits" Please state the level of confidence. Why does the NO_y channel have half of the LOD of the NO_x channel?

Our detection limits were based on instrument performance during the AQABA campaign in which the ship's motion degraded optical alignment and resulted in great variability in the zeros. We now report the LOD of both channels during operation in the laboratory, which is comparable to any stable platform.

Abstract: Detection limits, defined as the 2σ precision for 1 minute averaging, are 40 pptv for both NO_x and NO_y .

Sect. 2.2: The NO_x detection limit of 40 pptv (2σ , 1 minute average) for the present instrument (laboratory conditions) was derived from an Allan variance analysis and is worse than that reported by Thieser et al. (2016) (6 pptv at 40 s) due to degradation of the mirror reflectivity.

Sect. 3.4: Our present detection limit for both NO_x and NO_y is however worse than that reported (for NO_2) for the same instrument in 2016 (Thieser et al., 2016), which is a result of mirror degradation since that study.

pg 1 line 17, 18, 19 "significant interferences", "high particle transmission", "essentially complete removal" Please be quantitative.

Corrected

[...] and rule out significant interferences from NH_3 detection (< 2%) or radical recombination reactions under ambient conditions. While fulfilling the requirement of high particle transmission (> 80% between 30 and 400 nm) and essentially complete removal of reactive nitrogen under dry conditions (> 99%), [...]

pg 1 line 19 "denuder suffered from NO_x breakthrough" Does the breakthrough of NO_x not imply that the pNit measurement is inaccurate and does not work?

The breakthrough certainly indicates a potential bias. See replies to major comments (2) (c) and (5) (c). In the abstract we write:

The denuder suffered from NO_x breakthrough and memory effects (i.e. release of stored NO_y) under humid conditions, which may potentially bias measurements of particle nitrate.

pg 1 line 21-22 " NO_x measurements obtained from a ship sailing through the Red Sea, Indian Ocean and Arabian Gulf were in excellent agreement with those taken by a chemiluminescence detector of NO and NO_2 ." What about the NO_y and pNit data during this cruise?

The oven of the pNit channel broke down shortly after the time frame shown in Sect. 4.1. An analysis of the NO_y data set will be presented in a separate publication.

pg 1 line 23 "A dataset exploring variations in the NO_z to NO_y ratio (maximum value of 0.6) of air in a region (Mainz, Germany) with strong urban influence was measured over a one-week period in winter." and what was the conclusion?

We now write:

Summertime NO_x measurements obtained from a ship sailing through the Red Sea, Indian Ocean and Arabian Gulf (NO_x levels from < 20 pptv to 25 ppbv) were in excellent agreement with those taken by a chemiluminescence detector of NO and NO_2 . A dataset obtained locally under vastly different conditions (urban location in winter) revealed large diel variations in the NO_z to NO_y ratio which could be attributed to the impact of local emissions by road-traffic.

pg 2 line 1 - pg 3 line 21 Section 1.1 "Atmospheric NO_x and NO_y ". This paper is about a new instrument. The lengthy description of NO_x and NO_y chemistry and all those reactions (in particular R6-R10) are not needed and could / should be replaced by citations to the authors' own papers.

If this section stays, please fix R8. RH is already used as relative humidity and implies a saturated alkane, with which NO_3 barely reacts and usually does not form an alkyl nitrate.

See reply to major comment (7) (a). We replaced "RH" with a generic alkene.

pg 4 line 17 "Pyrolysis". Thermolysis or thermal dissociation are more appropriate here. Changed throughout the manuscript.

pg 4 line 25. "which overcome these limitations" Please be more specific here. One of the limitations discussed in the preceding paragraph mentions secondary chemistry by O-atoms formed from the decomposition of ozone, which wasn't addressed in this paper.

More detail has been added:

Compared to the setups described by Thieser et al. (2016) the following changes were implemented: (1) Addition of O_3 for NO_x detection; (2) higher oven temperature (to

detect HNO₃) and location directly at the front of the inlet; and (3) use of a charcoal denuder for separate measurement of pNit and gas-phase NO_z. The addition of O₃ (after the TD-inlet) ensures that we detect NO as well as NO₂ and thus removes bias caused e.g. by the pyrolysis of O₃ and reactions of O(³P) which reduce NO₂ to NO.

Since some of the co-authors have described multi-channel TD-CRDS instruments previously (Sobanski et al., 2016; Thieser et al., 2016), please add a short statement explaining how this new instrument differs from the old ones and what parts constitutes novelty (use of a denuder to quantify pNit).

Text has been added:

Compared to the setups described by Thieser et al. (2016) the following changes were implemented: (1) Addition of O₃ for NO_x detection; (2) higher oven temperature (to detect HNO₃) and location directly at the front of the inlet; and (3) use of a charcoal denuder for separate measurement of pNit and gas-phase NO_z.

pg 5 Section 2.1 "CRDS Operation Principals" How much of this section is duplication of (Sobanski et al., 2016; Thieser et al., 2016)? Please condense and focus on what has been changed since the earlier versions, and why.

Apart from the core optical NO₂ detection most key parameters were changed compared to the setup described by Thieser et al. which did not measure NO_γ.

pg 5 line 5 spell out / define STD

Corrected.

pg 5 line 21 Please give an uncertainty for l/d.

Corrected.

$l/d = 0.98 \pm 0.01$

pg 5 line 23 "aerosol particles" should simply be particles.

Corrected.

Does a 2 μm pore size filter truly removes all particles? In our experience, they do not, but they remove the size range that would interfere optically. Consider rephrasing.

We performed a quick check with laboratory air and a CPC and added the results:

The filter's efficiency, tested with laboratory air containing 1.8×10^3 particles cm⁻³ and a CPC (TSI 3025 A), was > 98%.

pg 5 line 27 "depending on flow, pressure and inlet set-up" State typical pressures and flows. Is the inlet described anywhere? Please call out the relevant section if it is.

Text added.

(see sections 2.2 and 2.3).

pg 5 line 29 300 pptv NO₂ equivalent and 6.5 Torr pressure difference seem like a lot. It seems to be caused by the peculiar addition point of the zero air between the valve/denuder/inlet converter and CRDS cells and probably could be avoided altogether if zero air were added at the tip of the inlet (with larger fittings). Please provide a rationale why zero air was added this way (state advantages and disadvantages).

The current set-up was implemented for a chamber study, where flowing hot air into the chamber was undesired. The pressure effect on NO₂ detection is well characterised and the correction worked consistently in all field and laboratory situations. We have

also zeroed by overflowing zero-air through the heated inlet (without denuder) and this option is now mentioned.

We have also used an alternative setup, in which the inlet is overflowed with zero air added close to the tip of the inlet (downstream if the oven) reduces the pressure difference, but has the disadvantage that hot air is blown out of the instrument when zeroing, which may interfere with co-located inlets. Addition of zero air upstream of the quartz inlets would remove this problem but increase the complexity of the inlet and potentially result in loss of sticky molecules such as HNO₃.

pg 6 line 9. "The maximum concentration of NO₂ (and thus optimal conversion of NO to NO₂)". Please state what fraction of NO that is converted and if the NO data were corrected accordingly.

We have added the conversion factor. No correction was performed:

The maximum concentration of NO₂ (corresponding to 96% of the NO in the gas bottle) was observed when the flow over the pen-ray lamp was between 60 and 80 sccm, which resulted in 19 ppmv O₃ in the reaction volumes.

pg 6 Section 2.3 How is temperature measured in these furnaces? Is the oven temperature identical to the temperature of the gas travelling through it?

The temperature is measured in the ceramic block that accommodates the quartz tube. See also the reply to major comment (1) (b) and the new Figure S3a).

sections 2.3 and 2.4. A critical parameter is the sample flow rate, which should be stated here.

Has been added:

The sampling flow through both heated inlets is 3.0 slm.

pg 6 line 20. How short is "short"?

An experiment of the inlet setups during the two field campaigns should be provided.

On AQABA sampling occurred directly through the denuder in the pNit channel and through the heated quartz inlet in the NO_y channel. During the ambient measurements in Mainz, the NO_x and NO_y channels sampled from a common overflow in a straight, 1 m long ½ inch OD PFA tube (as described in Sect. 4.1 and 4.2). Inlet lines, filter location and the pressure reduction were identical in both campaigns.

[...] was kept short (ca. 30 cm) [...]

pg 6 line 22. Describe the valve (make & size etc.). Are there memory effects? Pressure drops?

A description has been added:

An electronic, PTFE 3-way valve (*Neptune Research, Inc.*, type 648T032, orifice diameter 4 mm) under software control switches between the two heated inlets, one of which is equipped with a denuder. Memory effects for NO₂ on the valve surfaces were not observed. Bypassing the valve under normal sampling conditions led to an 0.6 Torr pressure change.

pg 7 line 11 "Results and discussion, 3.1 The fractional conversion of NO_z to NO₂ in the TD-inlets was investigated in a series of experiments in which constant flows of (separately) PAN, isopropyl nitrate and nitric acid were passed through the heated-inlet (bypassing the denuder) while the temperature was varied and NO₂ was monitored"

This section describes how the experiment was conducted and should be moved to the experimental section, and not appear under "Results and discussion"

We restricted the experimental section to basic features of the instrument that apply to all laboratory and field experiments. For better readability of the paper we prefer to add short (section specific) experimental details in the results section.

pg 7 line 20. ~400 C to dissociate PAN is very high. How and where exactly is this temperature measured? What is the difference between the measured temperature and the temperature of the gas stream?

The temperature is measured in a ceramic block that accommodates the quartz tube. See also the reply to major comment (1) (b) and the new Figure S3a).

pg 7 line 22 "We conclude that PAN is stoichiometrically converted to NO₂" Just because the curve has flattened does not imply stoichiometric conversion. Has this statement been verified, e.g., by comparison to a CL NO_y instrument or PAN-CIMS?

Both CL NO_y instruments and PAN-CIMS also require calibration. For PAN-CIMS, this has previously been done using TD-instruments operating in the plateau range. It makes little sense to reverse the logic and use the PAN-CIMS to calibrate the TD-CRD.

pg 7 line 24 it is also higher than Day et al. (2002), Paul et al. (2010), Di Carlo et al. (2013) and Sadanaga et al. (2016) and inconsistent with CIMS inlet performance (Slusher et al., 2004; Zheng et al., 2011; Mielke and Osthoff, 2012; Phillips et al., 2013). There is no reason to expect identical thermograms when comparing different experimental set ups with different oven-types, tubes diameters pressures and flows. Figure S3a) shows that the offset between the oven temperature readout and the approximate thermocouple measured temperature in the center of the gas stream is largest at lower temperatures (84 °C at 230 °C). This would contribute to explain the particularly large "apparent" difference in temperature needed to thermally dissociate PAN in the present study. In addition, we emphasise that our goal is not to measure PANs, ANs etc separately. This instrument was designed to measure NO_y and overlap of the "broad" thermograms is of no consequence.

pg 7 sections "3.1.1. PAN" and 3.1.2 "Isopropyl nitrate". Please comment on the possibility that the PAN and iPN sources contain impurities. PAN, for instance, will slowly decompose and form nitric acid and an alkyl nitrate.

We have remeasured the iPN thermogram with a new sample. The previously used iPN sample apparently contained a large HNO₃ impurity. See major comment (1) (a).

pg 7/8 "3.1.2 Isopropyl nitrate" and "3.1.3" I am skeptical about the accuracy of these thermograms. The overlap of iPN and HNO₃ is inconsistent with literature.

See major comment (1) (a).

pg 8 line 3 "expected" Expected how?

We now write.

Based on the mixing ratio of iPN in the canister and the dilution flows, 10.7 ppbv represents (101 ± 11)% conversion.

pg 8 line 20. Please also compare with Di Carlo et al. (2013).

Reference to Di Carlo (2013) has been made.

pg 8 lines 22-25. If the temperatures are truly that inaccurate, please consider at least rough-calibrating the temperature scale.

As shown in Fig. S3a), the temperature measurement of the oven is clearly inaccurate. However, we do not have experimental means to accurately determine the temperature distribution at 850 °C set point over the whole length and width of the oven tube and therefore prefer to continue working with the nominal set point temperatures. We emphasize that almost all of the experiments that report thermograms rely on temperature measurement at the external surface of the inlet and not in the gas-phase.

pg 8 line 26. "Rather short" Why so short? In such a short inlet, the gas stream is likely heated very unevenly, leading to considerable broadening of the TD profiles. Was this intentional, or is this a design flaw? Note the broadening would not explain the overlap of iPN and HNO₃ thermograms.

See new Sect. 3.4.

pg 8 line 29 if this calculation can be performed for 50% conversion, it can also be done for 10%, 20%, 30%, etc. to construct an expected TD profile, which in all likelihood will be inconsistent with Figure 2.

50 % conversion is the metric we also used to compare with literature thermograms. The overlap of iPN and HNO₃ has been resolved, the width of the dissociation steps due to the short residence times has been discussed above.

pg 8 line 32 "to ensure complete conversion of each trace gas to NO₂". Replace complete with maximum conversion.

Corrected.

pg 9 line 4 "verify quantitative ... conversion to NO₂". Quantitative conversion was not demonstrated in this work; In fact, Figure S2 suggests incomplete conversion (~85%; or 13/15 for HNO₃).

See answer to major comment (1) (c). We write:

The HNO₃ thermogram (Fig. 2 and Fig. S2c)) has a plateau at temperatures above ≈ 800 °C. In the plateau region of Fig. 2, the HNO₃ mixing ratio measured is 13.0 ± 0.8 ppb, which (within combined uncertainties) is in agreement with the expected value (15.2 ± 1.98 ppb) calculated from the permeation rate and uncertainty in the dilution factor.

pg 9 line 6. Section "3.1.4 NH₃" Womack et al. (2017) showed NH₃ to be non-issue under most conditions, which is the same conclusion reached here. Does this insignificant interference really warrant two full pages? Consider condensing.

We would prefer to keep this section as it is. The interference is suppressed in the ambient air samples which both Womack et al. (2017) and we used. However, as discussed in the paper, there might be ambient conditions under which it becomes significant. In addition to the findings of Womack et al. (2017) and Wild et al. (2014) we showed a strong linear relationship between the NH₃ interference and O₃ added, quenched the signal with individual organic species, and confirmed the influence of RH on the quenching in both artificial and ambient atmospheres.

If NH₃ can be converted to NO_x, what happens when NH₄NO₃ or (NH₄)₂SO₄ aerosol are sampled?

See reply to major comment (6).

pg 9 line 22 "addition of 30 ppbv isoprene to zero-air did not significantly reduce the NH₃-to-NO₂ conversion efficiency under dry conditions, but reduced it by a factor of two when the RH was increased to 50%" In the preceding section, it was shown that NH₃ converts when there is a lot of O₃ present; please clarify if isoprene was added in the absence or presence of O₃ (with which it would react)?

O₃ was added in all experiments on the quenching of the NH₃ interference, as the interference is barely detectable without O₃, as seen in the pure NH₃ thermogram. A note about the O₃ concentration was added:

We found that addition of 30 ppbv isoprene to zero-air (containing 330 ppbv O₃) did not significantly reduce the NH₃-to-NO₂ conversion efficiency under dry conditions, but reduced it by a factor of two when the RH was increased to 50%.

pg 11 R22. How much CH₃C(O)O₂NO₂ are expected in a heated inlet? Its dissociation reaction is missing.

The dissociation reaction has been added as R22a.

We also explored the potential for bias caused by the recombination of CH₃C(O)O₂ and NO₂ when measuring PAN (reaction R22b), following the thermal decomposition of PAN (reaction R22a).

pg 11 equation (2). Is this equation valid for the likely turbulent flow conditions in the inlet?

The calculation of the diffusion coefficient is not coupled to flow conditions. Equation 3 applies to laminar flows. Under turbulent conditions transfer to the walls is likely to be more rapid.

pg 12 line 24/26 "Particle loss calculator (PCL)" Should this be PLC?

Corrected

pg 12 line 26 "which was developed for cylindrical piping and not the square honeycomb shape of the denuder and also does not take into account losses due to impact at the finite surface area which the gas/particle flow is exposed to at the entrance to the honeycomb" Based on this statement, wouldn't it be reasonable to conclude that this calculator should not be used?

The PLC gives a rough guide and indicates that significant particle loss is likely to occur for super-micron particles. We write:

The PLC does a better job in predicting a reduction in transmission for the largest particles which we measured and indicates a transmission of 74% at 1 μm and 45% at 2 μm. In certain environments, nitrate associated with coarse mode particles represents a potential (negative) bias for TD-CRDS measurements of NO_y.

pg 13 line 6. "close to 100%". Please provide a table with the precise values and some statistics.

Table S2 has been added.

The precise values from which the removal efficiencies in Fig. 6 were determined are listed in Table S2.

"humidified significant" Grammar.

Corrected.

"RH-dependent breakthrough". During zeroing, dry air is added and some of it travels through the denuder; does the denuder require some conditioning then after the switch back to ambient air sampling?

Zero air is never flowing back through the denuder to avoid exposing it (and fittings) to hot air. The valves are switched during zeroing to guarantee that excess zero air leaves towards ambient or through the non-denuder oven.

pg 13 line 9. ">95%. Please give precise values. Since NO_x is usually the major component of NO_y, the partial and variable (as a function of RH) transmission of NO_x introduces a major bias when quantifying aerosol nitrate.

See Table S2.

pg 13 line 12. Why dry nitrogen (if the behaviour is different at high RH)? Is this really equivalent to 1 month of sampling ambient air? How was 2.30×10^{17} molecules derived at?

Dry nitrogen is the dilution gas of the iPN cylinder. The number of molecules deposited was calculated from the flow of iPN, the time of exposure and the cylinder mixing ratio.

pg 13 line 20 " 2.55×10^{15} " what are the units here?

It is a number of molecules: We write:

During this experiment, 2.55×10^{15} molecules of NO_x desorbed from the denuder, indicating that the major fraction of iPN molecules remained stored on the denuder surface upon humidification.

pg 13 line 23 "After loading the denuder with 5 sccm from a 0.831 ppm NO₂ gas bottle for 4.8 days" NO₂ cylinders usually co-emit HONO, HNO₃ and NO. Was this considered?

No, impurities in the NO₂ cylinder were not considered, as NO₂ is presumably still the dominant component. In a separate experiment we also observed that deposited HNO₃ is not re-released as NO_x upon humidification. In our discussion we speculate that HONO might be an intermediate in the formation of the released NO.

pg 13 line 24 "(a total of 7.60×10^{17} molecules deposited)" How this value determined?

An explanation has been added.

[...], derived from the flow rate, the exposure time and the gas bottle mixing ratio)

pg 15 line 14 sections 4.1 and 4.2 are not convincing since there is no independent measure of what to expect for pNit.

These sections illustrate the first deployment of the instrument and are not intended to provide validation of e.g. the pNit measurement by inter-comparison. In contrast, the case study in Sect. 4.1 serves to demonstrate that humidity related interferences in the pNit channel are likely to be a source of bias under field conditions. This information is important to those striving to measure pNit with similar denuders. See also reply to major comment (2) (c).

pg 16 line 10 Does the AMS quantify supermicron particles at all? A citation is needed.

A citation has been provided:

(Drewnick et al., 2005).

pg 17 line 18 "> 90% transmission for ammonium nitrate". Is this statement justified when the transmission varies with size as shown in Figure 5?

This is why we give a size range in this sentence. Between ~40 and 400 nm the transmission is consistently above 90 %.

pg 21 line 45. The accepted paper should be cited.

pg 22 line 28. The accepted paper should be cited.

pg 23 line 13 The paper by Womack et al. (2017) has been accepted and should be cited and not its discussion paper.

Corrected for all three papers.

pg 24 Figure 1. Please add more detail such as dimensions; for example, indicate the diameter of the critical orifice and air pressure, and show l and d.

The two orifices have diameters of ≈ 0.05 mm.

This information has been added to the caption.

Figure 1 shows that ambient air is drawn in through two valves ("V")? Are these described anywhere? How much of a pressure drop do they give? What is the internal surface made of (Teflon?)?

Information on the valves has been added. See above.

An electronic, PTFE 3-way valve (*Neptune Research, Inc.*, type 648T032, diameter 4.4 cm, height 5.2 cm, orifice diameter 4 mm) under software control switches between the two heated inlets, one of which is equipped with a denuder. Memory effects through the employment of this valve were not observed. Bypassing the valve under normal sampling conditions led to an 0.6 torr pressure change.

In Figure 1, "1/2 in PFA" should be in metric units; indicate if this is outer or inner diameter and how long this section is.

Corrected.

In Figure 1, what does the green line represent? A chamber wall?

That was indeed a left-over from a previous diagram. The line has been removed.

The Figure is inconsistent with the text as it shows a TD oven at 850 C which is roughly the same length as the denuder; in the text, the section actually heated is described as rather short or 3 cm long, and the denuder length is stated at 10 cm.

Dimensions of the heated inlets parts are now included in the figure. A note has been added in the caption that the figure is not to scale.

pg 25 Figure 2. The PAN and iPN thermograms are inconsistent with literature. The caption should state the level of O₃ present for the NH₃ experiment.

Literature inconsistencies are discussed above. O₃ level was added:

[...] NH₃ (without added O₃).

pg 26 Figure 3 is not essential to this paper and probably should be in the supplemental.

The linear correlation between added O₃ and the extent of the NH₃ interference is an important finding and one of the main novelties in the NH₃ section, compared to the study of Womack et al. (2017). Therefore, we would preferably keep the figure in the main manuscript.

pg 28 Figure 5. Please specify the type of aerosol diameter (geometric vs. mobility). State value of key parameters (flow rate, denuder diameter). Correct inconsistency between PLC and PCL.

Figure and caption amended accordingly.

An aerosol flow of 3.3 slm was directed through the denuder (diameter 3 cm, see Sect. 2.4) and subsequently a DMA sampled 0.3 slm from the stream exiting the denuder.

pg 29 Figure 6. Please zoom in to ~60% to 100% for NO and to 95% to 100% for the other gases. Often, NO and NO₂ are the largest components of NO_y. How accurate is the measurement of NO_z species if ~5% of NO₂ and ~35% of NO break through the denuder? How variable are the numbers shown in Figure 6 (add error bars)?

The Figure has been re/drawn with error bars and an inset. The direct breakthrough of NO and NO₂ at zero-humidity is indeed just as problematic as the humidity induced re-release of NO in zero air. See above for discussion of the usability of pNit measurements (major comment (2) (c)). See new table S2 for precise values and variability metrics.

pg 30 Figures 7. What do the blue shades represent and why does the RH change (state in caption). As stated in the comments above, I am not convinced this experiment provides relevant information for an ambient air measurement (conc. are simply too high).

The caption has been extended. We have replied above to the comment on the high mixing ratios used.

The blue shaded area signifies the period in which the inlet oven was heated to 850 °C. Changes in RH are achieved by flowing parts of the zero air stream through deionized water.

O₃ addition was switched off during the blue shaded period.

pg 31 The presentation of Figure 8 is unclear.

How this experiment conducted?

Is synthetic air equal to zero air (and why is it humid then)?

In panel (a), why is there a "bump" at 9:50?

In panel (b), what does the derivative mean to the reader? What time?

Why are there lines for different RH?

The caption has been extended. The discontinuity ("bump") during the drying phase is caused by the presence of different adsorption sites and/or phase transitions on the denuder surface (as discussed in Sect. 3.3.2). The derivative was calculated in order to locate the position of this feature. Several RHs were plotted to demonstrate, that the discontinuity is slightly shifted to higher RH when starting the drying from a higher RH.

a) RH of humidified synthetic zero air after passing through the denuder. The initial RH was determined by bypassing the denuder before and after the experiment. Zero air was humidified by flowing a fraction of the stream through deionized water stored in a glass vessel. The time at which the experiment was conducted is given on the x-axis. Until ca. 09:35 UTC air with constant humidity (RH ca. 68%) was sent through the denuder. Behind the denuder, the measured humidity increased with a delay. Afterwards the denuder was exposed to dry zero air. b) Derivative of the measured RH during the drying period. The step during the drying phase occurs in a higher RH area, when starting the drying from a larger RH value.

pg 32 Figure 9. Properly cite Kim et al. in the bibliography, and do not provide the full reference in the caption.

Corrected.

pg 33 Figure 10a. Is the slope correct? There seem to be many points above the line. Is the slope affected by outliers? In any case, it's great that NO_x data agree, but since the focus of this paper is mainly on measurement of NO_y, NO_z and particle nitrate, a more relevant plot would be TD-CRDS NO_y vs. CLD NO_y, TD-CRDS NO_z vs. NO_z measured by other techniques, as well TD-CRDS nitrate vs PILS or MARGA nitrate. We have added a histogram of the NO_x data points as Fig. S6. The histogram shows that 92 % of all data points are below 5 ppbv. These data points determine the slope of the overall correlation, explaining the visual misinterpretation caused by the relatively few data points between 10 and 25 ppbv. No other NO_z or NO_y measurements with which to compare were available during AQABA.

pg 33 Figure 10b I am not sure the OPC data add anything of value here since the nitrate fraction could be changing.

The OPC data set was added to exclude the possibility that the short term fluctuations in pNit were caused by coarse mode nitrates, undetected by the AMS, despite the non-nitrate-specific nature of the OPC signal.

Supplemental:

Figure S1. Please provide the mechanism used in the box model.

The reaction scheme has been added as table S1.

Figure S2, caption. "total uncertainty of the TD-CRDS measurements" - what is meant by this?

The caption has been refined.

Error bars represent the ~~total~~ measurement uncertainty of the TD-CRDS measurements (see Sect. 2.2).

Figure S2D is inconsistent with Figure 2 which shows the entire TD profile of iPN overlapping with that of HNO₃ - which is not observed in Figure S2D under any condition.

The iPN thermogram has been re-measured. See above.

Figure S3. A strange and confusing way to present data.

The figure helps to explain the reason why addition of O₃ to convert NO to NO₂ removes the need for complex data correction.

The simulations consider oxidation of NO₂ by O₃ to form NO₃ and subsequent formation of N₂O₅. Were NO₃ and N₂O₅ sinks been considered? Please provide the full mechanism.

See new table S1.

References

Barker, J. R., Benson, S. W., Mendenhall, G. D., and Goldern, D. M.: Measurements of rate constants of importance in smog, Rep. PB-274530, Natl. Tech. Inf. Serv., Springfield, Va., 1977.

Baulch, D. L., Duxbury, J., Grant, S. J., and Montague, D. C.: Evaluated kinetic data for high temperature reactions. Volume 4 Homogeneous gas phase reactions of halogen- and cyanide- containing species, J. Phys. Chem. Ref. Data, 10, 1981.

Bridier, I., Caralp, F., Loirat, H., Lesclaux, R., Veyret, B., Becker, K. H., Reimer, A., and Zabel, F.: Kinetic and Theoretical-studies of the Reactions $\text{CH}_3\text{C}(\text{O})\text{O}_2 + \text{NO}_2 + \text{M} \rightleftharpoons \text{CH}_3\text{C}(\text{O})\text{NO}_2 + \text{M}$ between 248 K and 393 K and Between 30-torr and 760-torr, Journal of Physical Chemistry, 95, 3594-3600, 1991.

Day, D. A., Wooldridge, P. J., Dillon, M. B., Thornton, J. A., and Cohen, R. C.: A thermal dissociation laser-induced fluorescence instrument for in situ detection of NO_2 , peroxy nitrates, alkyl nitrates, and HNO_3 , J. Geophys. Res. -Atmos., 107, doi:10.1029/2001jd000779, 2002.

Drewnick, F., Hings, S. S., DeCarlo, P., Jayne, J. T., Gonin, M., Fuhrer, K., Weimer, S., Jimenez, J. L., Demerjian, K. L., Borrmann, S., and Worsnop, D. R.: A new time-of-flight aerosol mass spectrometer (TOF-AMS) - Instrument description and first field deployment, Aerosol Science and Technology, 39, 637-658, 10.1080/02786820500182040, 2005.

Glänzer, K., and Troe, J.: Thermal Decomposition of Nitrocompounds in Shock Waves. IV: Decomposition of Nitric Acid, Berichte der Bunsengesellschaft für physikalische Chemie, 78, 71-76, 10.1002/bbpc.19740780112, 1974.

IUPAC: Task Group on Atmospheric Chemical Kinetic Data Evaluation, (Ammann, M., Cox, R.A., Crowley, J.N., Herrmann, H., Jenkin, M.E., McNeill, V.F., Mellouki, A., Rossi, M. J., Troe, J. and Wallington, T. J.) <http://iupac.pole-ether.fr/index.html>, 2019.

Sobanski, N., Schuladen, J., Schuster, G., Lelieveld, J., and Crowley, J. N.: A five-channel cavity ring-down spectrometer for the detection of NO_2 , NO_3 , N_2O_5 , total peroxy nitrates and total alkyl nitrates, Atmos. Meas. Tech., 9, 5103-5118, 10.5194/amt-9-5103-2016, 2016.

Thieser, J., Schuster, G., Phillips, G. J., Reiffs, A., Parchatka, U., Pöhler, D., Lelieveld, J., and Crowley, J. N.: A two-channel, thermal dissociation cavity-ringdown spectrometer for the detection of ambient NO_2 , RO_2NO_2 and RONO_2 , Atmos. Meas. Tech., 9, 553-576, 10.5194/amt-9-553-2016, 2016.

Tsang, W., and Herron, J. T.: Chemical kinetic data base for propellant combustion. I. Reactions involving NO , NO_2 , HNO , HNO_2 , HCN and N_2O , JPCRD, 20, 609-663, 1991.

Wild, R. J., Edwards, P. M., Dube, W. P., Baumann, K., Edgerton, E. S., Quinn, P. K., Roberts, J. M., Rollins, A. W., Veres, P. R., Warneke, C., Williams, E. J., Yuan, B., and Brown, S. S.: A measurement of total reactive nitrogen, NO_y , together with NO_2 , NO , and O_3 via cavity ring-down spectroscopy, Environmental Science & Technology, 48, 9609-9615, doi:10.1021/es501896w, 2014.

Womack, C. C., Neuman, J. A., Veres, P. R., Eilerman, S. J., Brock, C. A., Decker, Z. C. J., Zarzana, K. J., Dube, W. P., Wild, R. J., Wooldridge, P. J., Cohen, R. C., and Brown, S. S.: Evaluation of the accuracy of thermal dissociation CRDS and LIF techniques for atmospheric measurement of reactive nitrogen species, *Atmospheric Measurement Techniques*, 10, 1911-1926, 10.5194/amt-10-1911-2017, 2017.

Author's Response to Referee #3

In this response, the referee comments (in black) are listed together with our replies (in blue) and the changes to the original manuscript (in red).

This manuscript does an overall good job of describing an instrument designed to measure NO_x, NO_y, and particulate nitrate by thermal dissociation – CRDS. The most useful aspect of the work is the demonstration of problems with the use of activated carbon denuders for removing gas-phase NO_y compounds. This will be of great use to many other researchers who use these types of denuders and activated carbon in general!

I recommend it be published after addressing the minor comments below.

We thank the referee for the positive review of our paper and the helpful comments which we address in this response.

The detection limits are listed in the abstract (98 ppt for NO_x with 1 min averaging) but strangely are not described elsewhere in the manuscript. Is this for a signal-to-noise ratio of 2? 3? How the LOD is defined and these numbers are determined should be in the main text somewhere. Given how sensitive CRDS can be to NO₂, I am surprised that the LODs are as high as they are – I would have expected that with a minute of averaging the LOD would be quite a bit lower. Is this a result of the large correction (116 ppt) that must be made to account for the difference in Rayleigh scattering when sampling humid ambient air vs. dry zero air? In addition to that correction that must be made to account for the differences in humidity between sampling and zero measurements, doesn't the change in humidity also change the reflectivity of the mirrors (due to the change in the index of refraction of air), and thus the ring-down times?

We added a paragraph in Sect. 2.2 about the performance of the instrument and a critical comparison with other instruments (including LODs) in Sect. 3.4. The LOD we listed previously was from the AQABA campaign, where the ship's motions caused significant fluctuations in the ring-down times. We now list the performance obtainable on a stationary platform.

For NO₂, the performance of the instrument was first described by Thieser et al. (2016), who reports a measurement uncertainty of 6 % + (20 pptv*RH/100) which is dominated by uncertainty in the effective cross section of NO₂ and the wavelength stability of the laser diode. The NO_x detection limit of 40 pptv (2σ, 1 minute average) for the present instrument (laboratory conditions) was derived from an Allan variance analysis and is worse than that reported by Thieser et al. (2016) (6 pptv at 40 s) due to degradation of the mirror reflectivity. Corrections applied to take into account humidity and pressure changes are discussed in Sect. 2.1. The total uncertainty in NO_y will depend on the uncertainty in the conversion to NO_x of both gaseous and particulate nitrate and thus depends on the individual components of NO_y in the air sampled. For purely gaseous NO_y, the major problem is likely to be related to loss of sticky molecules at the inlet and we choose to quote a "worst case" uncertainty of 15%.

We have amended the LOD we quote to that obtained on a stationary platform (the one mentioned in the last version was derived from the AQABA dataset obtained on a ship):

In this context we note that the deployment on a ship resulted in a degradation in performance (LOD was ≈ 100 pptv) owing to the ship's motions, especially in heavy seas, which resulted in drifts in the instrument zero.

The zero air used for zeroes is "CAP 180, Fuhr GmbH" - please clarify what this means— is it compressed zero air from a cylinder, or is it from a zero air generator? Rather than deal with the effects of ambient sampling vs. dry zeroes, why not use humidity-matched air? (e.g., ambient air that has been scrubbed of NO₂ via purafil or a catalyst?)

The zero-air generator has been described in more detail. Generally, the humidity correction is ≤ 100 pptv and has small associated uncertainties. Essentially we are scrubbing ambient air that has passed through a compressor.

k_0 is typically determined every five minutes (for one minute) by overflowing the inlets with zero air from a commercial zero air generator (CAP 180, Fuhr GmbH) attached to a source of compressed ambient air.

pg 6, last line - define BET pg 13, "However, when the main dilution flow was humidified significant," This sentence appears to be missing a word. Or perhaps the last word should actually be "significantly".

Both corrected.

[...] we calculate a BET (Brunauer-Emmett-Teller (Brunauer et al., 1938)) surface area [...]

[...] humidified significant [...]

References

Brunauer, S., Emmett, P. H., and Teller, E.: Adsorption of gases in multimolecular layers, J. Amer. Chem. Soc., 60, 309-319, 1938.